ASPECTS OF FAR-FIELD CONTROL ON BUOYANT JET MIXING

By

STEVEN J. WRIGHT

ASSOCIATE PROFESSOR OF CIVIL ENGINEERING
THE UNIVERSITY OF MICHIGAN
ANN ARBOR, MICHIGAN USA

PROJECT CONDUCTED AT

THE INSTITUT FUR HYDROMECHANIK
UND WASSERWIRTSCHAFT

ETH ZURICH
SWITZERLAND

Project Sponsors

Swiss National Science Foundation
Grant No. 87.229.0.84

U.S. National Science Foundation
Grant No. INT-8404553

1986

TABLE OF CONTENTS

FOREWORD

This report describes the major details of a research project conducted in the laboratories of the Institut für Hydromechanik und Wasserwirtschaft of the ETH Zürich. This research was conducted from October, 1984 through July, 1985 while the writer was on a sabbatical leave from the University of Michigan. The project was supported in part from the following sources:

Swiss National Science Foundation from which the writer was awarded an International Postdoctoral Fellowship, Grant No. 87.229.0.84;

U.S. National Science Foundation from which the writer was awarded a Cooperative Exchange Grant, No. INT-8404553;

The University of Michigan through a Faculty International Grant;

The ETH who awarded a grant to provide for supplies and student help.

The support from each of these sources is gratefully acknowledged. In addition, the efforts of the Institut staff who supported my efforts in developing and conducting the research project must not go unrecognized. In particular, Dr. Th. Dracos provided the necessary institutional support to initiate the project. Dr. Johannes Bühler was the necessary liason during the planning stages of the project, helped develop components of the experimental system, and provided stimulating conversation on matters related to the theoretical aspects of the problem. He also provided valuable comments on this manuscript. Daniel Schläpfer was an invaluable resource for resolving problems with the data aquisition and reduction and only with his experience in those regards was I able to complete the work in the limited time available. Martin Gutman helped with the early experiments and Xaver Studerus provided much assistance related to the use of the computer system. The help of these persons and the many others who helped to assure the successful completion of the project is gratefully acknowledged.

The publication of this report is intended to fulfill several objectives. In part, it is to fulfill the requirements for reporting the research results of the National Science Foundation grants. Another major objective is to provide a detailed description of the experiments, since that information will not be available elsewhere. It is intended that this report provide the necessary documentation of the experiments, the data collected, and the nature of the experimental results. Because of the large volume of data collected, it has been recorded on magnetic tape, copies of which will remain at the ETH and the University of Michigan. Descriptions of the magnetic tape data are provided to assist in data retrieval.

Because of the short time between the completion of the experiments and the report preparation, a thorough attempt at interpretation of the experimental results is not performed herein; experience has

shown that some "digestion" of the data is necessary before final conclusions should be attempted. In spite of this, a theoretical framework for the interpretation of the results is developed. Existing theoretical arguments are outlined and applied to the specific problem. The approaches to the interpretation of the data are outlined, although much of the data analysis to verify such theoretical descriptions has yet to be undertaken. The data results available at present are given to provide some idea of the nature of the results and their limitations. These results are found to be in conflict with some of the theoretical descriptions and alternative methods of analysis which will be pursued in the near future are outlined.

CHAPTER 1
INTRODUCTION

The impetus for the research project arose from a number of observations in previous experimental studies that had the examination of turbulent mixing in submerged buoyant jets as their principal objective. In many environmental applications, a major analytical objective is to be able to predict the dilution and extent of a contaminant field within some specified proximity of the source. The submerged turbulent buoyant jet has been subject to numerous studies, not only as a classical free shear flow but also due to its relationship to these environmental applications. It is probably safe to state that the problem of estimating buoyant jet mixing has been more than adequately resolved by previous investigations. However, most environmental applications involve more complex flow systems in which the jet interacts with system boundaries, ambient currents, and/or ambient density stratification. Relatively fewer studies have been performed to examine the effects of these ambient influences.

When submerged buoyant jets are released into receiving fluids with little or no ambient velocity (often an important limiting or "worst case" flow condition with respect to dilution), the mixed fluid will eventually flow away from the site under the influences of gravity. A clear distinction is made between this situation and cases with a strong ambient current which removes the fluid from the source region without a "piling up" of the buoyant fluid. At zero or low ambient velocities, the situation is quite different and gravitational effects dominate the flow-away process; the two situations are indicated schematically in Fig. 1-1. For the problems considered in this text, the gravitational spreading process is assumed to dominate the flow-away dynamics; i.e. there may be an ambient current, but it only

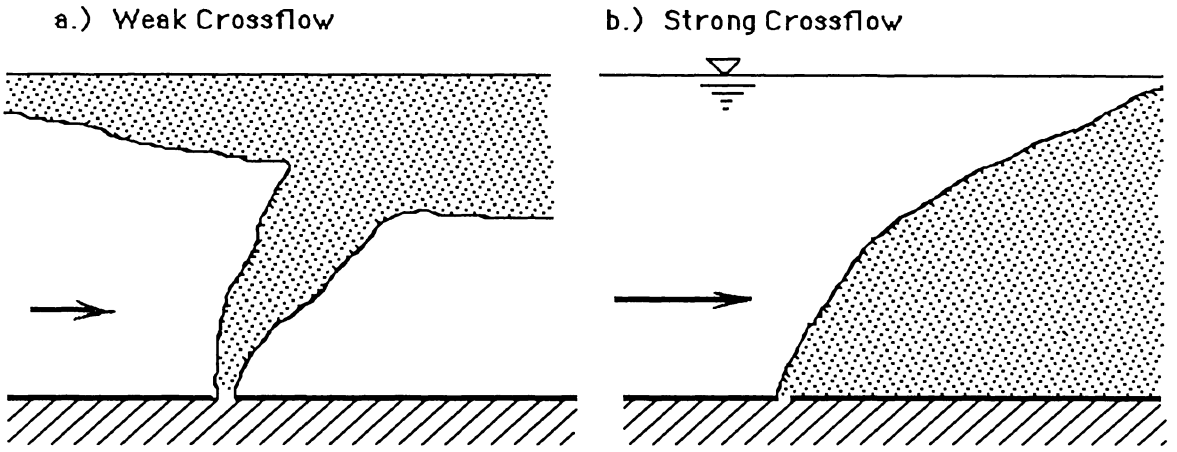

Figure 1. Schematic of Waste Field in a.) Weak Crossflow; b.)Strong Crossflow.

serves as a complement to the gravitational spreading process. The results of a number of previous studies, e.g. Cederwall (1971) and Roberts (1977) can be used to distinguish between the two different types of flow.

Within this context, there are a number of different generalized ambient configurations that can be visualized; several are indicated in Fig. 1-2. In general, three fundamentally different ambient density variations can occur:

1. A completely uniform vertical density distribution; An initially buoyant discharge will remain so and the discharge will continue rising (or sinking depending upon the initial density difference) up to a free surface and will commence spreading along the surface as in Fig. 1-2a.;

2. A continuously varying density distribution; In this case, the discharge may mix sufficiently with the underlying more dense fluid so that it attains a density equal to that somewhere within the ambient fluid column and therefore begin to collapse at an internal level as indicated in Fig. 1-2b. An essential component of this problem is that the collapse level is determined by the jet discharge (as it determines mixing rates) and the stratification which determines the density variations of the entrained fluid.

3. A discontinuous density distribution, approximated by the two discrete layers indicated in Fig. 1-2c. In this case, the rising jet may either be trapped at the density interface or continue to rise up to the surface depending upon the density change across the interface and the jet source conditions. For the first case, it may be possible to treat the interface as an analogue to the free surface in case 1, although this will not always be valid. It is possible for example, for the jet to be negatively buoyant after it passes through the density interface, but with sufficient momentum to penetrate well into the upper layer where it mixes with enough low density fluid to trap it in the upper layer.

These different cases describe the important limiting situations for the buoyant discharge case, although it is common to have ambient density distributions that may be intermediate; e.g. the two-layer fluid is an idealization since a density interface of finite thickness occurs in real fluid systems. A dense or negatively buoyant discharge may exhibit qualitatively similar types of flows with one important difference. If a negatively buoyant discharge encounters a sloping bottom such as indicated in Fig. 1-2d, it is possible for the dynamics of the resulting flow-away layer to be determined primarily by a balance between the buoyant weight down the slope and the bottom friction. This situation has some similarities with the other cases, but the nature of the overall force balance is different. This consequence was exploited in the experimental investigation to perform certain types of experiments that would not have otherwise been possible.

There have been previously suggested approaches that couple the behavior in the submerged buoyant jet flow with that in the spreading layer. One of the earliest is described by Koh and Brooks (1975) and has been updated to include the internal intrusion within a density stratified medium, Koh (1983). These approaches involve the coupling with a spreading density current; a relationship describing the propagation speed of a two-dimensional density current is combined with a prediction of the dilution within a rising plume to obtain both the thickness and the average dilution within the layer. These analyses assume that the jet dilution stops at the bottom of the spreading layer. Koh predicts layer thicknesses of approximately 30% of the depth for the case of a plume in a uniform density fluid

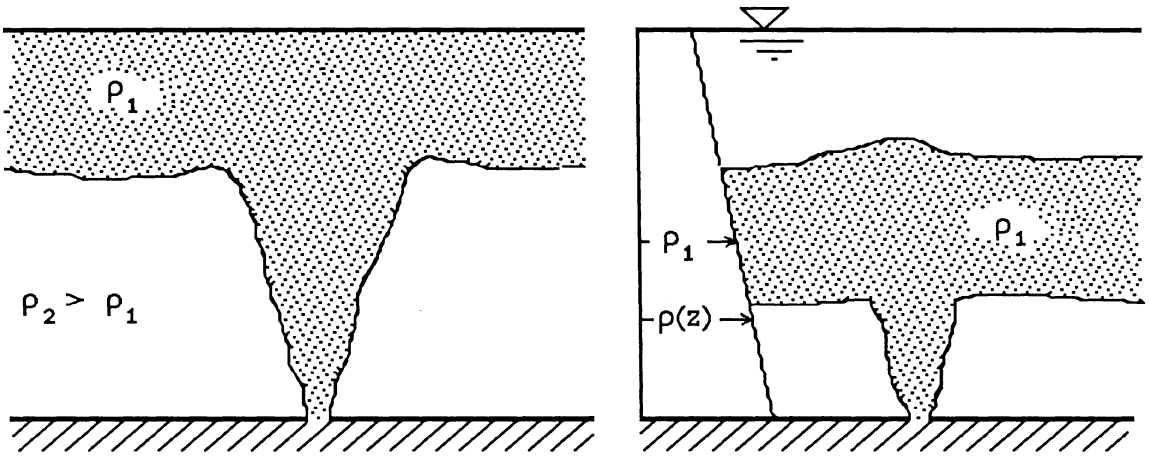

a.) Buoyant Discharge Into Uniform Ambient Fluid.

b.) Buoyant Discharge Into Linearly Stratified Ambient Fluid.

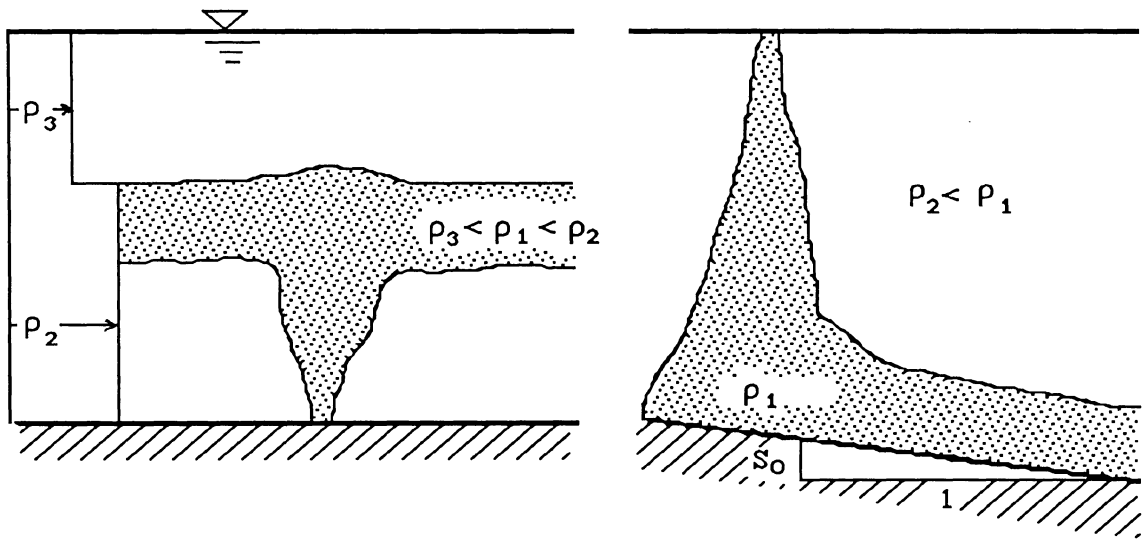

c.) Two Layer Ambient Fluid.

d.) Dense Discharge Into Ambient Fluid With Bottom Slope.

Figure 1-2. Schematic of Discharges With Different Density Configurations.

and 50% of the maximum height of rise for the case of a plume in a linearly stratified flow. Since the predicted layer thicknesses are quite significant fractions of the total plume rise, the computed reduction in dilution due to the blocking by the layer is quite significant. Wright (1985) discusses the lack of agreement between the dilutions predicted with these models and those experimentally observed. To demonstrate the magnitude of the discrepancies, consider the experimental data presented in Figs. 1-3 through 1-5. These data are taken from studies by Wallace and Wright (1980,1984) and Wong (1984). The data are nondimensionalized according to arguments developed in the respective references; these are not important to the discussion and are not repeated herein. Figs. 1-3 and 1-4 represent a comparison between the minimum dilutions predicted by a buoyant jet theory similar to that used by Koh. The predictions are for the minimum dilution at the maximum height of rise and the data are observed minimum dilutions within the spreading layer for two-dimensional and round buoyant jets, respectively. There has been no blocking correction applied in these predictions, yet the agreement between observed and predicted dilutions is quite adequate. Fig. 1-5 is a plot of minimum dilution along the jet axis from Wong and Wright (1985) and also fails to show the blocking effect of the

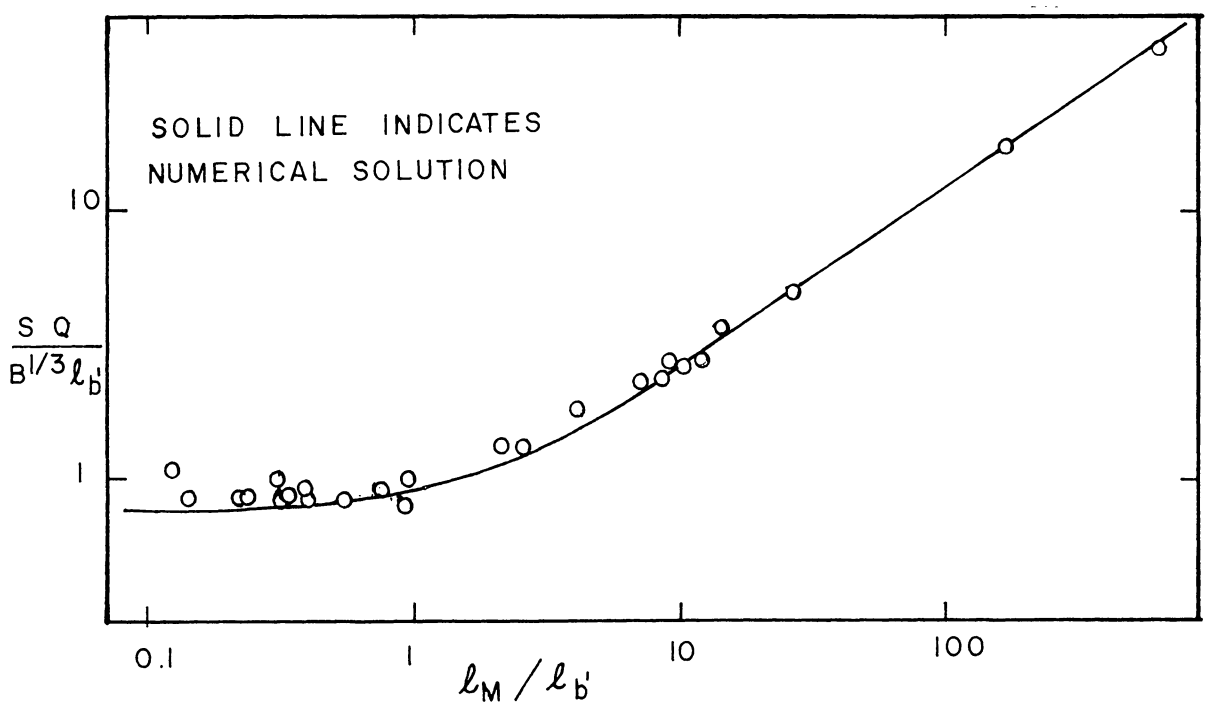

Figure 1-3. Comparison of Predicted Minimum Dilution at Maximum Height of Rise and Minimum Dilution Within Spreading Layer (From Wallace (1981)).

spreading layer, the extent of which is indicated in the figure. Therefore, the available experimental observations do not appear to validate the predictions by Koh's method. The data by Wright, et al (1981,1983) for discharges from a manifold diffuser into a linearly stratified fluid confirm these findings in that the layer thicknesses are even greater and yet no justification for a blocking correction can be found in the results.

Wong (1984) formulated an analysis similar to that by Koh but applied to the round buoyant jet in an internally stratified fluid. Since there is no indication of the internal hydraulic jump (as discussed below) in his experiments or those of Wallace (1984) for two dimensional flows, this was not considered in the analysis. One difficulty with such an theoretical approach is that a density current does not propagate with constant speed and thickness for the radial spreading problem. Nevertheless, Wong was not able to obtain realistic predictions of the dilution or the layer thickness with a blocking correction similar to that employed by Koh. He also observed a significant entrainment inflow towards the source in the ambient fluid above the spreading layer. Since the integral jet models predict vanishing jet entrainment at the maximum height of rise, it is not clear which, if any, aspects of the problem are described accurately in that region.

Another approach applied to unstratified fluids that can be considered as an alternative to the above is given by Jirka and Harleman (1979). This approach is basically similar to Koh's formulation, except for the consideration that the far-field spreading layer does not extend all the way back to the source but instead is connected with it by an immiscible hydraulic jump as depicted in the sketch in Fig. 1-6. The conditions within the thin surface layer preceding the jump are determined by applying an energy conservation argument for the impinging jet flow and the jump is analyzed by the theory of Yih and Guha (1955), which will be discussed in more detail later.

This type of analysis is later extended to the round buoyant jet problem, Lee and Jirka (1981). Their approach taken is essentially the same except that some jet mixing is assumed to occur as the flow spreads along the surface prior to the internal jump which is still assumed to be immiscible. The location of the internal jump was assumed to be relatively close to the source and the total dilution in the surface flow is relatively small (about 13%). In a related investigation, Wright, et al (1984) measured the surface dilution directly above a surfacing round buoyant jet and the surface dilution at a radial location three water depths away; these data are indicated in Figs. 1-7 and 1-8. A curve which predicts the minimum dilution in a submerged buoyant jet at an elevation equal to the free surface is plotted on each figure. It can be seen that significant increases in dilution in the flow along the surface occur for certain ranges of experimental parameters. From the data of Pryputniewicz and Bowley (1975) and Ryskiewich and Hafetz (1975) which are also indicated, the additional influence of the total water depth can be seen. Their experiments were conducted by altering the relative vertical source location within a system of fixed total water depth to simulate the effect of different depths. Note that although all the data appear to collapse onto a single curve (except for experimental scatter) directly above the source (Fig. 1-7), the data follow no consistent trend at the greater radial distance whereas the data by

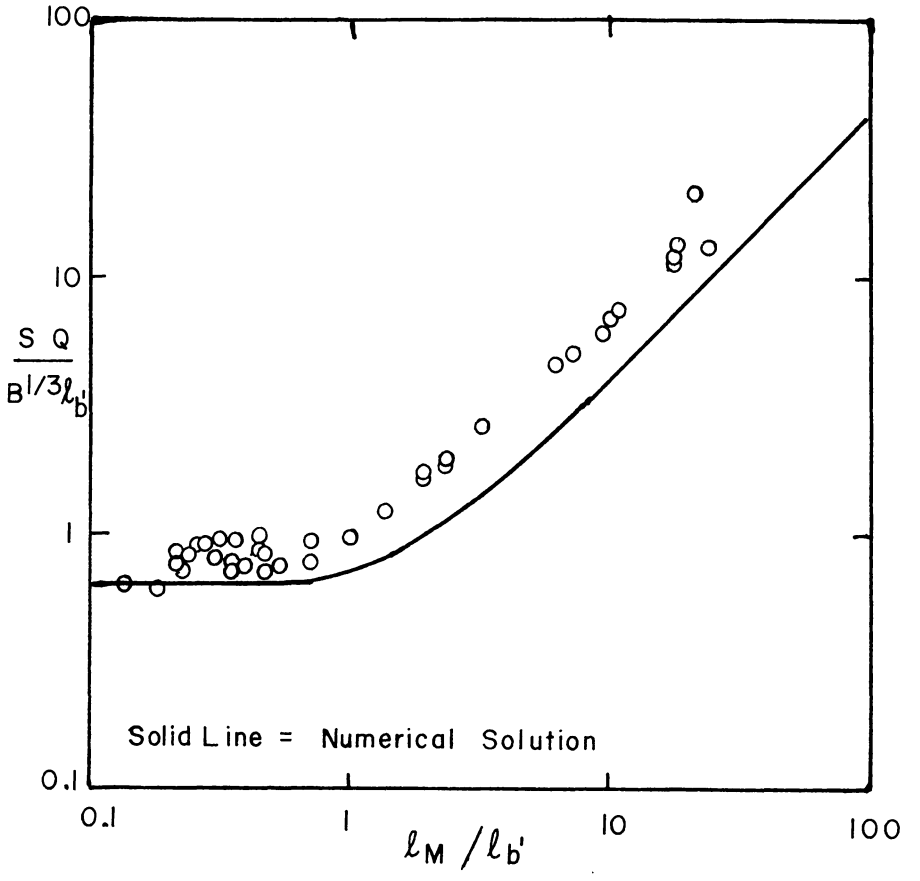

Figure 1-4. Comparison of Predicted Minimum Dilution At Maximum Height of Rise and Observed Minimum Dilution Within Spreading Layer (Round Buoyant Jets, From Wong (1984)).

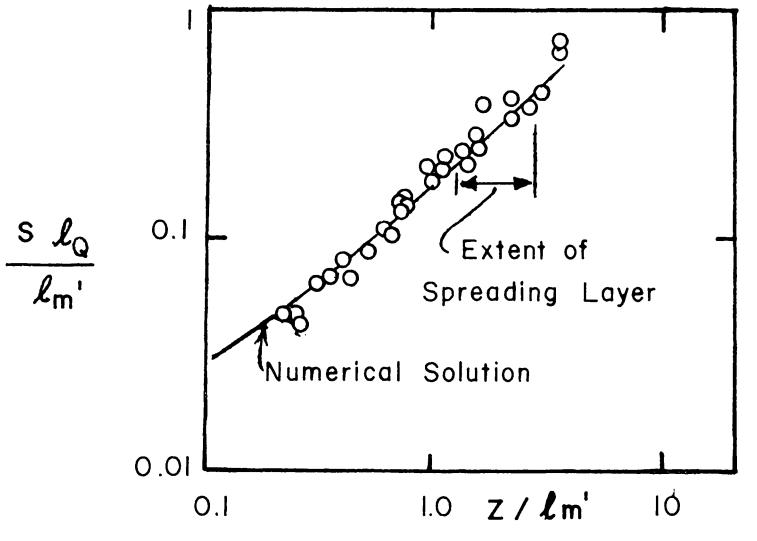

Figure 1-5. Predicted and Observed Dilutions Along Jet Axis (From Wong (1984)).

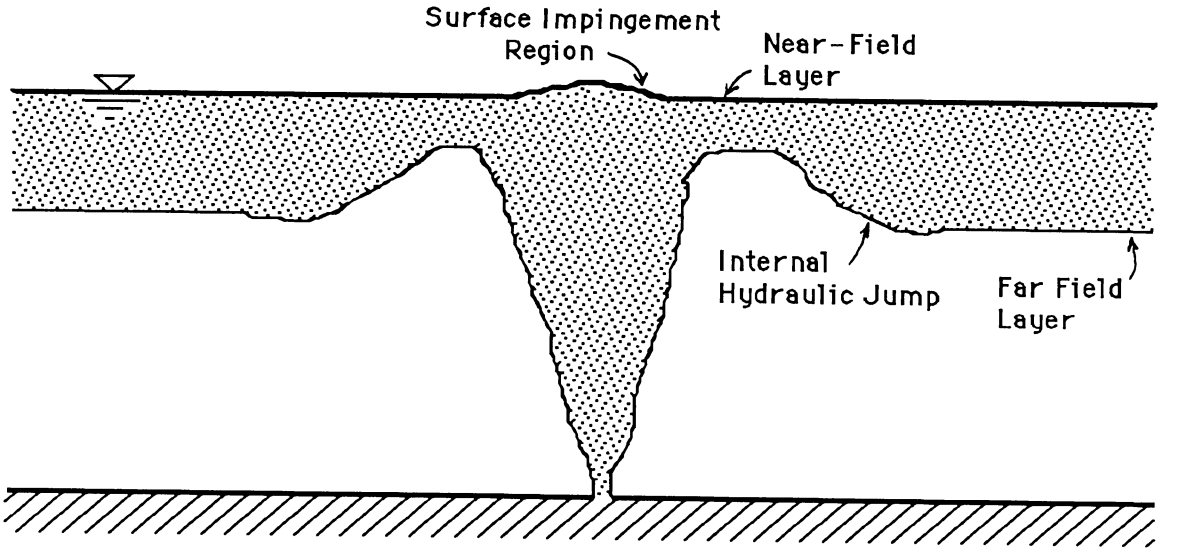

Figure 1-6. Schematic of Internal Hydraulic Jump From Surfacing Discharge.

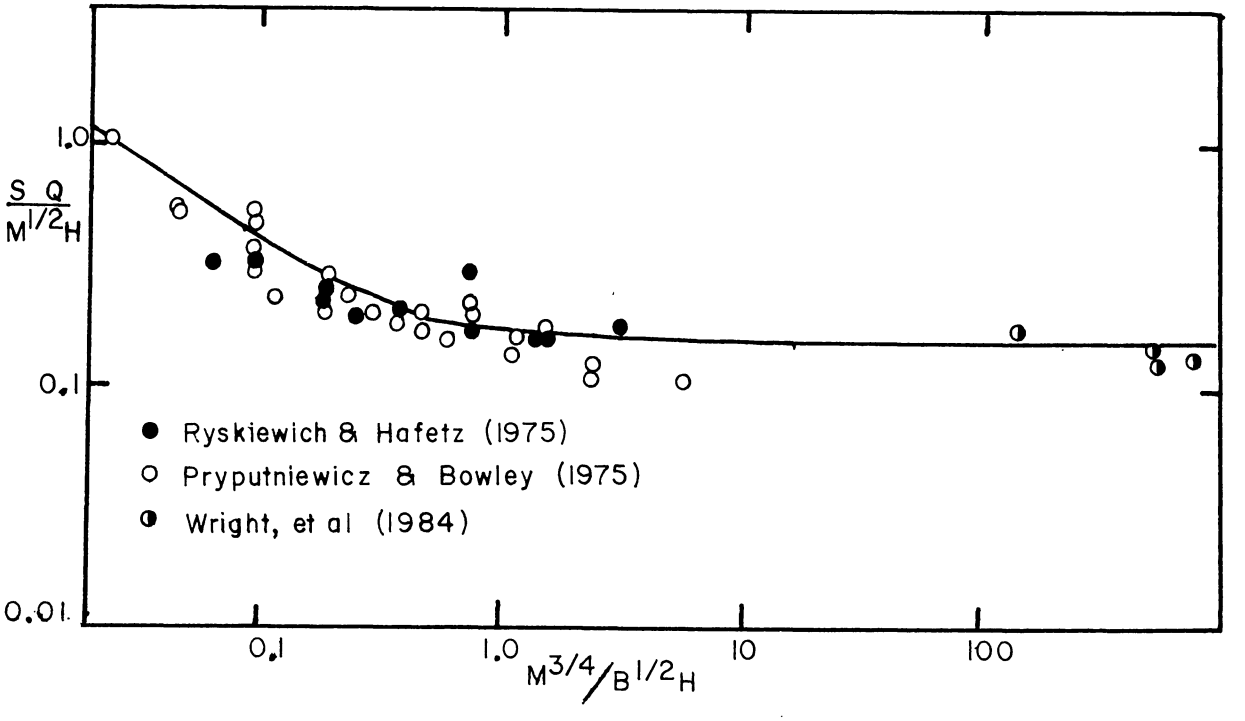

Figure 1-7. Minimum Surface Dilutions From Submerged Round Buoyant Jets.

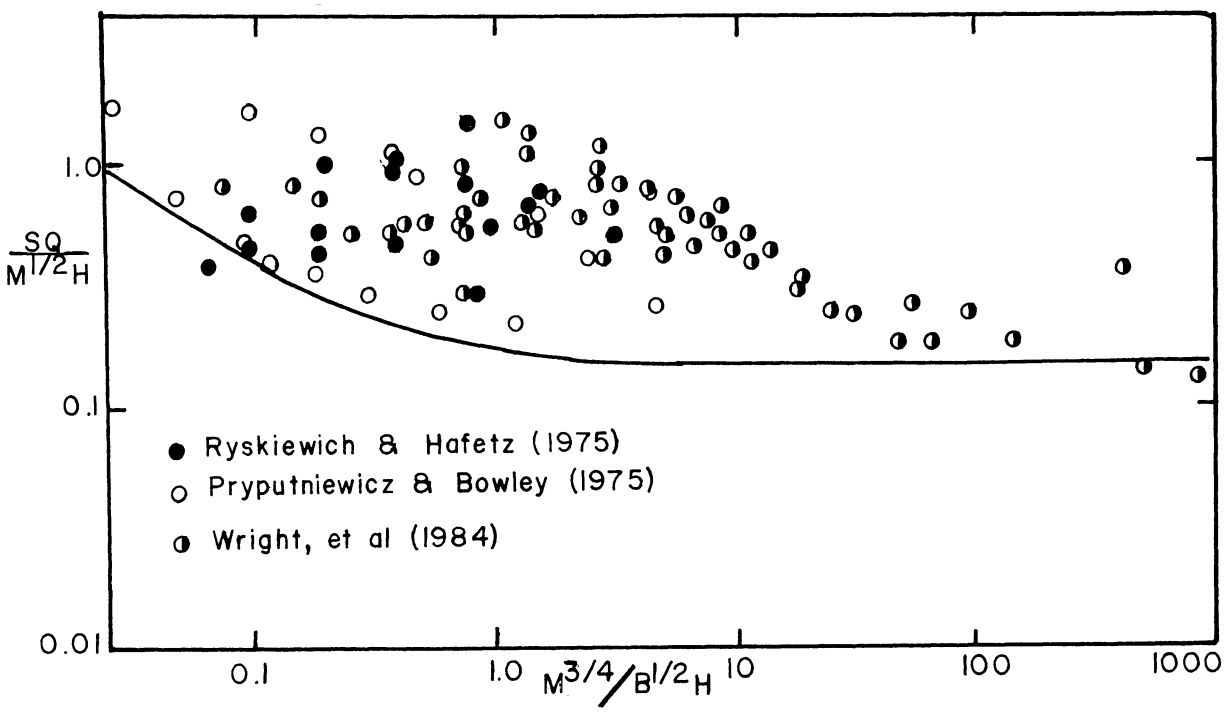

Figure 1-8. Surface Dilutions Three Water Depths Away From Submerged Round Buoyant Jet.

et al tend to follow a unique curve. This can be explained by considering that the total water depth and not the distance from the source to the surface is important in the additional mixing that occurs within the horizontal flow; therefore the experiments with the source at a variable position within the vertical column do not represent a unique set of experimental conditions due to the additional variable.

It can be concluded that either of the above methods appears to underestimate the total amount of mixing occurring between the jet source and a position within the gravitational collapse layer (henceforth referred to as "near-field" mixing) in certain circumstances and raises questions regarding the general applicability of the proposed analyses. It is known from previous studies, e.g. Roberts (1977), that the impinging plume does create a relatively thin surface layer which then expands to a greater thickness. There have been several studies on impinging jets (Rajaratnam, 1976 or Looney and Walsh, 1984 provide a good review) and it would appear that the method of Jirka and Harleman (1979) provides a reasonable means of estimating this behavior. Therefore, the major discrepancies must arise in the subsequent behavior of the jet fluid as it spread laterally. Since it is clear from the data in Figs. 1-7 and 1-8 that additional mixing occurs in this flow, an analytical method that correctly describes this phenomenon must be utilized.

Since it appeared that the dynamics of this counterflowing surface buoyant jet was the major problem that needed to be resolved, this problem was selected as the focus for the particular research project. Although it would be useful to develop a methodology applicable for the general problem (i.e. axisymmetric or two-dimensional, stratified or unstratified), a decision was made to focus on a particular aspect of the problem due to the limited duration of the project. The experimental program was dictated in part by constraints on the availability of laboratory apparatus and facilities, and was guided by a desire to examine the various aspects of the general problem that appeared most unresolved by existing data bases. Ultimately, a decision was made to concentrate on the two dimensional unstratified ambient fluid problem. However, it is expected that the proposed framework is sufficiently general to be capable of being extended to the other cases, although it is recognized that there may be important qualitative differences among them. Some of these differences will be referred to at appropriate places within the text. These additional cases are considered as directions for further research.

In the following chapter, the primary elements of the theoretical aspects of the problem are discussed. In Chapter 3, an overview of the experimental investigation is presented and a description of the laboratory apparatus is provided. The details of the experiments, the nature of the experimental results and a preliminary interpretation of some of them is provided in Chapter 4. Appendix A provides additional description of the data and methods of storage on magnetic tape.

CHAPTER 2
THEORETICAL ANALYSIS

Introduction

This chapter contains a discussion of the theoretical framework on which the initial data interpretation will be based. Although the data analysis is incomplete at the time of the report preparation, it has been observed that some of the theoretical details within this chapter are inconsistent with the experimental observations. These are discussed in more detail in Chapter 4, and suggestions for alternative analytical approaches are provided. With this in mind, what follows is an attempt to synthesize the basic elements of several different analyses into a format that is suitable for the description of the general problem. At the end of the chapter, this approach is applied to the example of a submerged two-dimensional plume and the predictions are compared against existing data. Also, some of the implications of the analysis with respect to the relationship between laboratory investigations and prototype applications is discussed. Finally, possible relationships between the behavior predicted herein and that for different flow configurations (i.e. radially symmetric discharges and/or with internal stratification) are discussed.

For the purposes of this development, the notation in the flow system indicated in Fig. 2-1 will be maintained. It is presumed that the flow can be separated into distinct layers, although in practice, this distinction may not be so easy to make. For most of the analyses, the layers are considered to have uniform density and velocity profiles, although some sort of continuous velocity and density distributions such as indicated in the sketch are actually observed. However, a consistent formulation can deal with most of the difficulties posed by this and the additional details are not important to developing a first understanding of the methodology. More attention may have to be paid to the exact definitions of the layer thicknesses in the final analyses. In the following discussion, the flow depth H is subdivided into a primary layer denoted with a subscript 1 and and secondary layer with subscript 2 as shown. The distinction between primary and secondary (or jet and external) flows is developed more completely below. The Boussinesq assumption is made from the outset so that situations with a buoyant surface flow or a dense underflow can be viewed as functionally equivalent. The theoretical development focuses on the dense underflow problem because it happens to be the experimental configuration. Later however, the example of the flow in a buoyant surface layer is considered. The duality of these flows is well accepted in the literature and many experimental investigations make use of this to develop more convenient experimental systems (e.g. Wright (1977), or Wright, et al (1981,1983)).

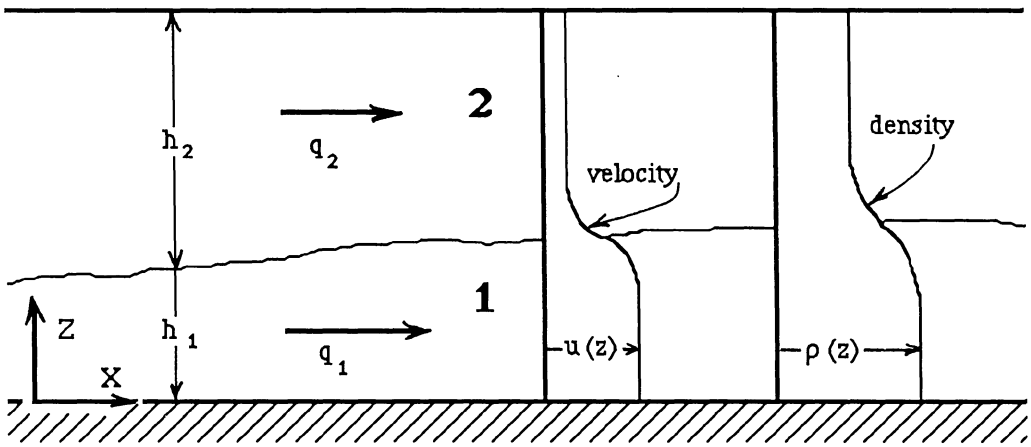

Figure 2-1. Schematic of General Flow System.

Stability Considerations

When the nature of turbulent mixing processes are considered, some important distinctions need to be made with respect to the generation of the turbulence. The phenomenon of most interest to this investigation is the turbulence generated by the shear between the two layers rather than turbulence due to bottom shear even though both are present in the experimental system. For the purposes of the analyses, the presence of the bottom shear is ignored although its effect on the interfacial processes is discussed below. The behavior of the flow at the interface can be regarded in two entirely different ways, and both are important. The first relates to the propagation of long internal waves at the interface while the second considers the stability of interfacial disturbances.

Long Wave Propagation

While this is not strictly a stability problem, it is discussed as a related concept. Long wave behavior at the interface can be regarded as an extension of free surface wave phenomena to the two-layer system. When each layer occupies a semi-infinite region, the only length scale describing the flow is the wavelength, Turner (1973), and the wave motion can be shown to decrease in amplitude with vertical distance from the interface. At the other limit, both layer depths are sufficiently small that the fluid velocities may be considered uniform over the entire layer thicknesses, a situation that is assumed to hold for the problems described herein. For this case, it can be shown, Schijf and Schönfeld (1953), that the propagation speed of long internal waves is given by

$$c_i = \frac{q_1 h_2^2 + q_2 h_1^2}{H\, h_1 h_2} \pm \sqrt{\frac{h_1 h_2}{H^2}\left\{g'H - \left(\frac{q_1}{h_1} - \frac{q_2}{h_2}\right)^2\right\}} \qquad 2\text{-}1$$

where q_1 and q_2 are the volume fluxes in the primary and secondary layers, respectively, and h_1 and h_2 are the corresponding layer thicknesses. H is the total depth and g' is the reduced gravitational acceleration $g' = g\,\Delta\rho/\rho_o$, where g is the gravitational acceleration, $\Delta\rho$ is the density difference across the interface and ρ_o is a reference density. When at least one of the disturbance velocities c_i is zero, the wave propagation is blocked in a particular flow direction. This critical flow state can be obtained by rearrangement of Eq. 2-1 to yield

$$\frac{q_1^2}{g'h_1^3} + \frac{q_2^2}{g'h_2^3} = \mathbf{F_1}^2 + \mathbf{F_2}^2 = 1 \qquad 2\text{-}2$$

where the layer Froude numbers $\mathbf{F_1}$ and $\mathbf{F_2}$ are defined in this relation. Eq. 2-2 is analogous to the critical state for free surface flow if only one layer is considered and can also be derived from a minimum energy principle. The wave speed in Eq. 2-1 with the negative sign describes a distinction between two important types of flow behavior. For subcritical flow ($\mathbf{F_1}^2 + \mathbf{F_2}^2 < 1$), and flow only in layer 1, disturbances may propagate upstream against the bulk flow, while for supercritical flow ($\mathbf{F_1}^2 + \mathbf{F_2}^2 > 1$), all waves will be swept downstream with most of the conventional connotations associated with free surface flow, Henderson (1966). When both layers are in motion, the situation is conceptually similar if one utilizes a frame of reference that brings the second layer to rest. If the upper layer flows in the reverse direction, upstream wave propagation is blocked at the internally critical state, only if $q_1 h_2^2 > q_2 h_1^2$; otherwise, it is the positive characteristic that is blocked from propagation. There is a special case where both characteristics will be blocked, e.g. if $h_1 = h_2$ and $q_1 = q_2$.

For the purpose of this study, only initially supercritical flows (i.e. at a source or discharge point) are considered. The primary layer is considered to be the layer with the largest Froude number. An important difference between the two layer system and single layer flows is that waves propagating along the interface between two miscible fluids may involve turbulent mixing across the interface, depending upon the nature of the disturbances. This implies that a source with velocity discontinuity (compared to the secondary layer) will generate disturbances due to the vorticity concentration at the interface and these will be propagated downstream. Conventional analyses for surface buoyant jets, e.g. Engelund (1976), are applied only for supercritical flows and indicate a reduction of the Froude number within the primary layer due to the turbulent mixing. The notion that Wilkinson and Wood (1971) applied to this problem is to argue that the Froude number can only decrease to a value of 1 due to mixing since the occurrence of a cross-section with this state represents a blocked condition with

respect to internal waves. Although downstream controls (e.g. geometry changes in the channel) can cause the occurrence of a subcritical flow, an initally supercritical layer will exchange momentum with the secondary layer until an internally critical state is reached in the absence of other influences.

Interfacial Stability

As mentioned above, the discussion of internal wave propagation is not necessarily related to the problem of turbulent mixing (due to either diffusion or entrainment) across the interface. For example, internal waves can propagate along the interface without breaking and no mixing will occur if the effect of molecular diffusion is neglected. Therefore, separate criteria have to be developed to describe the stability of the interface to mixing. The main theoretical focus in the past has been on the stability to inviscid disturbances in shear layers. The shear layer is a somewhat idealized flow with no spatial variations of mean velocity along the interface, i.e. two masses of fluid are uniformly set in motion relative to each other. Although there should be a clear distinction from the spatially varying mixing layers discussed in this study, this distinction is generally not made. Turner (1973) reviews some of the results of linear stability theory. The stability to small amplitude disturbances can be described in terms of a gradient Richardson number **R**:

$$\mathbf{R} = -\frac{g}{\rho_o}\frac{d\rho}{dz}\Big/\left(\frac{du}{dz}\right)^2 \qquad 2\text{-}3$$

where the vertical density and velocity gradients are defined locally. One can also define a flux Richardson number based upon the turbulent fluxes of buoyancy and momentum and a bulk Richardson number $\mathbf{R}_o = g'L/U^2$ where L and U are characteristic length and velocity scales, respectively, of the bulk flow. $\mathbf{R}_o$ is a form of inverse Froude number and therefore can be related to the long wave propagation problem, at least when there is flow only in a single layer. Therefore, in order to relate interfacial stability and wave propagation, some relationship between **R** and $\mathbf{R}_o$ must be specified.

The linear stability analysis cannot be formulated without specification of velocity and density profiles and usually some assumption is made as to their form. However, in general, the results are that the interface is stable to the growth of inviscid Kelvin-Helmholtz instabilities provided that **R** is greater than a value of approximately 1/4, an oft-quoted number. The stability calculations depend somewhat on the velocity and density profiles so this should be regarded as an approximate criterion, that is adequate for purposes of discussion for the shear layer.

A more serious problem is posed when the flow is not of the shear layer type as is the case in most experiments which are of the mixing layer or spatially evolving type. Generally, it is assumed that the same stability criterion is valid. The idea that is implied by the analysis, especially clear when viewed

as a turbulent energy balance is that there is a local balance between shear production and buoyant damping at some critical Richardson number such that turbulent motions are not amplified. This concept is only valid within the context of a local equilibrium argument. Long (1977) points out that **R** will be infinite for the case of two layers at rest and turbulence generated by another mechanism such as stirring. Gartrell (1979,1980) demonstrated that interfacial values of **R** can become much larger than 1/4 when the mixing is due to turbulence generated by boundary shear which then propagates to the interface. Nevertheless, he also showed that mixing is effectively damped for $\mathbf{R} > 1/4$ provided that the advection of turbulent kinetic energy from the boundary is unimportant in the turbulent energy balance. In the case of a mixing layer, the turbulent energy is advected from upstream, so this may be viewed as a local nonequilibrium process such that mixing still occurs for $\mathbf{R} > 1/4$. However, Chu and Baddour (1984) show that the critical **R** for damping of turbulent jet mixing occurs for a value on the order of 1/4. However, this still admits the possibility that within the jet mixing region, Richardson numbers in excess of 1/4 are possible, i.e. that velocity and density profiles change with distance in such as way as to allow $\mathbf{R} > 1/4$ before the collapse of the turbulence is complete. Jirka (1982) explicitly allows such a possibility in his model formulation.

Since many analyses are formulated in terms of buoyant jet theory, e.g. Chu and Baddour (1984), or related approaches, Ellison and Turner (1959), a further step is required to relate the stability criterion through the gradient Richardson number to a measure of the bulk or one-dimensional properties of the flow. This, of course, assumes a unique relationship between **R** and a suitably defined $\mathbf{R}_0$. However, it is noted that bulk Richardson numbers based upon average flow variables are found to have a magnitude of order 1 at the stability limit for several different flows. A broad extrapolation is thus that supercritical flows (low $\mathbf{R}_0$) are unstable to interfacial mixing, while subcritical flows (high $\mathbf{R}_0$) are stable. This is not to be interpreted as a precise argument, since, for example, at a source where there is a velocity discontinuity, the bulk Richardson number could have any value while **R** would be infinite and some initial mixing will occur, although it may be quickly damped in the downstream direction.

The analysis of Abraham, et al (1979) is also worth mentioning in this regard. They assume that the velocity and density profiles are linear across the interface and then can compute an exact relationship between the gradient and bulk Richardson numbers. Although the details of their analysis may not be precise due to the assumed profiles, they indicate that most wavelengths of disturbances will be amplified for supercritical flows. In addition, they indicate that instabilities in subcritical flows will result only in a rearrangement of the density and velocity profiles such that stability can be achieved without complete mixing over the layer thicknesses.

The above discussion has two implications. First of all, if one wishes to simulate the complete flow field numerically, such as with the methods described by Rodi (1980), then the assumption of a unique critical **R** can be questioned. It is unclear whether turbulence models based upon a local

equilibrium concept can ever be as general as required to describe the buoyant flows of interest in this investigation. Secondly, if a theory which only considers mean flow (one dimensional) variables is used, then a relationship between the bulk flow (through $\mathbf{R}_0$) and the stability (through $\mathbf{R}$ or a flux Richardson number) needs to be developed. If one makes similarity assumptions for velocity and density profiles as in the integral analyses, this can be performed in principle, but begs the fundamental questions raised above. The idea proposed by Ellison and Turner (1959) that there is a unique entrainment versus $\mathbf{R}_0$ relation for a broad class of turbulent flows is highly suspect, although perhaps sufficiently accurate for engineering purposes. The essential point to be made in the next section is that the interface may well adjust to the constraints of the mean flow rather than the reverse situation so that while this concept of a critical $\mathbf{R}$ or $\mathbf{R}_0$ is not only difficult to specify, it is also unnecessary.

Mixing Between Layers

Introduction

Given the general arguments presented in the previous section, the problem of mixing between two layers with supercritical flow is to be considered. This development is subdivided further for purposes of clarity in the presentation. This section discusses the nature of the mixing process in the absence of any downstream influence, while the next section considers the nature of different downstream controls. A generalized analysis requires the combination of the two separate components.

There have been numerous studies on the mass and momentum exchange between two fluids flowing horizontally with differences in density and velocity. There are many theoretical approaches that have been developed that could be used to describe the general phenomenon. When both fluid layers have considerable depth, the problem is analyzed as a mixing layer such as considered by Champagne, et al (1976). The only length scale for this problem is distance from the source and the total flow depth does not enter the analysis. If one of the fluid layers has a relatively small thickness so that its flow is supercritical with respect to the propagation velocity of disturbances along the interface, the problem is usually considered as a horizontal buoyant jet such as described by Tamai, et al (1969) or Chu and Baddour (1984). The integral models solve a system of first order ordinary differental equations obtained by integrating appropriate continuity, momentum, and energy equations over the vertical and making suitable similarity assumptions to describe velocity and density profiles. It is not generally possible to include the dynamics of the flow in the secondary layer in these formulations. For the buoyant surface jet, the solution encounters a singularity in the equations when a local jet Froude number is of order 1 (depending upon the exact definition of the Froude number) and the solution breaks down, e.g. Stolzenbach and Harleman (1973). This condition is basically analogous with the attainment of the internally critical state if the flow in the secondary layer is ignored. Buoyant jet analyses require, in addition to the profile assumptions, an expression for the entrainment of ambient

fluid by the jet. The role of buoyancy in reducing the entrainment rates has long been recognized and formulations such as those by Stolzenbach and Harleman (1973) or Jirka (1982) explicitly include this effect in the entrainment relation.

Ellison and Turner (1959) take a slightly more general approach to the same situation so that they can also describe the related problem of the dense flow down a sloping channel. Their development describes the entrainment as a function of the bulk flow Richardson number and a similar decrease in entrainment due to the stabilizing effect of buoyancy is found in their experimental observations. The major difference in their formulation is in its application to dense flow down slopes where the flow attains some sort of uniform flow state in rough analogy to the single layer open channel flow problem. However, the uniform state does not necessarily correspond to constant layer thickness and velocity since a nonzero entrainment rate will result in increases in the lower layer volume flux.

From a basically different point of view, Yih and Guha (1955) ignore the mass exchange due to entrainment and develop an analysis for an internal hydraulic jump. Analyses by Hayakawa (1970), Jirka and Harleman (1979) and others represent applications of this analysis to different flow systems. A result of the assumptions employed (specifying the pressure distribution along the face of the jump and that the fluids are immiscible) is that specification of a downstream control is not required to complete this analysis. This is opposed to the situation for a conventional free surface hydraulic jump in a single layer system (i.e. free surface flow) where the downstream control is a necessary component of the analysis. In fact, all of the above analyses for mixing layers and surface jets presume only upstream control on the mixing process. While this is analytically convenient, there are logical reasons to question the validity of this concept. For example, the analysis by Yih and Guha predicts the flow to pass from a supercritical to a subcritical state, which permits internal disturbances from the downstream region to propagate upstream and influence the nature of the jump itself. There are certain circumstances in which this theoretical approach may be reasonably valid, but, as Wood and Simpson (1984) indicate, it is not general enough to describe all possible ranges of flow behavior.

An analysis proposed by Wilkinson and Wood (1971) directly includes a downstream control in the formulation of what they refer to as a density jump. The density jump involves entrainment into the supercritical layer; however specification of entrainment rates or pressure distributions in the mixing zone is not required, in contrast to the other methods. This type of analysis makes the classification by Rajaratnam and Subramanyan (1985) of surface discharges into buoyant surface jets and internal hydraulic jumps somewhat superfluous since they are only the two extremes in a continuum of flow behavior. While Wilkinson and Wood's original analysis was for a single flowing layer and an infinitely deep stagnant layer, later studies (e.g. Stefan and Hayakawa (1972), Bewick (1974), Baddour and Abbink (1983) and Wood and Simpson (1984)) extend this to more general cases of two flowing layers and/or finite depth.

The simplicity of this method makes it appealing, although it only provides predictions regarding the limiting state of the flow, i.e. downstream from the mixing zone, whereas the jet or mixing layer

theories also provide predictions through the mixing region. However, if attention is restricted to the case of a discharge into an otherwise stagnant fluid, a limitation of these latter analyses becomes apparent. All integral analyses are formulated on the basis of the boundary layer approximations, the most important of which in this regard are the assumptions of a prevailing flow direction and the lack of coupling between upstream and downstream flows through the pressure gradient. The resulting equations are parabolic in nature and therefore do not admit the possibility of a recirculation in the overall flow field. Considering the situation sketched in Fig. 2-2, the entrainment inflow into the mixing region must come from downstream in order to satisfy continuity. This counterflow violates the assumptions inherent in the boundary layer approximations and will be negligible only when the secondary layer depth becomes large; therefore, the buoyant jet theories (or Ellison and Turner's approach) should only be valid in that limit. However, from the discussion in Chapter 1, it has been shown that layer thicknesses are a significant fraction of the entire depth for the submerged discharge problems of interest. This indicates that the buoyant jet and other theories are applicable only for circumstances which are not generally encountered in most environmental applications.

When viewed in the context of Wilkinson and Wood's original theory, it may be shown that in the absence of any other downstream control, the total depth (due to the entrainment counterflow) serves as a control on the mixing due to shear. As indicated by Stefan and Hayakawa (1972), the large momentum in a thin layer of high velocity counterflow affects the total momentum balance so as to result in significant decreases in entrainment. Therefore, the problem of constraints on total jet mixing due to a limitation in the total depth is important as well as the influence of other downstream controls.

Induced Counterflow

Consider the situation indicated in Fig. 2-2 with the more dense underflow and a free surface. Ambient entrainment flow is not allowed to come from upstream of the source in analogy to the submerged discharge problem in Fig. 1-2a where the symmetry of the flow away from the source results in a similar configuration. In the analysis formulated by Wilkinson and Wood and extended by Bewick (1974) and others, the following assumptions are required: 1) Hydrostatic pressures at the source and downstream from the mixing zone; 2) Energy conserving flow in the external fluid; and 3) the Boussinesq approximation of small density differences. The analysis is only valid when the discharge is supercritical with respect to internal disturbances. A momentum balance is obtained (neglecting turbulent transport and bottom friction) over the depth at the two sections:

$$\frac{q_o^2}{b_o} + \frac{1}{2} g'_o b_o^2 + \frac{1}{2} g H_A^2 = \int_u^{H_B} g' z \, dz + \int_u^{H_B} u^2 \, dz + \frac{1}{2} g H_B^2 \qquad 2\text{-}4$$

where the first two terms define the total source flow force M_o with discharge q_o, slot opening b_o, and

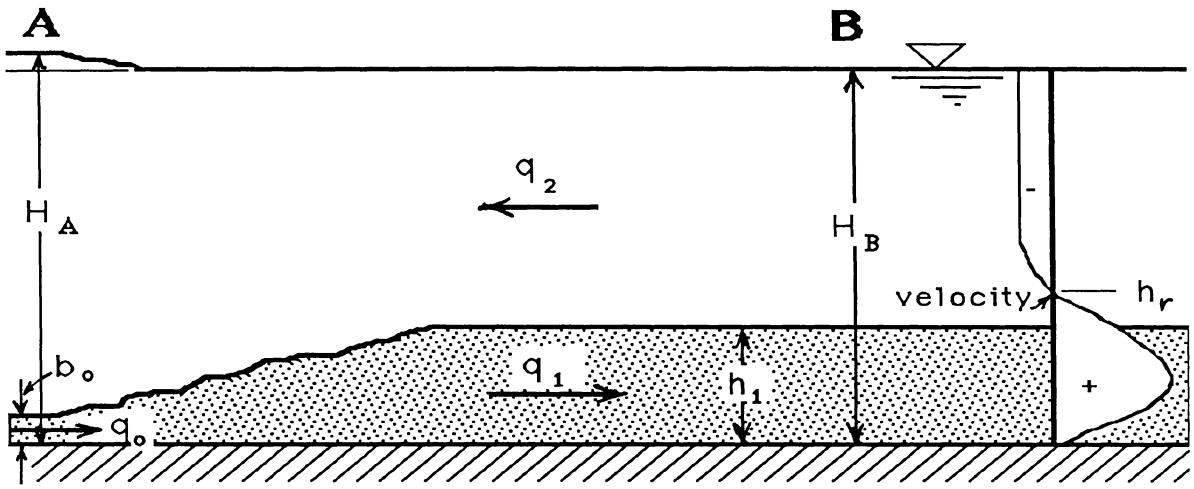

Figure 2-2. Definition Sketch For Counterflowing Density Jump.

effective gravity g'_o. H_A and H_B are the total depths at the respective sections. In Eq. 2-4, the effects of velocity and density profile variations are included explicitly through the pressure and momentum flux integrals at section B. Following the approach by Bühler (1983), the thickness and density scales are determined from the first two moments of the density distribution:

$$g'_1 h_1 = \int_0^{H_B} g' \, dz \qquad 2\text{-}5$$

$$\frac{g'_1 h_1^2}{2} = \int_0^{H_B} g' z \, dz \qquad 2\text{-}6$$

For the purposes of this theoretical development, these may be considered to be merely a set of consistent scales to describe the density distribution. However, these are also convenient for the comparison of experimental results since most of the data is in the form of density profiles. If the flow at the downstream section is resolved into forward and reverse components, Eq. 2-4 becomes

$$M_o + \frac{\gamma_3 q_2^2 H}{2(H-h_1)^2} = \frac{\gamma_1 q_1^2}{h_1} + \frac{\gamma_2 q_2^2}{H-h_1} + \frac{1}{2} g'_1 h_1^2 \qquad 2\text{-}7$$

where the distinction between H_A and H_B has been dropped in the geometry relations, q_1 and q_2 represent the volume fluxes in the respective layers and the momentum correction factors γ_1 and γ_2 are defined by

$$\frac{\gamma_1 q_1^2}{h_1} = \int_0^{h_r} u^2 \, dz \qquad 2\text{-}8$$

$$\frac{\gamma_2 q_2^2}{H-h_1} = \int_{h_r}^{H_B} u^2 \, dz \qquad 2\text{-}9$$

h_r represents the elevation of the point of velocity reversal. The last term on the left hand side of Eq. 2-7 arises from energy conservation along the free surface and represents an additional pressure force due to the stagnation pressure above the discharge point. The quantity γ_3 is an energy correction factor to describe the kinetic energy in the return flow at section B. Fluid continuity implies

$$q_1 = q_o + q_2 \qquad 2\text{-}10$$

The conservation of the flux of density difference between the two sections yields

$$B_o = q_o g'_o = \int_0^{H_B} u \, g' \, dz = \gamma_4 q_1 g'_1 \qquad 2\text{-}11$$

where γ_4 is an additional scale factor as defined in the above expression. This latter expression could also be used to defined a characteristic velocity as did Bühler, but the use of volume fluxes in the equations will be retained as a matter of consistency of presentation.

Closure to the above system of equations is achieved by specifying the downstream control. As previously discussed, Wilkinson and Wood's approach assumes that in the absence of other controls, the mixing proceeds until the condition for the jump to be stationary is reached, namely that the flow is internally critical. For the two layer system, this is expressed from Eq. 2-2 as

$$\frac{q_1^2}{g'_1 h_1^3} + \frac{q_2^2}{g'_1 (H-h_1)^3} = \text{constant } (\gamma_5) \qquad 2\text{-}12$$

where γ_5 is now only of order unity and depends upon the layer definitions and the density and velocity profiles. In fact, since Eq. 2-12 arises from Eq. 2-1 which has assumed uniform velocity and density profiles, it should be expressed in terms of the wave propagation characteristics in a continuously stratified fluid. Such a level of complexity is not consistent with the other approximations in the analysis, however. Eqs. 2-7 and 2-10 through 2-12 can be manipulated and nondimensionalized to yield the following two nonlinear equations, with $S = q_1/q_o$ and $\eta = h_1/H$:

$$\frac{H M_o}{q_o^2} = \frac{\gamma_1 S^2}{\eta} + \frac{\gamma_2 (S-1)^2}{1-\eta} - \frac{\gamma_3 (S-1)^2}{2(1-\eta)^2} + \frac{B_o H^3 \eta^2}{2\gamma_4 q_o^3 S} \qquad 2\text{-}13$$

$$\left[\frac{S}{\eta}\right]^3 + \frac{S(S-1)^2}{(1-\eta)^3} = \frac{\gamma_5 B_o H^3}{\gamma_4 q_o^3} \qquad 2\text{-}14$$

These equations cannot be solved explicitly except in the limit as $H \rightarrow \infty$. For this case, $q_2/(H-h_1) \rightarrow 0$ with the following solutions for S and η:

$$\frac{S q_o B_o^{1/3}}{M_o} = \left[\gamma_1 (\gamma_5/\gamma_4)^{1/3} + \frac{1}{2\gamma_4}(\gamma_5/\gamma_4)^{-2/3}\right]^{-1} \qquad 2\text{-}15$$

$$\frac{\eta B_o^{2/3} H}{M_o} = \left[\gamma_1 (\gamma_5/\gamma_4)^{2/3} + \frac{(\gamma_5/\gamma_4)^{-1/3}}{2\gamma_4}\right]^{-1} \qquad 2\text{-}16$$

If all the integral constants are assumed to be unity, the right hand side of both expressions reduces to a value of 0.67. The experiments reported by Chu and Baddour (1984) show the constant in Eq. 2-15 to be about 0.62 for both what they term buoyant surface jets and mixing layers. These definitions correspond to differences in observed mixing behavior between low and high (but still supercritical) source Froude numbers. The analysis presented above distinguishes between the two cases only if the integral constants are different, which they were found to be. The experimental value of the constant in Eq. 2-16 was found to be about 0.41 for jets and somewhat greater for mixing layers. It is also interesting to note that Chu and Baddour use different scaling relations for their results on mixing layers and a great deal of scatter is found in their results. However, when scaled in the above form, their experimental results for mixing layers are more consistent.

In the more general situation of limited depth, the above equations are solved numerically to find roots that are physically admissable according to the constraints that

$$S \geq 1$$

$$0 \leq \eta \leq 1$$

and that the total energy in the flow cannot increase from A to B. This latter condition further constrains η to be greater than or equal to b_o/H. The influence of depth on the solution can be visualized for an arbitrary set of source conditions in the plot in Fig. 2-3. Although the layer thickness doesn't change significantly, the dramatic decrease in dilution as $\eta \rightarrow 1$ is clearly seen in this plot. The effect of the depth appears to be negligible when the layer thickness is less than about 30 percent of the depth indicating that buoyant jet theories may be applicable for this range of conditions. It can also be realized that there are certain combinations of source conditions in which no solution that satisfies

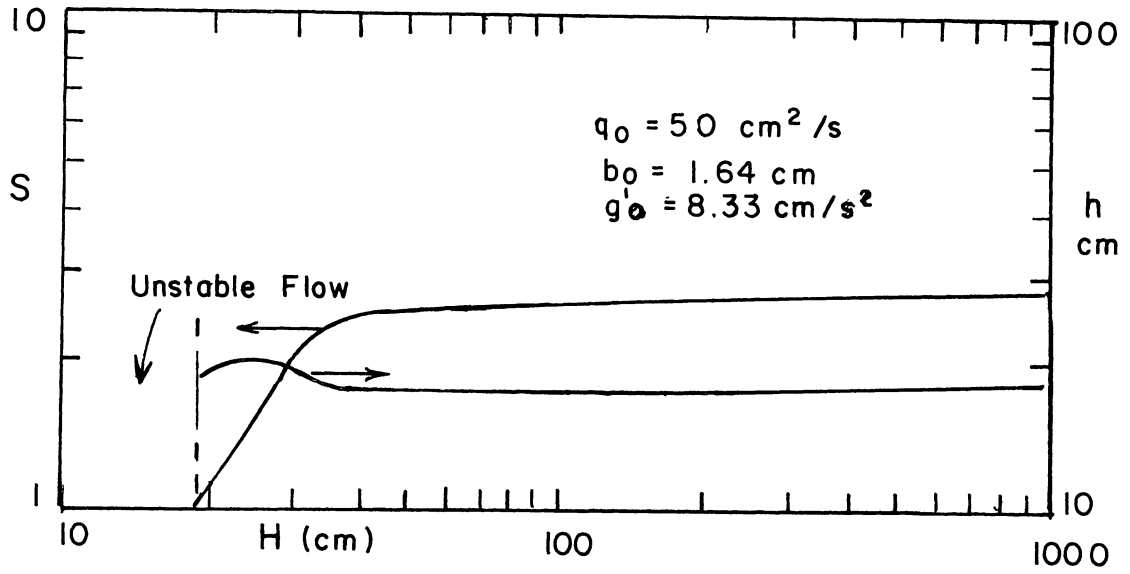

Figure 2-3. Predicted Variation of Dilution With Depth For Arbitrary Source Conditions.

Eqs. 2-13 and 2-14 along with the constraints. For these situations, Eq. 2-16 would predict the layer thickness to be greater than the total depth. Jirka and Harleman (1979) refer to this situation as "unstable flow" although their problem and theoretical approach are somewhat different. Baddour and Abbink (1983) suggest that the onset of the unstable condition can be predicted from the theory by taking the limit as $\eta \rightarrow 1$ and $S \rightarrow 1$. It is not clear how they actually accomplish this since there is only one source condition and the two equations to simultaneously satisfy. Inspection of the form of Eqs. 2-13 and 2-14 indicates a resolution to this question as the terms related to q_2 in the momentum equation, Eq. 2-13, vanish more rapidly than the one in the critical flow relation, Eq. 2-14. Numerical experimentation with the solution to these equations indicates that $\mathbf{F}_2^2$ can be quite significant even as the terms in the momentum equation vanish. Therefore the condition for onset of instability it determined by algeabraic manipulation of the momentum equation:

$$HM_o/q_o^2 = \gamma_1 + (B_o H^3)/(2\gamma_4 q_o^3) \qquad 2\text{-}17$$

or in terms of the basic source variables with $\gamma_i = 1.0$:

$$2\, q_o^2 = g'_o\, (H + b_o) H\, b_o \qquad 2\text{-}18$$

A clear distinction must be made between this unstable state and the occurrence of the "roller

region" described by Wilkinson and Wood and others in which there is recirculation of the dense fluid. They describe situations where the source mixing region is at least partially submerged by the downstream control, resulting in the recirculation of the discharge fluid with very little entrainment of external fluid in the recirculation zone. If the solutions to Eqs. 2-13 and 2-14 are compared to Eqs. 2-15 and 2-16, it can be shown that, for all other variables fixed, S increases with depth to its asymptotic limit as $H \rightarrow \infty$. Therefore, a decrease in H results in less entrainment of the external fluid. It can be visualized that this is accomplished by a recirculation of the dense fluid such that the total entrainment remains approximately the same, but with some of it being re-entrained primary layer fluid. Numerical solutions to Eqs. 2-13 and 2-14 indicate that when the solution for internally critical flow is achieved, the negative characteristic is blocked from upstream propagation at small values of h_1/H while it is the positive one that is blocked from downstream propagation at larger values of this parameter. From this result , it can be reasoned that at large relative layer thicknesses, there can be a "roller region" (as defined by Wilkinson and Wood, 1971) formed in which the discharged fluid is recirculated back into the mixing zone. The decrease in dilution can be explained physically by this phenomenon; the experiments that are described in Chapter 4 indicate that this is conceptually correct. Use of the "unstable" criterion herein refers only to conditions where the dense fluid occupies the entire depth over a region near the source. There is a special limiting case which can be found by examining the parameter $\mathbf{F}_*^2 = q_o^3/(B_o H^3)$, the form of which appears in Eqs. 2-13 and 2-14. In the special case of $\mathbf{F}_*^2 = 1$, this refers to a situation where the layer is uniformly mixed over the depth and

$$\mathbf{F}_*^2 = \mathbf{F}_1^2 = q_o^2/(g'_o H^3) = q_o^3/(B_o H^3) = 1 \qquad 2\text{-}19$$

The flow is thus internally critical with the layer extending over the entire depth and for $\mathbf{F}_*^2 > 1$, the only possible solution is the primary layer to extend over the entire depth with an unmixed discharge fluid; the overall momentum balance can only be satisfied by a decrease of H above the source as in a submerged hydraulic jump. It can be shown that the unstable condition will generally occur for much smaller values of $\mathbf{F}_*$, although the exact values depend on b_o/H through Eq. 2-17 or 2-18 . Therefore, the onset of unstable flow does not necessarily imply that no mixing will occur. This is consistent with the findings of Jirka and Harleman (1979) that indicate significant dilution in submerged discharges, even with unstable near fields.

Density Jump in a Coflowing Stream

Up to this point, the assumption has been that the flow in the external layer is imposed by the entrainment due to the supercritical discharge. In fact, this situation is only a specific case for the more general case of a flowing ambient fluid. Since a relatively comprehensive discussion has already been

given for the entrainment supplied from a counterflow, only the major differences between this and the flowing ambient fluid are discussed in detail. Wood and Simpson (1984) and Bewick (1974) provide most of the basis for this development.

Consider the situation sketched in Fig 2-4. The buoyancy flux and critical flow relations given by Eqs. 2-11 and 2-12 are unchanged for this situation. The continuity equation is more generally given as

$$U_A(H-b_o) + q_o - q_1 \pm q_2 = 0 \qquad 2\text{-}20$$

The negative sign on the upper layer flow rate q_2 represents the ordinary solution, but it is possible for the downstream flow to be reversed in certain circumstances, i.e. small U_A. The ambient flow is described in terms of the velocity U_A which is that above the source; otherwise all previous conventions remain the same. The momentum equation is

$$M_o + U_A^2(0.5H - b_o) = q_1^2/h_1 + q_2^2(0.5H - h_1)/(H-h_1)^2 + 0.5\, g'h_1^2 \qquad 2\text{-}21$$

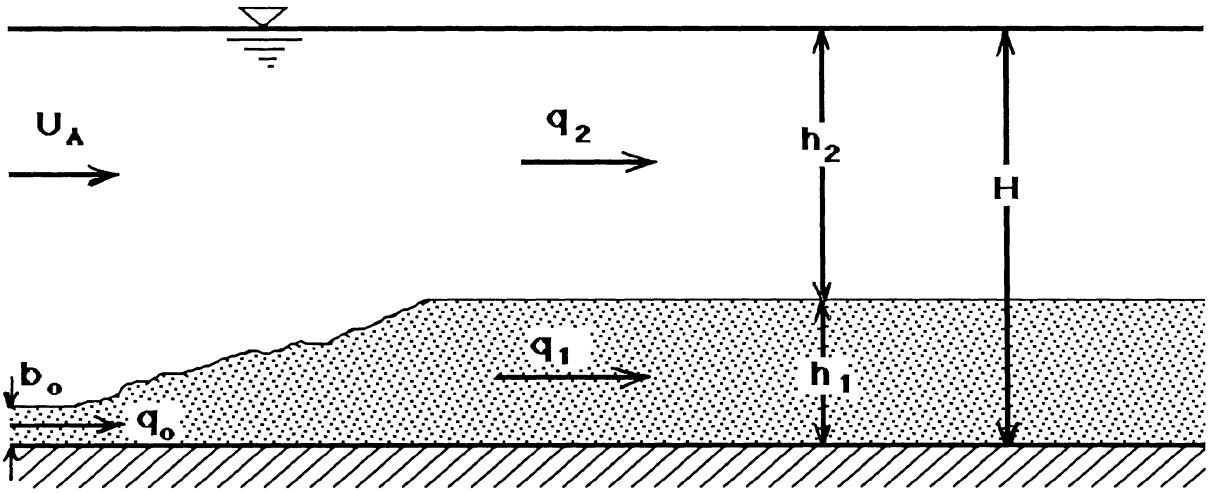

Figure 2-4. Definition Sketch For Density Jump in Coflowing Stream.

In these equations, no attempt has been made to include the integral factors such as given in Eq. 2-7 although they should be included in a more complete formulation. Their omission has made the inclusion of the energy conservation assumption for the external flow fairly direct. The solution to this system of four equations proceeds in a similar fashion to that discussed above.

A few comments regarding the nature of the solution are in order. Fig. 2-5 indicates the nature of the numerical solution as influenced by the ambient velocity. Again, an arbitrary set of conditions are used for this case with a single value of the depth and variable U_A. One can see that the entrainment of the secondary flow increases with ambient velocity up to a limit, after which it decreases. The same happens with respect to the layer thickness; this phenomena needs to be further considered to develop a more detailed description. The questions of stability are basically similar to those in the counterflowing system. The ultimate stability of the flow depends upon the parameter

$$\mathbf{F}_{**} = \frac{[q_o + U_A(H-b_o)]^3}{B_o H^3} \qquad 2\text{-}22$$

which is analogous to the parameter $\mathbf{F}_*$ and the criterion suggested in Eq. 2-19. When $\mathbf{F}_{**}$ is equal to 1, the entire layer will be uniformly mixed over the depth and the flow critical. This is conceptually equivalent to the criterion by Bühler (1974), Roberts (1977) and others who use this to describe the transition to what they refer to as forced entrainment or supercritical flow for submerged discharges.

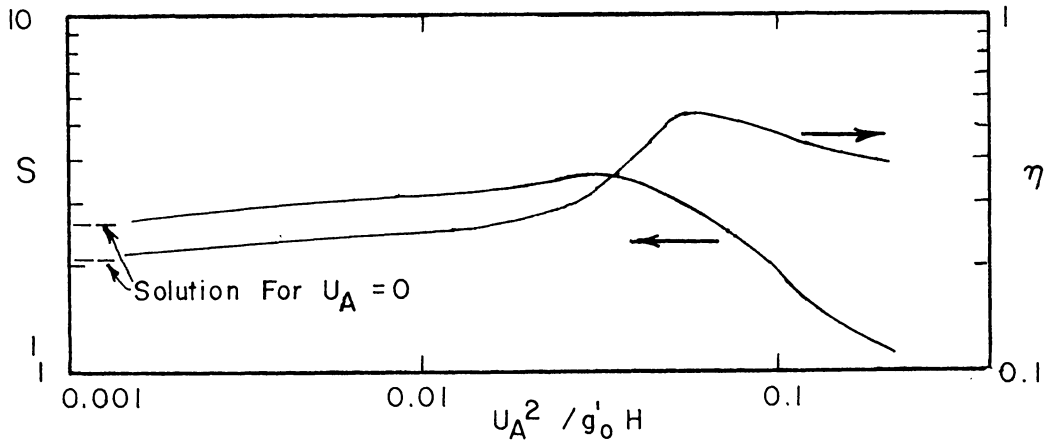

Figure 2-5. Predicted Influence of Ambient Velocity on Near Source Mixing.

Controls

There are a number of different phenomena that could be analyzed in this section. Rather than attempt an exhaustive treatment of the various possibilities, only those situations which are relevant to the particular experimental program will be discussed. From a more basic point of view, the issue of

the relationship to possible prototype applications is relevant. In practice, the issue of downstream control in prototype problems is very difficult to address because a whole host of influences, such as weak but nonzero ambient velocities, the finite length of a line source, and the loss of buoyancy due to heat loss may contribute to prototype applications because of the long distances over which the effect of a downstream control may be felt.

A more clearly defined situation occurs in most laboratory experiments. Generally speaking, two types of downstream control can be identified for the vast majority of experimental investigations. By far the most common is to perform an unsteady experiment in a facility of limited size. The implied assumption is that during the time that the flow is spreading away from the source region, the flow field is essentially steady near the source. In other experiments, such as Jirka and Harleman (1973), Wallace and Sheff (1984), and others, there is an experimental configuration in which the test channel expands into a larger facility. A steady flow will develop with a control at the expansion section for these types of experiments. Although this situation may be more difficult to relate to a prototype configuration, the advantage is that a truly steady flow can, in principle, be established.

Density Current Control

The following analysis represents a major extension of the ideas presented by Koh (1976,1983) coupled with the different near-source description from the previous section. The objective is to develop a closure relation to replace that given by the critical flow relation given in Eq. 2-12. In this regard, it is obvious that any flow control must represent a subcritical flow state, since the discharge will otherwise approach the critical flow state through turbulent mixing. Any control relation that represents a supercritical flow state cannot therefore serve as a control on the near-source mixing process even though it may describe a valid flow state.

The analysis developed by Benjamin (1969) is utilized for this purpose. A discussion of potential shortcomings of the basic model is reserved until later. Britter and Simpson (1978) and Simpson and Britter (1979,1980) have proposed modifications to the basic theory which may somewhat improve the agreement with experimental observations. However, the basic nature of the solution is not significantly altered and it is not clear that these additional analyses represent significant improvements in an understanding of the flow phenomena.

The theory developed by Benjamin was initially applied to the problem of an air cavity intruding into a fluid filled channel. However he extended it to the problem of a density current propagating into an otherwise stagnant fluid. In the present framework, it will be considered that there is a discharge q_o to the left (to facilitate extension to the present application and the experimental configuration) superimposed on the system. Fig. 2-6 indicates the flow system and the same basic assumptions as mentioned in the previous section are made; hydrostatic pressures, the Boussinesq assumption, and

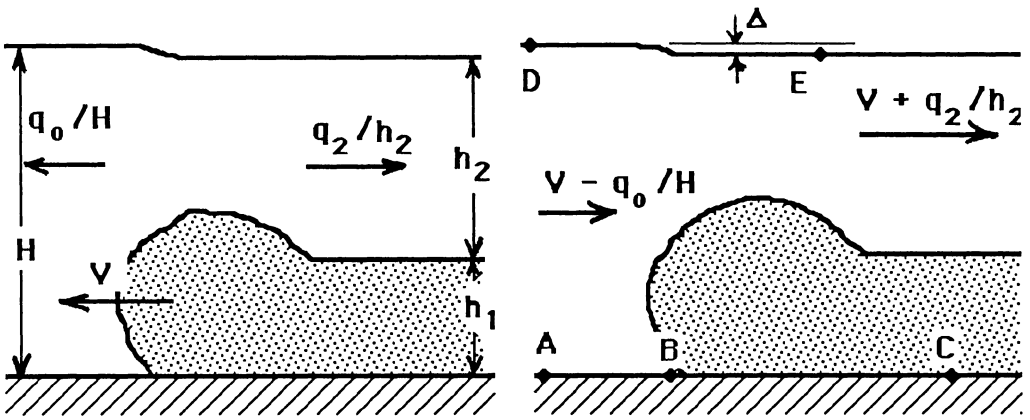

Figure 2-6. Definition Sketch For Density Current.

uniform density and velocity profiles. These latter approximations are employed without adjustment although a series of integral constants could be introduced into the equations below to account for nonuniform profiles.

The problem is formulated in a coordinate system moving with the head of the density current. It has been assumed that the free surface gravity waves propagate so fast compared to internal waves or the density current head that the flow is uniform with a velocity of q_o/H ahead of the density current, an assumption that is valid due to the free surface and internal waves scaling with the square root of g and g', respectively. Again, the effect of bottom friction is ignored. The inclusion of friction in the formulation results in the inability to maintain a steady flow within the density current as suggested by the analyses of Chen (1980) and others, although Kranenburg (1978) includes the effect of friction at the head in an approximate fashion. Assuming steady flow, the following equations are obtained:

Continuity

$$U_1 H = U_2 h_2 \qquad 2\text{-}23$$

Momentum

$$U_1^2 H + \frac{g H^2}{2} = \frac{g}{2}(h_1 + h_2)^2 + \frac{g'}{2} h_1^2 + U_2^2 h_2 \qquad 2\text{-}24$$

Energy A to B to C

$$\frac{\rho_o U_1^2}{2} + p_A = p_B = p_C \qquad 2\text{-}25$$

Energy D to E

$$\frac{U_1^2}{2} + g(\Delta - \delta) = \frac{U_2^2}{2} \qquad 2\text{-}26$$

Hydrostatics $p_A = \rho_o g H$ 2-27

$$p_C = \rho_o g (h_1+h_2) + \rho_o g' h_1 \quad 2\text{-}28$$

where $U_1 = V - q_o/H$ and $U_2 = V + q_2/h_2$ are the relative velocities in the respective layers and V is the propagation velocity of the density current. Δ represents the drop in the free surface level necessary to satisfy Eq. 2-24 with the energy loss δ behind the head of the density current. These equations, along with the geometrical relation $H = h_1 + h_2 + \Delta$ are insufficient to solve for the number of unknowns even if it were assumed that the reduced gravity g' is a known quantity. That is, there are an infinite number of depths that can satisfy the above equations, although Benjamin demonstrates that $\eta = h_1/H$ must be less than 0.5 to satisfy the constraint that energy cannot be gained from D to E. For layer thicknesses h_1 smaller than 0.5H, there are two conjugate states, i.e. depths that satisfy the equations with the same propagation speed, but with different amounts of energy dissipation. The particular depth $\eta = 0.347$ represents a single valued solution with the maximum amount of energy dissipation. Benjamin argued that it was not likely to find layer thicknesses greater than this value. However, Kranenburg (1978) argues that the flow discontinuity associated with the head can only be maintained when the flow behind the head and relative to it is subcritical or at most, critical. This critical flow condition can be shown to occur at $\eta = 0.347$. Greater layer thicknesses than this involve supercritical flow in the secondary layer and the inability to maintain a steep front to the density current. Therefore, Kranenburg argues that the maximum layer thickness possible is 0.347 H according to this analysis.

It is important for interpretation of experimental results to distinguish between the condition within the head itself and the layer somewhere behind. It is assumed that the energy loss is concentrated in a region between the head itself and the section with assumed constant conditions. Yuan (1984) argues that both conjugate depths of Benjamin's analysis occur with the greater of these representing the head thickness and the lesser is the layer thickness h_1. However, the basis for this conclusion is not clear since the head is in a region of possible nonhydrostatic pressures and therefore need not satisfy the basic equations as formulated. The results of Faust (1977,1981,1984) indicate head thicknesses greater than Kranenburg's limit of .347 H, but it is not clear from the discussion whether the thickness referred to is actually the head thickness or the steady layer thickness. A private communication with E.J. Plate indicates that the steady layer thickness was the quantity measured.

The nature of the above solution may be used to couple the density current with the near-source mixing region. For subcritical discharges ($q_o^2/g'_o b_o^3 < 1$), there should be little or no near-source mixing and the source values of q_o, g'_o, and b_o represent known conditions. If it is stated that $g' = g'_o$

$V = q_o/b_o$, and $h_1 = b_o$, the solution is overprescribed. Therefore, the only possible solution consistent with the no mixing hypothesis is to assume that the layer thickness adjusts to some value other than b_o such that Eqs. 2-23 through 2-28 can be satisified. Therefore g' and q_1 are known quantities with the unknown h_1. On the other hand, supercritical discharges entail some mixing and both g' and h_1 are not directly specified. Therefore, the system of equations remains unclosed even with the use of Eqs. 2-7 through 2-12. This dilemma can be partially resolved by further consideration of the nature of the solutions to the density current equations. The nondimensional solution for the velocity $U_1 = V - q_o/H$ from Benjamin and Kranenburg is

$$\frac{U_1^2}{g' h_1} = \frac{(1-\eta)(2-\eta)}{1+\eta} \qquad 2\text{-}29$$

For a specified source discharge, the Froude number $\mathbf{F_1}$ in a fixed coordinate system can be computed. In the limit as $\eta \rightarrow 0$ and $q_o/H \rightarrow 0$, (the great depth case), $\mathbf{F_1}^2 \rightarrow 2$ and the density current head is supercritical with respect to a fixed coordinate system. Therefore, disturbances from the head of the density current cannot propagate back to the source and the solution must be independent of the density current head. That is, the discharge mixes up to its internally critical state and then propagates in the form of a supercritical density current, i.e. the source mixing determines g' and q_1, but not the density current thickness. A fact that must be kept in mind is that the question of the internal flow state at the source and in the density current must be viewed in two different reference frames, moving with the head for the density current and in a fixed reference system for the near source mixing. One difficulty with this point of view is that it is not possible to satisfy the momentum balance between the density jump and the desnity current head; this dilemma can only be resolved by arguing that steady flow at the density current head cannot be maintained. In the discussion of the experimental results, more serious objections to this description of the flow arise.

In the more general case of finite total depths, the combined Froude number $\mathbf{F_1}^2 + \mathbf{F_2}^2$ can be computed from the solution in Eq. 2-29 and the continuity relationship. This information is presented graphically in Fig. 2-7 as a family of curves with the parameter $\mathbf{F''}^2 = q_o^2/g'H^3$ as the additional variable. This parameter is related to $\mathbf{F_*}^2$ described previously but not the same because g' is not generally equal to g'_o. It can be seen that the flow state changes from supercritical to subcritical at around 0.293H for the case for $\mathbf{F''}^2 = 0.0$ but does not at all for $\mathbf{F''}^2$ greater than about 0.005. This has a number of very interesting implications. First of all, for the no net throughflow case, the control

must shift from the source to the density current at around $\eta = 0.293$ (In this and further discussions, source control refers to the existence of an internally critical state at the end of the mixing zone). Within the narrow range of $0.293 < \eta < 0.50$, the solution must then be obtained by using the information in Fig. 2-7 to relate the Froude numbers and the relative depth. According to Kranenburg, once the limit of $\eta = 0.347$ is exceeded, the solution must be uniquely determined according to Eq. 2-29 with η set equal to the limit of 0.347. This equation can be manipulated to yield:

$$S(S/\eta - 1)^2 = \frac{B_o H^3 \eta (1-\eta)(2-\eta)}{q_o^3 \quad (1+\eta)} \qquad 2\text{-}30$$

which for the limiting value of $\eta = .347$ suggested by Kranenburg, yields the unique solution

$$S(S - \eta)^2 = B_o H^3/q_o^3 [\eta^3(1 - \eta)(2 - \eta)/(1 + \eta)] \quad \text{or} \quad S \approx 0.323 B_o^{1/3} H/q_o \qquad 2\text{-}31$$

with the approximation that $S >> 1$. A more relevant question is whether the layer thickness, and thus the dilution, adjusts to this theory or whether the theory must be adjusted to the description as a consideration of cases for $\mathbf{F''}^2 > 0.005$ points out more clearly. For these conditions, the sum of the Froude numbers given in Fig. 2-7 always indicates a supercritical flow state, thereby implying source control. However, Kranenburg's criterion (or even Benjamin's energy conserving flow for that matter) implies a limit on η which is independent of $\mathbf{F''}^2$, (i.e. the analysis is independent of the superimposed ambient velocity.) This leads to a conclusion requiring both source control and density current control and an overspecified problem for some ranges of source conditions.

There are perhaps two ways to resolve this problem. One is to deny the existence of a steady state flow for these conditions, in which case the density current and the source mixing are independent of each other. However, so long as the density current behaves as a steady state flow, a contradiction due to continuity considerations arise as the density current would pass more flow past it for certain source conditions than can be entrained. The probable resolution to the problem is to deny the applicability of Benjamin's analysis for density currents with significant thickness. The general area of open channel hydraulics has always been faced with the problem of the choice of governing equations to describe various flow phenomena. Consider if the density current head were replaced by a solid body. The situation is sketched in Fig. 2-8. In this classical hydraulics problem, there are two situations that can occur: Case 1.) subcritical control; the water level drops over the body but the flow is not affected upstream. The energy in the upstream flow is considered to be conserved. Case 2.) critical control; the flow is critical above the obstacle and the upstream flow adjusts to energy conservation with the flow energy on top of the body fixed. In an extension of this idea to the density current problem, the

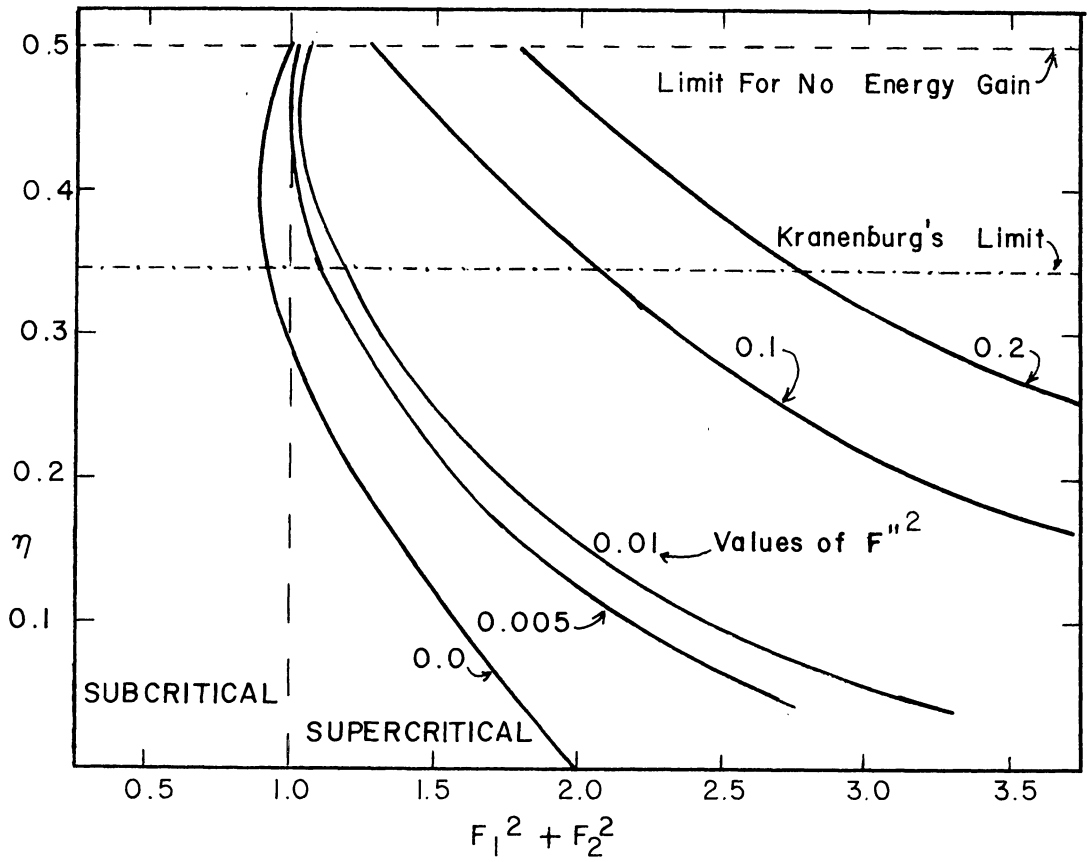

Figure 2-7. Variation of Froude Number With Density Current Thickness.

occurrence of critical flow then only defines a limit for which the analysis in Eqs. 2-23 through 2-28 is valid, i.e. $\eta \leq 0.347$. For other conditions, the occurrence of critical flow at the density current head fixes the necessary upstream condition to satisfy an appropriate set of equations. In Chapter 4, the data that led to these conclusions is presented. If this conclusion is drawn, the information in Fig. 2-7 would then no longer be valid for $\eta > 0.347$ and a correct formulation of the problem would resolve the contradictions posed in the above discussion.

An important implication is that there are two distinct possibilities, one with control at the source and the other with control at the head of the density current. This makes the unsteady flow problem very useful to test various aspects of the basic theory. It also appears that there may be a very important difference between flows with a net throughflow and $\mathbf{F''}^2 > 0.005$ and those with lesser values. The density current problem will be one of the first areas for further investigation as the data analysis continues.

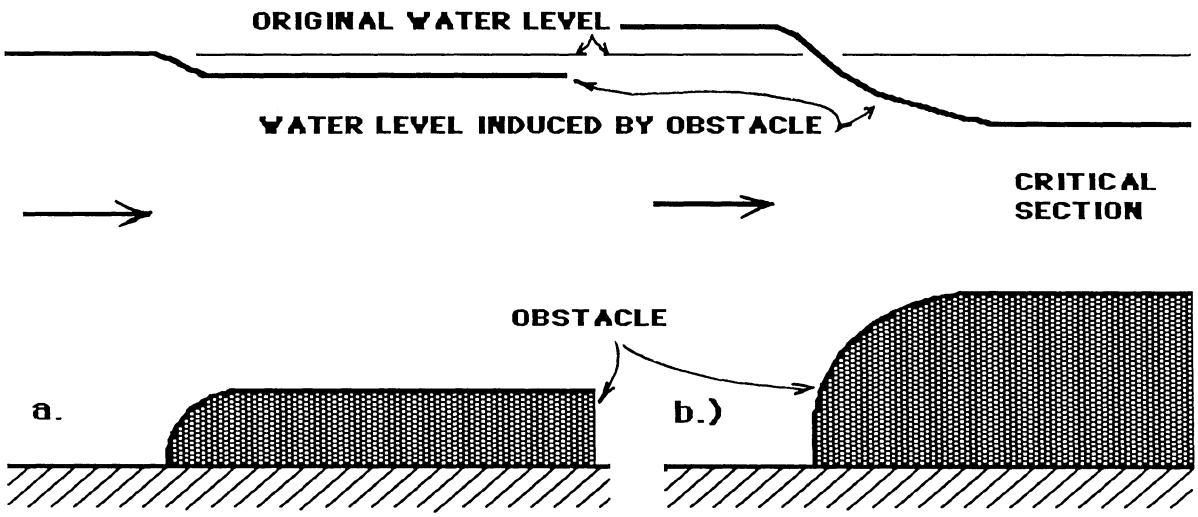

Figure 2-8. Flow Over Obstacle in Free Surface Flow.

Free Overfall

This situation can be handled quite adequately by extending the approach of Rigter (1970), who considered the problem of exchange flows in channels of limited length. However, he did not provide a basis for describing the problem of the mixing between the two layers at a discharge point at one end of the channel. The situation is sketched in Fig. 2-9. The Schijf and Schönfeld (1953) equations that describe the two-layer flow with the Boussinesq approximation are

Upper Layer

$$\frac{f_i(q_1/h_1 - q_2/h_2)^2}{h_2} - \frac{1}{2}\frac{d(q_2/h_2)^2}{dx} - g\frac{dH}{dx} = 0 \qquad 2\text{-}32$$

Lower Layer

$$-\frac{f_i\,(q_1/h_1 - q_2/h_2)^2}{h_1} - \frac{f_b(q_1/h_1)^2}{h_1} - \frac{1}{2}\frac{d(q_1/h_1)^2}{dx} - g\frac{dH}{dx} + g'\frac{dh}{dx} \qquad 2\text{-}33$$

where the interfacial and bottom friction are assumed to be given in terms of friction factors f_i and f_b, respectively. The formulation also employs the conventional assumptions that the interfacial friction is given in terms of the square of the velocity difference between the layers and the wide channel approximation (neglect of side wall friction) is made. The term dH/dx can be regarded as small with respect to dh_1/dx and thus $dh_1/dx \approx -dh_2/dx$. When dH/dx is eliminated from the above equations, a single equation is obtained:

$$[F_1^2 + F_2^2 - 1]\frac{dh_1}{dx} = f_b F_1^2 + f_i H\frac{[q_1/h_1 - q_2/h_2]^2}{g'h_1h_2} \qquad 2\text{-}34$$

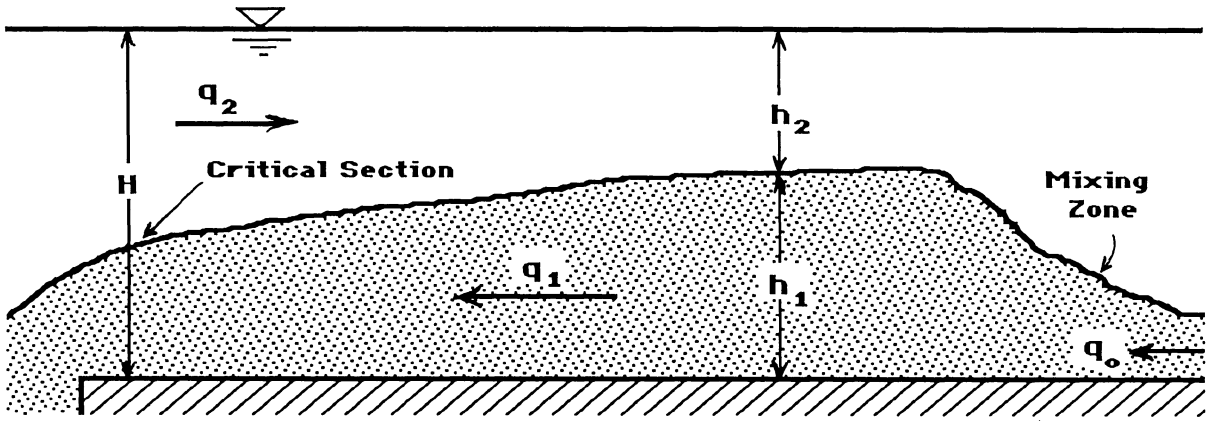

Figure 2-9. Definition Sketch For Counterflow Channel System.

The effect of friction is an important component to this problem. Critical flow is assumed to occur at the downstream end of the channel which is analogous to a free overfall in open channel hydraulics. Thus, Eq. 2-34 along with the critical flow state at the downstream end (assuming a free overfall or similar expansion) and the known length of the channel and the friction factors are sufficient to completely compute the amount of near source mixing. In the limit of negligible friction, the solution simply corresponds to that for internally critical flow near the source. The channel friction produces a subcritical state at the discharge point through a backwater curve. This will always result in less dilution than when the internally critical state is used as the downstream control. If the flow depth predicted by the backwater curve is used as the near source layer thickness h_1, the system of equations 2-7 through 2-12 are then closed. Note, however, that the solution is not direct in the sense that the volume flux and g' must be known to compute the profile while the profile must first be known to compute these. Therefore, an iterative solution will be necessary.

For certain idealized situations, it is possible to get direct solutions, e.g. for the stationary wedge problem described by Singh and Shah (1971) and others. For this particular situation, the effect of friction is sufficiently great and does not permit the fluid in the secondary layer to penetrate up to the source mixing region. It should be clear that if this happens, there will be no dilution of the source discharge. However, this is not analogous to the unstable flow condition discussed earlier, because the control is imposed from downstream and depends upon additional parameters, including the channel length and the friction factors.

The above equations and reasoning can also be extended to cases where the channel bottom slopes or otherwise changes elevation. A short qualitative discussion of the consequences is developed below since a prototype situation would rarely have a constant depth over a large distance.

If there is a singular high point on the channel bottom, then it may act as a control section in the

sense described by Long (1970). There is a direct analogy with single layer flow where the elevation change at the rise must be sufficiently large to create critical flow for the two layer system as well. Bewick (1974) and Wilkinson and Wood (1971) used this sort of configuration as their typical downstream control and formulate the problem on that basis while Baddour and Abbink (1983) do a similar thing with a width contraction.

For the case of a continuously decreasing total depth, the flow velocities generally increase downstream. Therefore, if the critical section remains at the downstream end, the flow only becomes more subcritical upstream and the flow will be qualitatively similar to the constant depth situation with a decrease in near-source mixing due to the reduced downstream depth.

With a continuously increasing total depth, there are two distinct possibilities. The buoyant surface layer and the dense bottom layer will behave somewhat differently; the former is considered first, For small bottom slopes (the friction slope is less than the bottom slope), the control remains at the downstream end, but more near-source mixing than for the constant depth case will occur. However, for steeper slopes, a loss of control at the downstream end is implied. The flow will then mix up to the internally critical state near the source and a certain layer thickness attained. The flow will then become subcritical downstream due to reduced velocities in the external layer, so no further mixing should occur. For the case of dense flow on a small bottom slope, the flow will be no different from the surface flow problem. As indicated by Britter and Linden (1980), the flow either subcritical or supercritical, depending upon the slope. Therefore, for steep slopes, the flow within the layer will remain supercritical due to the slope effect alone. There will be a near source mixing region that adjusts to a local momentum balance in which the effect of friction is negligible. The flow will then approach a uniform supercritical flow state over a longer distance according to the analysis of Ellison and Turner (1959). Their analysis also implies further entrainment in this region so that the uniform flow state does not necessarily imply constant layer properties. Koh (1971) suggests the same could occur in a constant depth channel due to heat loss or other similar loss of buoyancy (decreasing g' and therefore increasing Froude numbers). He suggests further mixing as the flow attempts to maintain an internally critical state. Although this is implied on the basis of the near-source analysis, this may not be valid due to possible rearrangement of velocity and density profiles which can promote stability without further mixing. Further entrainment should therefore perhaps not be regarded as an inevitable consequence. Ellison and Turner's experimental results imply further mixing in the downstream region as long as Froude numbers are somehat greater than critical so that the mixing is not confined to a region near the source. However, the causes for the mixing are different in the two regions as the flow downstream is assumed to be controlled by a balance between bottom friction and the excess weight down the slope. Therefore, there may be no connection between these two phenomena although it is interesting to speculate on this.

Application to Submerged Plume Problem

The development in this section is for the same problem considered by Koh (1983) with the thickness of the surface layer assumed to be controlled by the density current spread. However, as discussed in Chapter 1, he assumes the mixing in the submerged plume to be blocked at the level of the downstream surface layer. The following is an extension of the discussion in Wright (1985) in which the density current formulation suggested by Koh was used without modification. In this section, the discussion from the previous sections is now considered in the analysis. The results may be easily extended to the more general problem of the two-dimensional buoyant jet; this is not done herein.

The example is indicated in the sketch in Fig. 2-10. For computational convenience, it is assumed that the dilution within the rising plume is sufficiently large so that the surface volume flux is much greater than the source discharge. In practice, this is likely to be a very good approximation for sewage outfall diffusers where dilutions of 100-200 are typical. Otherwise, all other assumptions are as specified for the analytical developments previously presented. The flow will split equally at the surface so that the fluxes in the layer considered are compared to one-half of the source values.

The analytical solution for the volume flux within the rising plume is given by Koh as

$$q = \alpha^{2/3} B^{1/3} z \qquad 2\text{-}35$$

where α is the plume entrainment coefficient with a magnitude of about 0.14, z is the vertical distance above the source, and B is the total source buoyancy flux per unit length. q is one half of the total plume volume flux, i.e. the flow that proceeds in one direction. At the surface, the submerged jet mixing is assumed to be blocked by the thin surface layer at A; the thickness is computed on the basis

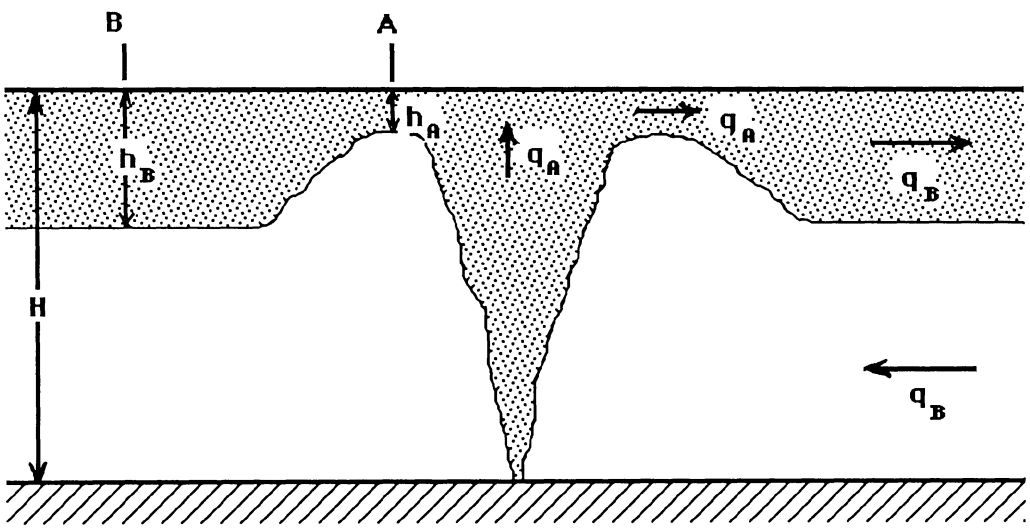

Figure 2-10. Definition Sketch For Surface Flow From Submerged Plume.

of assuming energy conservation in the impinging flow. This appears to be a reasonable assumption for impinging flows according to the experimental observations of Beltaos and Rajaratnam (1973). The density and velocity profiles within the surface layer are assumed to be uniform, in accordance with the observations of Jirka and Harleman (1973). The use of a gaussian velocity profile within the rising plume relates the plume characteristic width b (the width to where the velocity decreases to e^{-1} of its centerline value) to the layer thickness h_A (from Wright (1985))

$$b/h_A = \sqrt{2/\pi} \qquad 2\text{-}36$$

and the analytical solution for b is

$$b = 2\alpha z/\sqrt{\pi} \qquad 2\text{-}37$$

With $\alpha = 0.14$, solving for the vertical level where Eqs. 2-36 and 2-37 are satisfied results in a surface layer thickness of 0.165H. This defines all conditions at section A. The application of the momentum equation across the density jump (neglecting the change in surface elevation as in Eq. 2-7 due to the change in velocity in the outer layer) gives:

$$\frac{q_A^2}{h_A} + \frac{q_A^2}{H-h_A} - \frac{q_B^2}{h_B} - \frac{q_B^2}{H-h_B} = -\frac{g'_A h_A^2}{2} + \frac{g'_B h_B^2}{2} \qquad 2\text{-}38$$

Using the conservation of buoyancy flux and a downstream control relation allows for the solution of $\eta = h_B/H$ and $S = q_B/q_A$. Two different controls are selected; 1.) the internally critical flow state given by Eq. 2-2; and 2.) the density current critical flow solution by Kranenburg (1978) of $\eta = 0.347$. This latter is used in spite of the uncertainties associated with the applicability of the analysis as discussed earlier in this chapter. Use of the critical flow criterion of Eq. 2-2 yields a nondimensional expression for η in terms of α and $\lambda = h_A/H$ as

$$\frac{\alpha^{4/3}(1-\lambda)}{\lambda} + \frac{\lambda^2}{4\alpha^{2/3}(1-\lambda)} = [\eta(1-\eta)]^{1/3}\eta^{2/3} + \frac{\eta^{5/3}}{4}[\eta(1-\eta)]\alpha^{2/3} \qquad 2\text{-}39$$

Solving this expression numerically yields $\eta = 0.33$ and $S = 1.12$. Using the second relationship with $\eta = 0.347$ yields a direct solution (from the concept of Eq. 2-29) for S of 1.13. In terms of the total source discharge Q, the average dilution in the surface layer may be expressed as

$$\frac{S_{avg} Q}{B^{1/3} H} \approx 0.504 \qquad 2\text{-}40$$

One conclusion is that the two solutions are identical for all practical purposes. Using any downstream layer thickness $0.29 < \eta < .347$ results in only minor differences in predicted dilution. Therefore, it would be difficult to distinguish for this particular situation whether the near-field mixing is source or density current controlled.

There are some data available against which the validity of certain aspects of the above analysis can be checked. Experiments by Jirka and Harleman (1973) and Wallace and Sheff (1984) have been performed with a free outfall section at the end of a two dimensional channel. However, the section used by Wallace and Sheff (a 155 cm long section in a longer 80 cm deep channel) is so short that frictional effects cannot be important. In fact, the test section may have insufficient length to achieve the internally critical flow since Jirka and Harleman indicate that the density jump occupies a horizontal length of about two water depths. Therefore, mixing may be incomplete since there is only about one water depth on either side of the source in Wallace and Sheff's measurements. Their data consists of concentration profiles in the spreading layer near the outflow section. Most of their experiments are for a two layer ambient fluid, but there are four experiments with a uniform ambient density. These profiles were numerically integrated to compute the scales defined by Eqs. 2-5 and 2-6. The averages for three of the experiments (the concentration profile in the fourth is difficult to interpret) yield estimates of $\eta = 0.27$ and $S_{avg} = 0.509\, B^{1/3}H/Q$. Although the layer thickness is a little smaller than predicted, the average dilution is quite close. Probably, measurements in a somewhat longer section would yield larger layer thicknesses and dilutions. However, it can be seen that a realistic description of the mixing process has apparently been given. The data of Jirka and Harleman may also be analyzed in this manner, although their channel is somewhat longer and the effect of friction may need to be included.

The experiments by Roberts (1977) with a density current propagating in the test channel yield a reported result for minimum surface dilution as

$$\frac{S_{min} Q}{B^{1/3} H} = 0.27 \qquad 2\text{-}41$$

Roberts also provides a photograph of the resulting flow which quite clearly demonstrates of the density jump along the surface. The jump does not appear to include any roller region. Assuming that the relation between average and minimum dilutions from Wallace and Sheff is appropriate ($S_{avg}/S_{min} \approx 1.18$), this results in a coefficent of 0.319 for the average dilution relation. This is considerably less than estimated in Eq. 2-40. However Roberts' measurements were performed with a very small source and source Reynolds numbers were quite low and turbulence had to be artificially generated in the discharge structure. Therefore, it appears likely that the observed dilutions are too low due to the low

Reynolds number effects. Other data that are available, such as those by Isaacson, et al (1983) yield results that are more consistent with the above estimates as discussed by Wright (1985).

An additional result for density current controlled experiments that can be quite easily demonstrated is that any factor that increases the dilution within the submerged jet (i.e., horizontal discharge or increased momentum) will result in larger predicted downstream layer thicknesses (h_B)when the internally critical flow relation is used as the control on the mixing. The implication is that the critical condition at the density current head becomes operative and the dilution is fixed by the density current rather than the diffuser structure. Therefore, the possibility exists of the relationship in Eq. 2-31 or some equivalent being valid. The experiments by Bühler (1974,1977) are interesting in this regard. His experiments were performed with models of manifolds with a variety of port spacings and discharge conditions. Nevertheless, when his measurements downstream from the mixing region are analyzed, they give a quite consistent result of $S_{min}Q/(B^{1/3}H) = 0.46$ (average value of all Series 2 experiments, Bühler, 1974) and average dilutions about 10 percent higher, or very close to the prediction in Eq. 2-40. This information can be interpreted in support of the implications of Kranenburg's argument (through Eq. 2-40) or simply that the discharges were in sufficiently deep water so that the flows were dominated only by the initial buoyancy flux. Further analysis of these data may be of significant value in understanding the nature of the density current control in the case of significant layer thicknesses. (**Note:** Further analysis of Bühler's data has been performed and is reported by Wright and Bühler, 1986).

Implications with Respect to Prototype Applications

The analyses developed in this chapter have several important implications in spite of several unresolved aspects. One important item is the relationship between model and prototype studies. Because of apparatus constraints, most experimental investigations are performed in a mode where the flow is unsteady with a density current propagating away from the source. The interesting question is how this situation matches up with a prototype problem for a continuous discharge. First of all, there will be no density current head in most prototype situations because many prototype problems are associated with continuous releases. This raises the possibility of no downstream control (due to the denisty current) in the model and some as yet undefined downstream control in the prototype. However, it is probably not realistic to consider the limit of a steady layer with frictional influence extending to a control at infinity, the solution of which would be no dilution. Instead, other influences such as end effects from a finite length diffuser, ambient currents that advect the waste field away from the source, or loss of buoyancy due to heat transfer or sedimentation of particles may be considered to be the factors that establish the far field layer control. However, the analyses presented herein provide a framework for understanding how these might enter into the problem. It is possible to estimate the

maximum total dilution that can be attained, i.e. that in the absence of a downstream control. The length over which this is developed is only on the order of one or two water depths according to Jirka and Harleman (1979) which is negligible with respect to lengths over which other influences will be important. It is also possible to estimate a length scale associated with friction effects. This could be the distance over which interfacial friction must act to reduce the expected dilution by, say, 25 percent. This gives a measure against which other length scales can be compared. For example, the finite length of a prototype diffuser will result in the loss of a two-dimensional control in the far field where the speading will be more three-dimensional in nature. By considering a surface spreading analysis, the distance over which this occurs can be estimated. If this length is not large with respect to the friction length, then it can be established that interfacial shear plays a relatively minor role in the overall process and that the three dimensional nature of the flow field is more important. Although this argument is not pursued further herein, it is expected that many prototype problems will satisfy this type of situation, and that the inability to define an exact downstream control is therefore, not necessarily important to the overall problem and that the analysis with internally critical flow is a reasonable means of estimating the near-field dilution.

In spite of this argument, it is also clear that more attention needs to be made to the nature of laboratory investigations where the nature of the control may be well defined. Rather than some ill-defined notion that the laboratory measurement is satisfactory until the spreading fluid strikes the end of a tank or some similar criterion, it is possible to understand how the laboratory experiment is actually controlled. Therefore there is a means available to help guide experimental design to avoid possibly misleading results. A further development of the theory for the unsteady flows with a density current head is required, but the implications of various effects may be seen in the above discussion.

Applications of Analysis to Related Problems

As mentioned in the introduction, there are a number of variations to the basic problem description that can be considered as extensions of the above analysis, e.g. axisymmetric flows or ones into stratified fluids. Although no effort has been made to analyze these other problems in detail, it appears that there may be important differences when compared to the present situation. A discussion of some of these are presented below.

Chen (1980) presents a unified analysis for the surface spreading of axisymmetric and radial flows in both uniform density and linearly stratified fluids. However, he has overlooked many aspects of the problem that have been discussed within this chapter. In particular, he considers spreading in infinitely deep environments and further assumes that energy conservation is valid. The effect of a limited depth limits the applicability of his results on several grounds; nevertheless, the solutions give a functional form for the spreading relations that provides a basis for further reasoning.

Consider the problem of the submerged discharge in a linearly stratified environment such that there

is an internal collapse as in Fig. 1-2b. The inviscid energy conserving solution of Chen yields a constant thickness and intrusion velocity. Because the solution can be considered as a balance between buoyancy and form drag, the energy conserving solution predicts an internally critical state with respect to the propagation of internal waves just as Benjamin's energy conserving solution is critical with respect to interfacial waves. Both Benjamin and Britter and Simpson (1978) indicates energy loss due to wave breaking and subsequent mixing behind the head for density currents in fluids of finite depth and uniform density. The loss of energy in stratified fluids is more likely to be attributed to internal wave propagation as noted by Manins (1976a, 1976b) or Amen and Maxworthy (1980). Faust 's (1981, 1984) findings of little wave breaking behind the head of a density current in a linearly stratified fluid is consistent with this view. Since the internal wave speeds scale with the entire depth, the depth is again an important element of the problem.

An important difference between the two cases is for the submerged discharge case. As noted Jirka and Harleman (1979) and a logical consequnce of the more detailed analysis presented herein, the near-field flows become unstable for low buoyancy discharges in uniform density fluids. In the stratified fluid, this need not necessarily be the case. This is because the maximum height of rise is the important length (analogous to the depth in the unstratified case) and therefore the vertical extent of the rising flow is not uncoupled from the source dynamics as it is in an unstratified fluid. Therefore the range of possible flow configurations is more limited. This is consistent with the observations of Wallace and Wright (1984) that the intrusion layer thickness is constant for momentum dominated flows (but different than that for buoyancy driven flows) and an unstable flow state is not observed. An additional consideration is that if internal wave propagation is related to the depth, it is possible that both the maximum height of rise and the total water depth are important to the flow dynamics.

Finally, there may be near-source entrainment in the horizontal intrusion flow. Even though Wallace (1981) and Wright et al (1982) observe no density jump (i.e., there is no apparent increase in layer thickness away from the source such as observed by Roberts, 1977 for unstratified flows), this is not inconsistent with the general idea of a source region partially submerged by the far field intrusion. The findings of Wong (1984) that indicates significant entrainment inflow above the top of the intrusion layer could be attributed to near source mixing associated with the horizontal intrusion.

In these situations, the equivalent to the surface impingement analysis is likely to be extremely complicated. Methods must be developed to compute the potential energy stored as the jet overshoots its neutrally buoyant position and to convert this into energy in the horizontal flow. The coupling between the near-field horizontal momentum and the far field intrusion would thereby give a means of estimating the entrainment at the source attributed to the horizontal flow in a similar manner as developed for uniform density fluids herein. There is less certainty of the ability to formulate this accurately because of the breakdown of the jet model near the maximum height of rise and a number of other complications, but the conceptual idea would remain the same. The radial flow problem in an unstratified ambient fluid will probably bear more similarities to the present analysis than cases with

internal stratification. However, there are also some important differences. Because of the radial spreading, the length of the density jump enters the governing equations and it is also necessary to specify the jump location. The specification by Lee and Jirka (1981) of a constant length and location is unlikely to be valid over a wide range of source conditions, but the nature of the results may not depend too much on these assumptions. The expansion in the radial dimension along with the finite length indicates that the analysis will show relatively more mixing for radial density jumps. Therefore, the observations reported in Chapter 1 in Figs. 1-7 and 1-8 which show relatively large dilutions in the horizontal flow for certain ranges of source conditions should probably not be unexpected.

The density current interaction is somewhat more complex. As Chen (1980) shows, there is no steady state solution with a constant layer thickness even if the effect of friction is ignored. The solutions show an increasing layer thickness with time which leads to possible changes in control with time in the density current control. It should be expected, however, that two differences between the axisymmetric and two dimensional cases result. First, the spreading in the extra dimension should reduce the constraint on the density current spread enough so that the mixing will be source controlled over a broader range of conditions, perhaps under all cases. Also, the areas subject to interfacial shear will increase as the spreading radius squared so that interfacial friction should be more important.

There will be considerable efforts required to formulate these extensions to the analysis presented herein and many experimental and theoretical studies are required. Nevertheless, a basis for understanding the nature of the flow behavior has been laid out and it can be used to guide such work in the future. Also, the experimental findings of this study should shed much light on what are likely to be the most relevant issues in further research efforts.

CHAPTER 3
EXPERIMENTAL INVESTIGATION

Introduction

Given the background in the previous chapters, this chapter describes the experimental program that was undertaken to explore various aspects of the analysis. There were several major objectives in the experimental investigation:

1.) The examination of the concept of the global momentum balance establishing the control on the mixing process. Specific issues to be considered included the effect of the limited depth and the internally critical state in the absence of other downstream control. Unstable flows were also to be studied in regards to the mixing under those circumstances.

2.) The imposition of various downstream controls. Since laboratory investigations are usually performed as unsteady flows or as steady flows with some sort of artifical downstream control, the relationship between the results with these different configurations was to be investigated. The uncertainties in presently existing theories for density current propagation made the careful examination of this problem necessary. Any time dependent behavior of the flows with density current control is of interest and also the study of situations with significant interfacial friction influence was desirable.

3. The effect of background current on the problem. Since the work by Wood and Simpson (1984) is perhaps unique in terms of experimental results for this problem, there is need for more investigation on this subject. Their studies actually involved unsteady flows that are considered as equivalent steady flows and they did not measure the experimental detail that would be desirable in interpreting results. Also, situations with large layer thicknesses were not examined.

In order to achieve these objectives, a series of different experiments were performed. After a description of the experimental apparatus in this chapter, the experiments along with a limited analysis of the results are presented in Chapter 4.

Experimental Apparatus

The general flow system is sketched in Figure 3-1. The important components of it are indicated and are more completely described in the following paragraphs.

Channel

The test channel is actually two flumes; an inner working section installed within a larger flume that receives the flow from the inner one. The inner channel is 1 m deep x 40 cm wide and is constructed of 2.4 m long segments that can be removed. Thus, the length of this channel could be adjusted by removing end sections. Two different channel lengths of 4.8 and 14.4 m were utilized during this

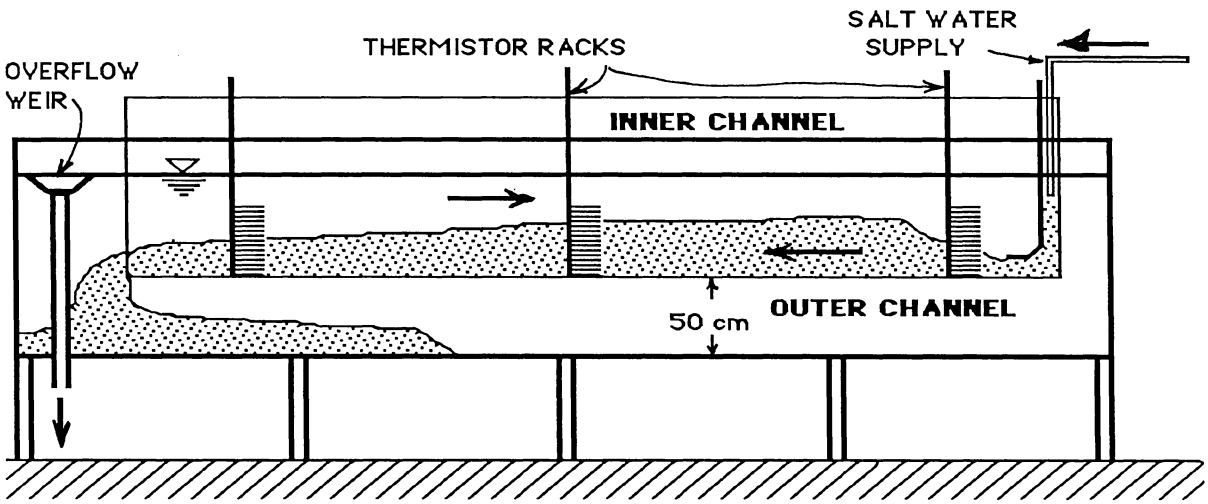

Figure 3-1. Experimental Facility.

investigation. The inner channel is suspended above the bottom of the outer channel on hangar brackets that allow it to be adjusted to an arbitrary bottom slope. The vertical separation between the bottoms of the two channels was about 50 cm. This allowed the dense fluid in the inner channel to drop from its downstream end and to slowly fill up the bottom of the outer channel. Measurements could be made so long as the level of dense fluid within the outer channel was below the bottom of the inner one. For typical source discharges, the time required to fill up the outer channel ranged from about 15-40 minutes. As discussed later, this provided one limit on the feasible experimental discharges. The water level within both flumes was controlled by means of an overflow weir at the downstream end of the outer channel. After initiation of an experiment, there was an initial water level rise in the channel up to the final steady state level due to the increasing head on the overflow weir. The total increase in water depth depends upon the flow discharge but varied over a range of about 0.3-2.0 cm. The time to achieve the steady level (say to within 1 mm) also varies with the discharge but is typically on the order of 3-5 minutes. Thus, the unsteady density current experiments were actually conducted with a slowly increasing depth. The depths recorded in the compilation of all steady state data were the ones at the final water level. For the unsteady flow experiments, an average depth during the propagation time was estimated from observations of the change in depth with time in a few tests.

The test channel is made from 0.5 cm thick polycarbonate and is not entirely rigid. That is, the unsupported portions of the channel may sag slightly resulting in a nonplanar bottom. Also, the bottom elevation varied across the channel width with the center generally somewhat higher than the edges. The difference was as much as 3 mm in some locations. There were variations in channel width as well, but these are less than 1-2 percent of the entire width and not as significant. The procedure for

changing the channel bottom elevation allowed independent adjustments at the hangers at the end of each segment. The effects of the channel bottom variation could be partially compensated by this adjustment process. The water depth at each side and the center of the channel was measured at both ends and the center of each section. The standard deviation of the water depths in these measurements was only 1.3 mm with no consistent trend in the variations along the channel. Therefore, the effect of depth variations is assumed to be negligible.

A more serious problem arose due to these channel bottom variations at the source itself. The discharge source was an adjustable gate with a rounded entrance. The channel bottom changes resulted in a variable source opening with rather significant variations due to the small source openings. For typical values for b_o of 1-1.5 cm, the variation across the channel was between 22 and 31 percent for the different gate settings utilized. To avoid difficulties in interpreting results associated with this influence, the discharge opening was not considered as a basic variable. Instead, only a few settings (six for the entire experimental study) were used. The discharge opening heights were measured at two cm intervals across the channel for any particular gate setting to the closest 0.5 mm and integrated to give the total area of the opening. The slot openings reported are this area divided by the channel width.

The gate itself was curved with a radius of approximately 10 cm. So far as could be detected, no contraction of the flow occurred beyond the gate.

Both flumes were filled with tap water at a temperature of 17-20 ° C prior to each experiment. This water was mixed with a portable pump to try to obtain as uniform an ambient temperature as possible. Typically, temperature variations of around 0.2° C were observed over the depth of the outer channel. The upward displacement of the bottom water by the dense fluid during an experiment resulted in a slight decrease in water temperature within the test channel over the course of an experiment. Although these variations are insufficient to cause density effects, they introduced a systematic influence on the temperature measurements discussed below.

Salt Water System

The important elements of the discharge system are indicated schematically in Fig. 3-2. The mixing tank consisted of an insulated box with a capacity of about 3000 liters in which the salt water was mixed. A separate system circulated the salt water through the refrigeration system which chilled the salt water to about 4° C. This refrigeration process was completed prior to an experiment. The chilled salt water was then pumped up to a constant head supply tank and entered the flume through a PVC line metered with an Annubar flow meter connected to a differential manometer. Separate valves for adjusting the flow rate and initiating the injection into the flume were installed in this line. The fluid then passed into a region behind the discharge gate, most of which was filled with styrofoam. Ambient water was displaced from this volume during the initiation of flow and clearly some initial mixing of the ambient and salt water occurred within this region. However the volume is estimated to be about 3

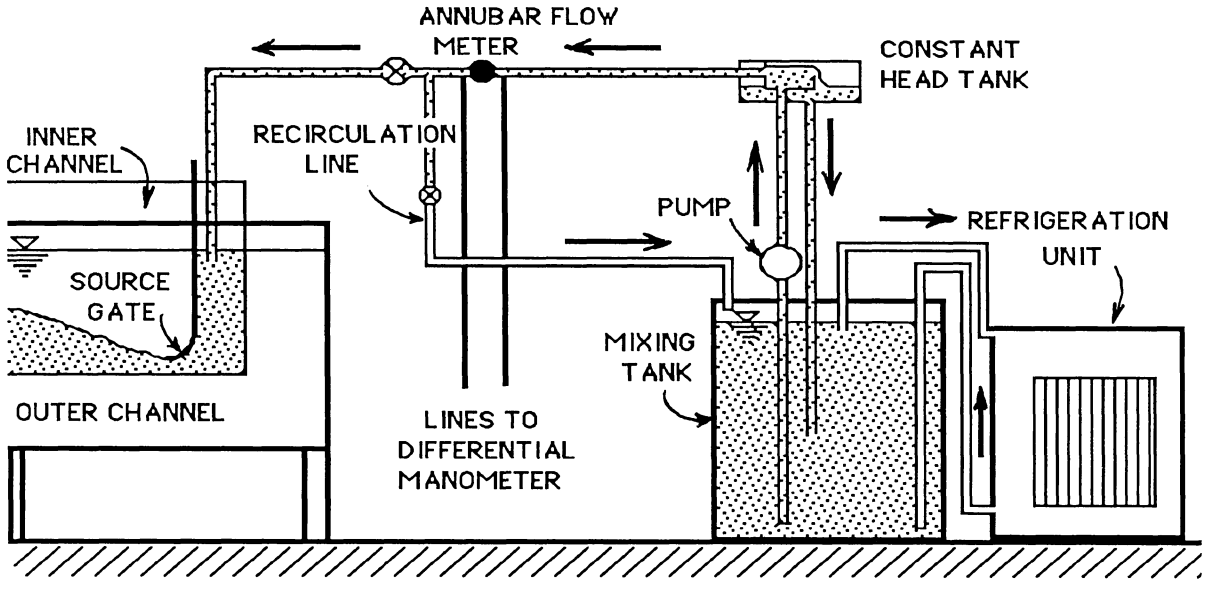

Figure 3-2. Schematic of Salt Water Delivery System.

liters so it would be displaced in only 3 seconds with a typical source discharge of 1.0 l/sec.

Heat transfer to the apparatus also would result in some initial discharge temperature rise. However, it was possible to circulate water through the system up to the quick closing valve; this was typically done for 5-10 minutes prior to the commencement of the experiment for those experiments in which the unsteady starting flow was measured. The combined effect of the mixing with the ambient water and this heat transfer can be assessed since the bottom temperature in the flow at the discharge gate was measured in most experiments. A detailed analysis has not been made at present, but it appears that this only causes variations on the order of 0.1-0.2 ° C except right at the density current head. An additional effect was the slow heating of the chilled water by the circulating pump. Again, the exact influence can be determined from the temperature records, but temperatures were measured with an accurate thermometer in the mixing tank during the experiment in some cases. It was observed that the temperature only increased by about 0.1° C until perhaps 1000 liters were left in the tank. The remaining fluid was heated more quickly and it was possible to measure an additional 0.2 degrees rise in an experiment that lasted about 35 minutes. For a few experiments, the salt concentration at the same sampling locations as temperature measurements was determined by withdrawing fluid samples and analyzing with a conductivity cell. This was done partially to verify that temperature could be used as a conservative tracer. Because the conductivity cell required at least a 250 ml sample, it was not possible to examine rapid changes of flow conditions, but the concentration distribution when the flow was essentially steady was found to be similar by either salt or tempertature measurements. Therefore,

except for the effects during the initiation of the flow, the use of temperature as the tracer did not result in significant measurement errors.

The density of the salt water was measured with a set of hydrometers that could be read to the nearest 0.00005 gm/ml. They were calibrated to give the density directly at 17.5 °C. Because the fluids were generally not at this temperature, a correction was required. A calibration showed that a density correction of $-2.8X10^{-5}$ gm/ml/°C was necessary to account for this temperature effect; this is within the range of reported volumetric expansion coefficients for glass. Therefore, any density was computed by noting both the hydrometer reading and the temperature. A temperature correction was made to the density reading. In the case of the discharge fluid, the density reading was often taken prior to the chilling process, say at about 10°C. A final correction was then made to account for the density change due to the temperature change to 4°. This was made on the basis of the density change for fresh water over the same temperature ranges since most discharge densities were only on the order of 1.005-1.009 gm/ml and salt concentrations were fairly low. In all cases, the salinity made up the majority of the density effect with temperature contributing up to a maximum of about 10 percent. The corrected densities are recorded to the nearest 0.0001 gm/ml.

Circulating Pump

For the final set of experiments, a circulating pump was necessary to create the ambient flow; Fig. 3-3 indicates the elements of this system. The intake for the pump was installed at as high a level as possible to avoid withdrawing the salt water, but since some experiments were at relatively low depths, it was not possible to place the bottom of the suction pipe higher than the bottom of the inner flume. A flat plate was installed below the inlet to withdraw fluid in a horizontal plane insofar as possible. Towards the end of an experiment, it was still possible that the salt water would be withdrawn as the level of the salt water rose in the outer channel. A digitial thermometer installed within the inner channel was used to distinguish if any recirculation of this fluid occurred. In cases where this was seen (as a drop in ambient temperature within the flume), the experiment was ceased and its occurrence was recorded in the laboratory notes. So far as was observed, the densities in the upper layer never increased more than about 0.0002 gm/ml due to this recirculation. There are about 6 experiments in which this occured and only in the last portions of the temperature measurements.

An orifice meter connected to a differential manometer just upstream from the circulating pump was used to meter the ambient flow. The setup suffered from an insufficient length of straight pipe in which the meter could be installed so a direct calibration of the meter was made. A calibrated V-notch overflow weir was installed at the end of the inner channel (only for the calibration) and provided the discharge determination for the calibration. One problem was that the manometer registered an 11.2 cm deflection with the valve completely closed. This was reproducible, however and all manometer deflections were measured relative to that. Also, manometer fluctuations were considerable, so a visual

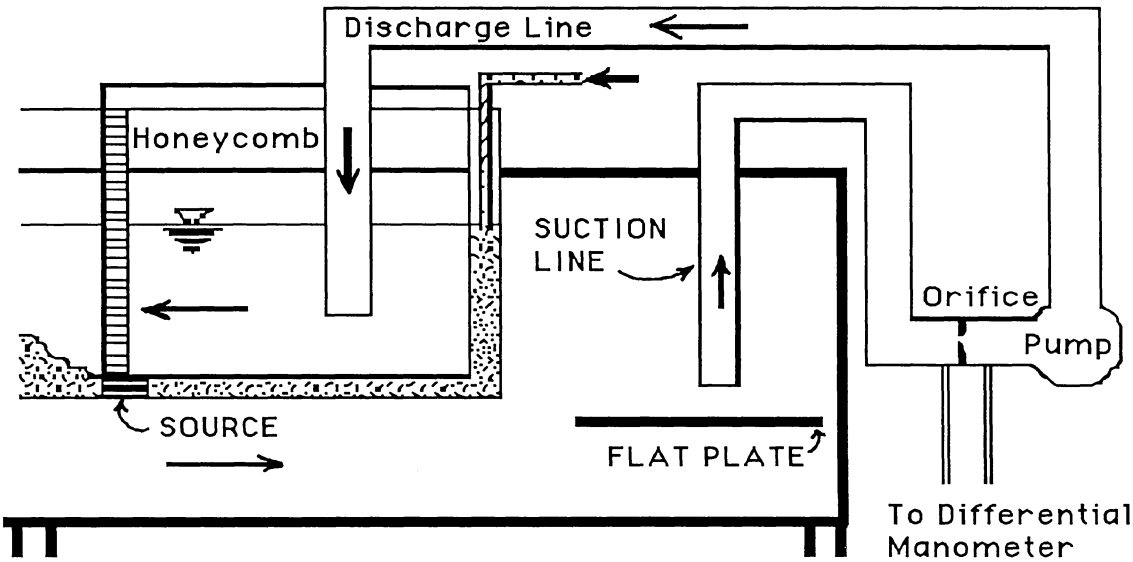

Figure 3-3. Circulating System For Series 3 Experiments.

averaging was required. It is expected that the calibration is no better than about 2% with larger errors at the smallest flow rates. In some instances, it is also possible that air in the system caused unknown errors in the manometer readings although considerable care was taken to avoid this problem.

The entrance section had to be reworked to produce the ambient flow. An insert of about 1 m length was installed at the upstream end of the flume. The ambient water flowed within this insert while the salt water passed underneath. This created a somewhat larger initial volume for the salt water to displace. One source width b_o was used for all of these experiments because of the need to seal the edges of the insert to prevent leakage of salt water at the sides of the flume. In the area where the salt water discharged, a honeycomb section approximately 5 cm thick was installed to destroy the boundary layer and create a uniform entrance velocity distribution. In the upper layer, 10 cm of honeycomb material along with a fiber mat were used to straighten the flow and create sufficient head loss to create uniform velocity distributions. The insert was made out of 0.5 cm thick material so this represents an initial vertical discontinuity between the ambient and salt water flows; also the inlet width is 1 cm less than the rest of the channel. Reported ambient velocities are the flow rate divided by the inside area of the insert. This was done because the most important aspect of this flow according to the analysis is the initial momentum in the ambient flow and this was felt to be the best way to describe it.

Downstream Control Device

For a number of experiments in the second series, an artifical downstream control was desired. The device indicated in Fig. 3-4 was constructed to create a backwater effect in the salt water layer without restricting the inflow of ambient water at that location. The plate position was adjusted by moving the second piston which was installed outside of the tank. In some cases, the salt water flowed between the plate and the end of the flume while in other cases, a portion of it flowed over the top of the plate. No attempt was made to characterize the blockage effect as a function of plate position since a thermistor rack was installed near the channel exit to measure the downstream end condition.

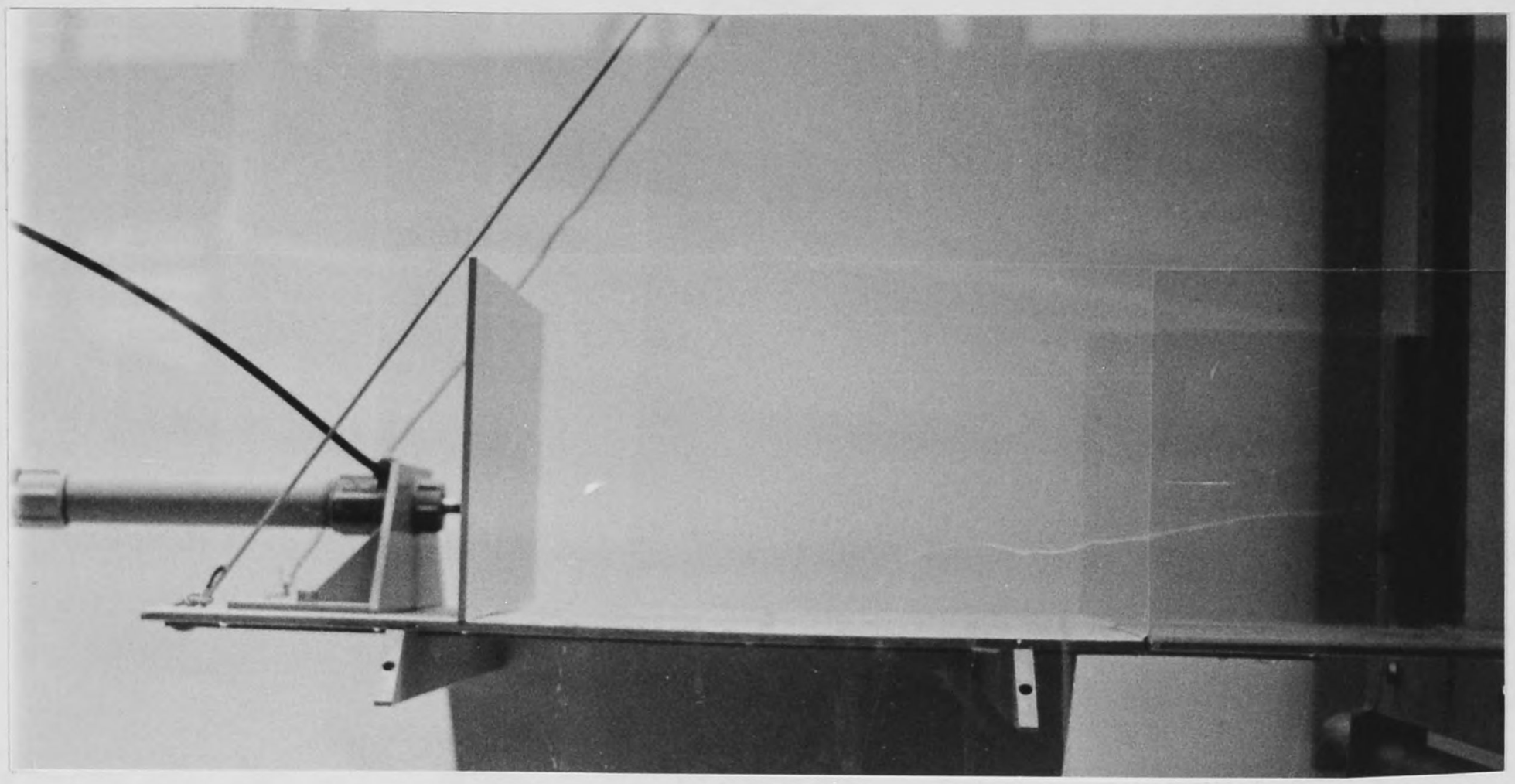

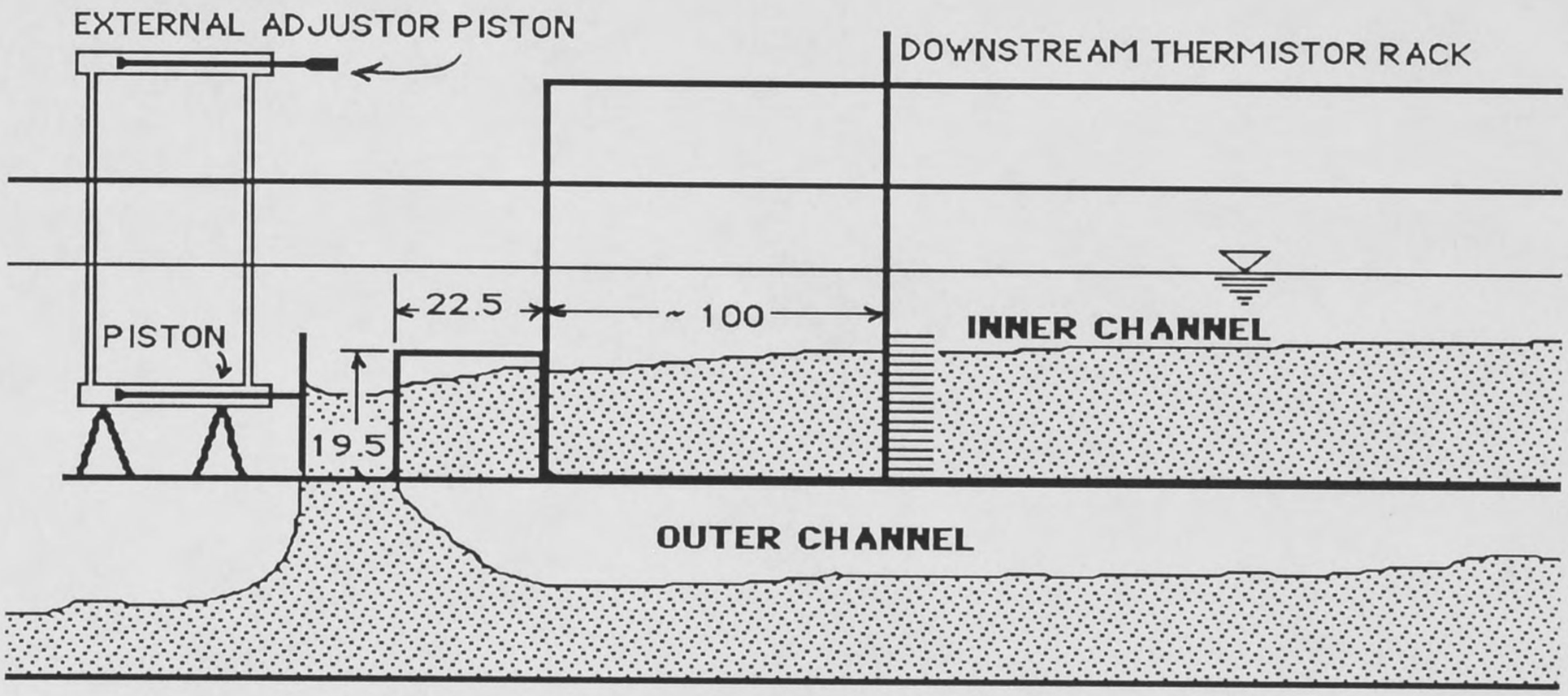

Figure 3-4 b. Device to Block Downstream End of Channel

Measurement Apparatus

Three basic methods for recording data were employed in this study. In general, it was desirable to make measurements of both density and velocity fields in order to obtain an idea of the deviations from the idealized uniform distributions within each layer. In many previous studies, the only information reported is on the visual thickness of layers. It was also an objective to try to relate the visual thickness to other more precise definitions and photographs were taken of many experiments.

Photographs

Semi-quantitative data could be obtained from these photographs. The other measurement apparatus described below could not always be located at the most desirable locations for a particular experiment. Instead, the temperature and velocity data were taken at a few fixed locations with the photographs providing a more or less continuous view of the flow. With an approximate relationship between the visual characteristics (e.g. layer thickness) and the measured profiles, it is possible to extrapolate to obtain further description of the flow. Approximately 350 different photographs were taken in addition to the hydrogen bubble photos. More details are given of the specific types of information recorded in this manner in Chapter 4.

Hydrogen Bubble Measurements

Velocity distributions were also measured for at least representative cases in each of the different series of experiments. In all, approximately 250 separate velocity profiles were measured. These were obtained by means of the hydrogen bubble method. A 0.001 cm diameter platinum wire was attached vertically over the depth and was pulsed with direct current from a square wave generator with a typical period of 0.20 seconds. An electronic flash was used to illuminate the flow section from above. The electrical voltage was about 80 volts and the current level was adjustable; this was necessary because of the different salt concentrations and velocities. Too high of an applied current resulted in substantial bubble rise especially in regions with low velocities, i.e. less than about 2 cm/sec. Since the salt water was more electrically conductive than the fresh water, an electrical current to obtain reasonable bubble concentration in the salt water layer would result in very little bubble visibility within the fresh water layer. In these cases, visualization of the flow in the upper layer was normally sacrificed, although in some cases both were obtained by using different current levels. In the steady state flows, it was possible to adjust the current to obtain good bubble traces whereas in the unsteady density currents, it was not possible to easily adjust the current during the course of the measurement.

The resulting bubble traces were photographed with a 35 mm camera. In the density currents, photographs were taken at several times after the passage of the density current head past the measurement location. In a few instances, bubble traces prior to the arrival of the density current (and also prior to the initiation of the salt water flow in the last series of experiments) were photographed to determine the flow pattern prior to the density current arrival. Typical times after the passage of the

head were 30, 60 and 90 seconds although more frequent recording was done in some experiments. For the steady flows, several photographs (up to ten per experiment) were taken of the measurement section and additional photos were made to measure the velocity in the counterflowing layer.

The resulting negatives were then used to make 8 X 10 inch enlargements. The bubble patterns were then traced on a digitizer table to determine the coordinates of successive electrical pulses. Photographs of a fixed grid at the center of the flume (prior to an experiment) gave a scale from which a coordinate system relative to the wire could be established. Up to about ten bubble traces per photograph were digitized and the coordinate locations stored on magnetic tape. The resulting data files were then processed to obtain vertical profiles of horizontal velocity. The wake correction method of Wilkinson and Willoughby (1981) was applied in the data reduction. Basically, this is a semi-empirical correction that was developed to describe the velocity reduction due to the wake behind the wire. Although this does not have any major influence except for the bubble traces closest to the wire, the correction was up to about 15% for the closest profiles. The actual bubble profiles were analyzed by piecewise linear interpolation of the digitized points and the velocities are the separation distance between two traces along a horizontal plane divided by the pulse interval. The data from multiple traces were averaged to get the mean velocity; from a minimum of perhaps three to a maximum of about 70 traces defined these average values.

In most of the experiments, a point where the velocity reverses direction occurs within the flow. Near this point, bubble rise is significant and the interpretation of the results should keep this in mind. Also in some measurements near the source, the high level of turbulence made it difficult to distinguish the bubble traces and these data are likely to be subject to more error. All information on the velocity profile data including the raw data files and the processed results are stored on magnetic tape as described in Appendix A. It is also possible to determine the velocity reversal point from the individual photographs in most instances and the interface between the salt and fresh water is also clear in some experiments due to an abrupt change in the bubble concentration (from the change in electrical conductivity).

Temperature Measurements

The bulk of the data collected were temperature profile measurements. The temperature histories at up to 75 points in the flow field are recorded in this fashion. The probe locations included a series of points spaced along the channel bottom and four racks to measure vertical profiles at specific horizontal locations. The bottom probes were intended to give information from which the propagation speed of the density currents could be computed and to give an idea of the bottom temperature variation along the channel. Generally the probe racks were concentrated near the source. The probes themselves were high frequency response thermistors sealed within 1.5 mm L-shaped stainless steel tubes. Each probe rack contained 16 probes and a device to clamp them together. Two of the racks were constructed so

that all tubes were parallel to the flow to minimize the wake. However, a visible wake could be seen behind these and some mixing at the interface was created. For probe racks at close spacings, these were replaced by wall-mounted brackets that held the tubes at right angles to the flow and positioned the thermistors near the center of the flume. These probably produced a somewhat greater wake but the effect was concentrated at the sides of the flume rather than near the thermistor locations. The overall effect on the experiments was some additional (and unknown) amount of mixing created by the wakes of the probes and racks but no measurements were made within the immediate wake of another probe rack.

The thermistors in the racks were spaced vertically to resolve the temperature profile through the entire salt water layer. For smaller depths, the probes extended over the entire depth; however, for larger depths, they only extended over a fraction of the depth. In a few experiments, some of the racks did not extend over the entire salt water layer. The vertical probe elevations above the center of the channel was measured to the closest 0.05-0.1 cm and all probe positions are recorded as basic data for each experiment. The horizontal probe locations were recorded to the nearest 0.5 cm.

The probes were sampled at a frequency of 3-12 Hz, the value varying among experiments and sometimes also within an individual experiment. A constraint on the total record size was dictated by the size of minicomputer disk which was used to store the data as it was collected. 12 Hz was the maximum sampling rate. The actual time intervals between samples were obtained by the data aquisition program by reading the computer clock at periodic intervals. The data records consist of successive digital (temperature) values for each probe and the time after each 16th scan of all probes.

All probes were calibrated twice during the study, once prior to the experiments and again after the completion of the first series. The calibrations consisted of sampling at fifteen different temperatures over the temperature range encountered in the experiments and fitting a third order polynomial to the points. These calibrations were rechecked in every experiment by comparing a measured temperature (the ambient temperature in the channel) against the calibration prediction. If there was a discrepancy, the constant (zero order) term in the poynomial was adjusted to yield agreement between the two. Calibration shifts were noted, for example, for the probes that were close to the hydrogen bubble wire, presumably because the electrolysis process which was observed to generate bubbles on the probes affected surface deposits on the thermistors. (Note that the hydrogen bubble measurements were not made simultaneously with the temperature measurements but both systems were in place during the final set of experiments.) The calibration changes were inspected before final data reduction and if there appeared to be an unusual discrepancy, the recalibration was not used and another obtained for a preceding (in time) or following experiment was substituted for it. In six experiments in the final set, a switch on one probe rack was reversed. The altered and original calibrations have been saved, however and the correct temperatures were recovered.

Measurements were begun at the initiation of the salt water discharge for the last two series of experiments and a short time after the density current head left the channel for the first set. The data

files contain the individual temperatures recorded during a particular experiment. In a few instances, two separate records were obtained for a single experiment.

Experimental Procedure

Although the exact procedures varied among the different types of experiments, a generally similar approach was followed. The following generalized description gives the important details of the experiments with variations among the different series noted parenthetically.

1. Mix salt water to desired density level, record density prior to chilling, then refrigerate to about 4° C.

2. Fill flume with water at a temperature of 17-20° C, mix with portable pump, and record ambient density and temperature.

3. Set ambient and discharge flow rates to desired levels. Perform hydrogen bubble measurements for density current (this latter was done only in the last set of experiments where it was possible to expell all salt water from the inner channel due to the shear by the ambient flow. Otherwise all hydrogen bubble measurements were made in separate experiments).

4. Recalibrate thermistor probes

5. Initiate flow, start thermistor sampling immediately (for the last two series; the sampling was begun after the density current left the inner channel for the first series) and visually record information on the propagation speed and size of the density current head. Take photographs of density current propagation as desired.

6. Make observations of the nature of the flow; record and photograph if desired. The meters were read and manometer deflections recorded. Let experiment proceed to steady state. (For the experiment with artificial downstream control, once steady state was attained, temperature measurements were made and sampling was halted while a new plate position was set. Further temperature samples were made after the attainment of a new steady state.) Thermometers were often used to record temperatures at selected locations in the flow field; the source, the mixing tank, the collapsed layer, and the ambient fluid, etc.

7. Make hydrogen bubble measurements in steady flow.

For all experiments, relevant visual observations and the temperatures observed with the digital thermometer are recorded on data sheets. All of this is available to help guide the later interpretation of results.

Experimental Error

A preliminary assessment of the data has yielded estimates of the experimental error. The following discussion provides an assessment of the reliability of each type of measurement.

The quality of the hydrogen bubble measurements depend in part on the number of photos taken

since the flow is turbulent and a suitable average is necessary to obtain the mean flow velocity. Of course, in the unsteady density current, it is not possible to obtain other than an instantaneous view of the flow. In the steady flows, a small number of photos was analyzed in some cases simply to keep the data processing requirements at a reasonable level. It was felt to be more desirable to get velocity profiles for more different experiments and accept some of the uncertainty due to insufficient data in a single experiment. Also there were the previously discussed problems with the bubble rise and the difficulty of interpreting bubble traces in the highly turbulent near-source region. However, a reasonable estimate of the error can be made by integrating the forward and return flows in the computed profiles and checking continuity for those cases without ambient flow. A typical profile is shown in Fig. 3-5; the information is contained in files BUBBLE68.DAT and BUBBLE69.DAT as described in Appendix A. The integrated forward discharge and the reverse flow are 66.7 and 29.5 cm^2/sec, respectively. Compared to the initial source discharge of 35.0 cm^2/sec, this results in a continuity discrepancy of 6.3%. For the few cases that have been checked, these continuity errors are less than about 15%, so this provides an estimate of the estimated maximum error. One case that grossly violated continuity apparently was due to an incorrectly recorded source discharge since other details of the flow appear to be inconsistent as well. The biggest errors arise at the top and bottom of the profiles where bubble rise is important and only a few traces are available. Since the velocities are low at these locations, the effect on continuity is not important, but the velocities at those locations may be in error by more than 10%, so any interpretation of velocity profiles should be made with this in mind.

The temperature measurements will be interpreted in the form of a relative concentration c , i.e. as

$$c = \Delta T/\Delta T_o = (T_a-T)/(T_a-T_d)$$

where T is a local temperature, T_a is the ambient temperature, and T_d is the discharge temperature. Therefore, errors enter through all three temperatures. It is also possible to obtain a continuity check as

$$q_o = \int_0^H u\, c\, dz \qquad 3\text{-}1$$

For the same information given in Fig. 3-5, the integral in Eq. 3-1 and the measured temperature profile (From Run 19) in Fig. 3-6 gives a value of 41.7 cm^2/sec, while Run 19 has an actual source discharge of 40.5 cm^2/sec. Temperature profiles from both Runs 19 and 20 are indicated in Fig. 3-6 as both have experimental conditions similar but not exactly equal to the data in Fig. 3-5. This continuity check is about as accurate as the velocity integral itself and there is some difficulty in interpreting results because the velocity and temperature measurements were not made with precisely the same discharge. Other such checks on other experiments yielded even better continuity checks. Therefore, the errors in such a computation are mostly associated with the velocity and it is concluded that the temperature

measurements are much more accurate than the velocity ones. This is also born out by inspection of the temperature profiles for experiments with similar discharge conditions (e.g. Runs 19 and 20 in Fig. 3-6), which show quite similar temperature profiles.

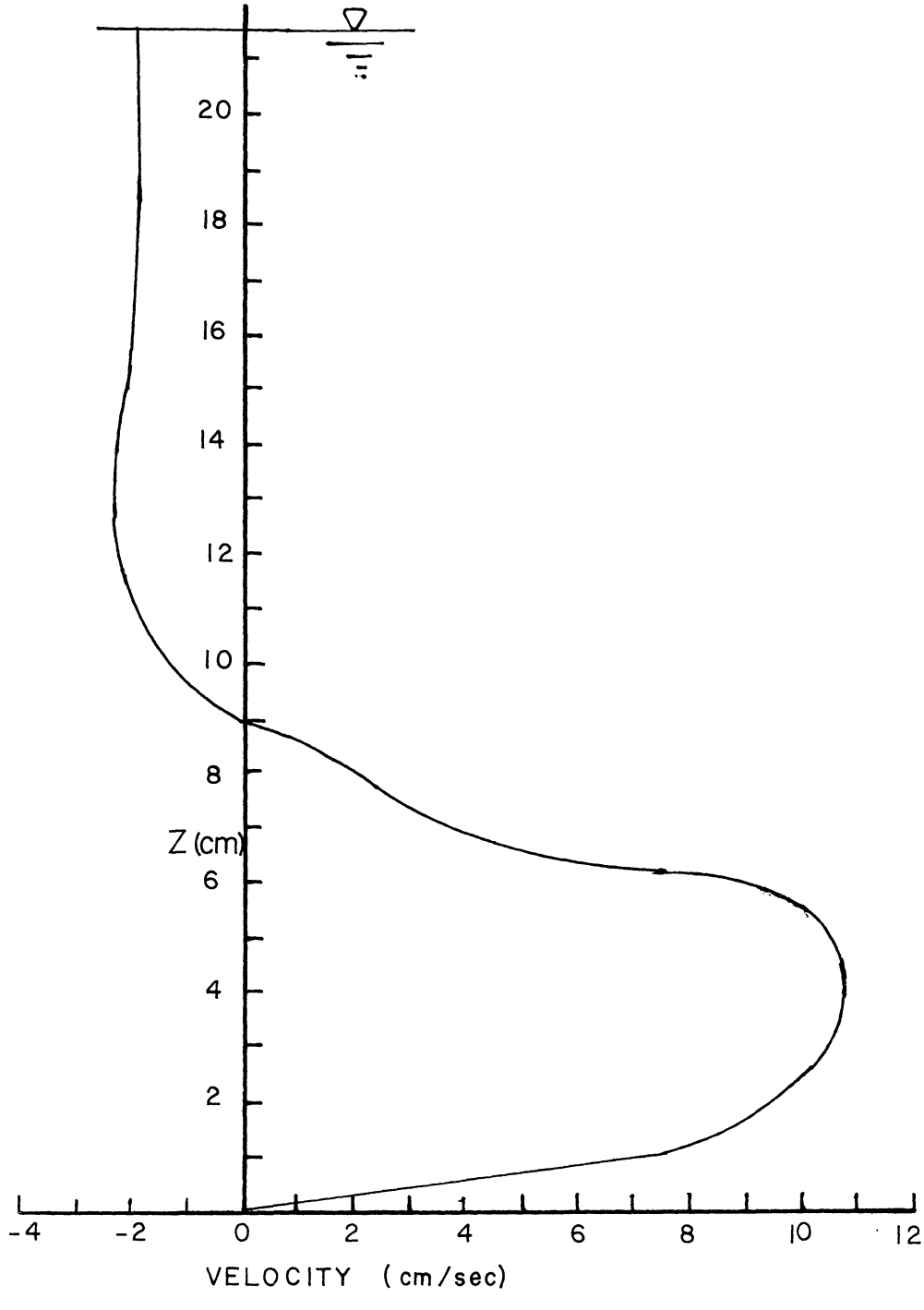

Figure 3-5. Typical Velocity Profile.

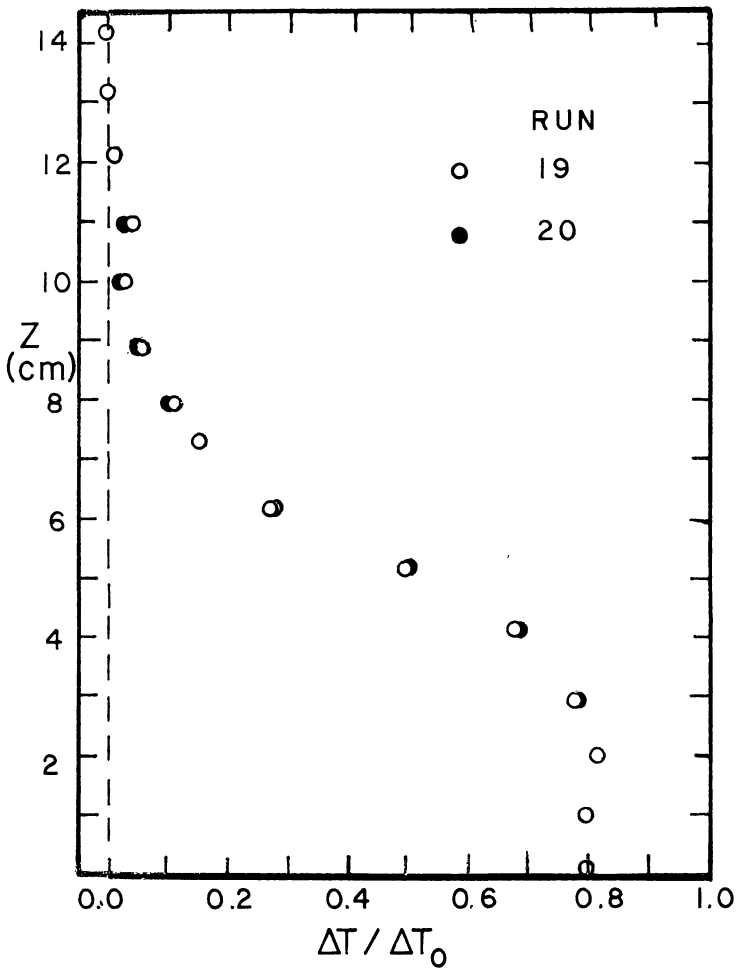

Figure 3-6. Temperature Profiles From Runs 19 and 20.

It is estimated that all temperature measurements are correct to within about 0.1° C. However, the discharge temperature rose due to the heating by the pump as discussed previously and also the ambient temperature often changed by up to about 0.2 °C due to incomplete mixing of the ambient fluid at the start of the measuement. This was due to the upward displacement of the colder water in the bottom of the outer channel as discussed previously. In principle, both of these effects could be removed by using the local (in a temporal sense) values of the two temperatures and computing the concentrations accordingly. However, this doesn't avoid the basic problem since this approach presumes that the fluid within the channel at any time is only composed of fluid discharged at that instant which of course, will not generally be true. However, such an approach will remove most of the error due to

these effects. In a few experiments, the source thermistor probe was not functional and a complete history of the discharge temperature is not available. Therefore, the interpretation of results will probably be accurate to within a temperature error of 0.1-0.2° C for each of the three temperatures in Eq. 3-1 and the error in meaurement can be estimated accordingly.

If there is heat tranfer to the apparatus, then temperature cannot be considered to be a conservative tracer. In a few experiments, the temperatures were compared to conductivity measurements of samples withdrawn from the flow and agree to within the accuracy indicated by the above estimate of temperature errors, and it is concluded that heat tranfer has a minor effect. These comparisons were made in essentially steady flows, however, and in the early stages of the density current propagation, this conclusion may not be valid.

The largest error in the determination of the experimental parameters is in the measurement of the source dimension b_o, a discussion of which was given previously. Since the source momentum flux is proportional to q_o^2/b_o, there is a potential variation across the channel of up to 20-30% due to the variation in the channel bottom. However, if one assumes that the most important variable is the total momentum flux in the flow, which then quickly adjusts to a two-dimensinal state, the error in estimated flow behavior is much less. Therefore, the error due to this effect is more important close to the source, say 10-20 b_o downstream. Beyond this, the maximum error in the momentum is probably on the order of 5-10 percent.

All other experimental parameters were measured with precisions that far exceed the above uncertainties and are not presumed to contribute significantly to the overall experimental error. The only other significant errors may come at low discharges where the precision in the manometer deflection reading becomes important. All other conditions are assumed to be accurate to within 1-2 percent.

CHAPTER 4
EXPERIMENTAL RESULTS

This chapter contains the description of the specific experiments and the results obtained to date. The presentation is subdivided into separate sections describing each of the three series of experiments. A qualitative description of the experimental results is also given to describe the general findings.

Series 1 - Experiments on Sloping Bottom

Objectives

This set of experiments was intended to examine the mixing process in the absence of any downstream control. This information has also been reported within this framework in Wright (1985). Although some of the experiments by Stefan and Hayakawa (1972) were also devised for this purpose, a somewhat different approach was taken in this investigation in order to cover a wide range of experimental variables. The basic problem is that the length of the near source mixing region varies among experiments as indicated in the results of Stefan and Hayakawa. Any physical apparatus will generally have a fixed length and therefore may be too short and not encompass the total mixing region or else it will be too long and possibly exhibit some interfacial friction or other downstream influence. It is known from previous studies on dense flows down sloping channels (e.g. Britter and Linden (1980)) that there is a slope beyond which the flow will be supercritical. Denton (1980) suggests this to be on the order of 1 percent. Therefore a supercritical discharge into a channel set with a slope slightly greater than this value will result in a flow that should mix up to the internally critical state and collapse into a slightly supercritical layer as the effect of friction and the sloping bottom is felt. It can be argued that the momentum balance in the discussion of Chapter 2 is negligibly affected for flow on a slope of about 1 percent. One consideration is that it is not obvious that the flow has to collapse, i.e. it could pass directly to the supercritical uniform downstream flow state. The basis for assuming the critical state is reached is that the length of the near-source mixing zone is short compared to the distances over which friction effects are important. Preliminary visual observations indicated the validity of the basic hypothesis in the sense that a collapse in layer thickness beyond the initial mixing region was noted. Therefore, these experiments are taken to be representative of the constant depth problem with the downstream control removed.

Results

23 different experiments in which temperature measurements were made were performed in this series. Table 4-1 summarizes the experimental conditions for all experiments. The last column gives

results computed from the measured temperature profiles. In addition, hydrogen bubble measurements were made at three locations (35., 97., and 564. cm) that corresponded approximately to thermistor probe rack locations. These were done for conditions that are roughly equivalent to some of the experiments described in Table 4-1. It was difficult to exactly reproduce a set of experimental conditions, so the velocity measurements are for experiments that are only approximately the same. Appendix A lists the exact experimental conditions for the velocity profile measurements. In addition, visual observations were made for a few preliminary experiments and limited results may be obtained from them.

Three different water depths (at the source) of about 12.0, 17. and 23. cm were studied with flow discharge as the other primary variable; the source density was also varied over a more limited range. A single channel bottom slope of 0.0175 was used; this was felt to be sufficient to ensure supercritical flow for any test condition. In retrospect, it would have been useful to look at the mixing in unstable flows at more than one slope to examine possible differences. A related study by Schläpfer (work in progress) found the bottom temperatures for this slope to increase by about 0.2°C over the length of the channel (16.7 m) for similar experiments in which the effect of near source mixing was minimized. This minor mixing is apparently due to turbulence generated by bottom shear which then propagates upwards to the interface before it is damped out.

Information on the propagation histories of the density currents associated with the initiation of these flows were obtained. The discharge was dyed blue and visual observations of the head size and the final layer thickness (as determined by the location of the dye interface) at four locations along the channel were recorded. Fig. 4-1 indicates the propagation histories for some typical flows. The description of the data files in Appendix A explains how this information can be retrieved along with additional information regarding the density current head and steady layer thicknesses. Straight lines are indicated in the plot to show the deviation from a constant propagation velocity. The results quite clearly show increasing propagation speed with depth (or distance along the channel) and are in direct contrast to the results of later experiments (with constant depth) in this study which show declines in propagation speeds with distance along the channel. This is generally consistent with the ideas presented in Chapter 2 which indicate that the velocity increases with depth so long as other variables are fixed. The density current head also increased in size along the channel which tends to indicate a larger amount of mixing in the head since the steady layer thickness did not change appreciably along the channel. These findings are different from those by Denton (1981) who suggests a constant propagation velocity. However, his experimental channel was only 3.8 m long. Fig. 4-1 indicates that an apparently constant velocity would be deduced from the present experiments over that length of channel; therefore his conclusion is basically invalid. Although further data interpretation is necessary, it appears possible that the density current behavior can be partially explained as an adjustment of the head to the imposed return flow in the upper layer and these data may shed some light on questions raised in Chapter 2.

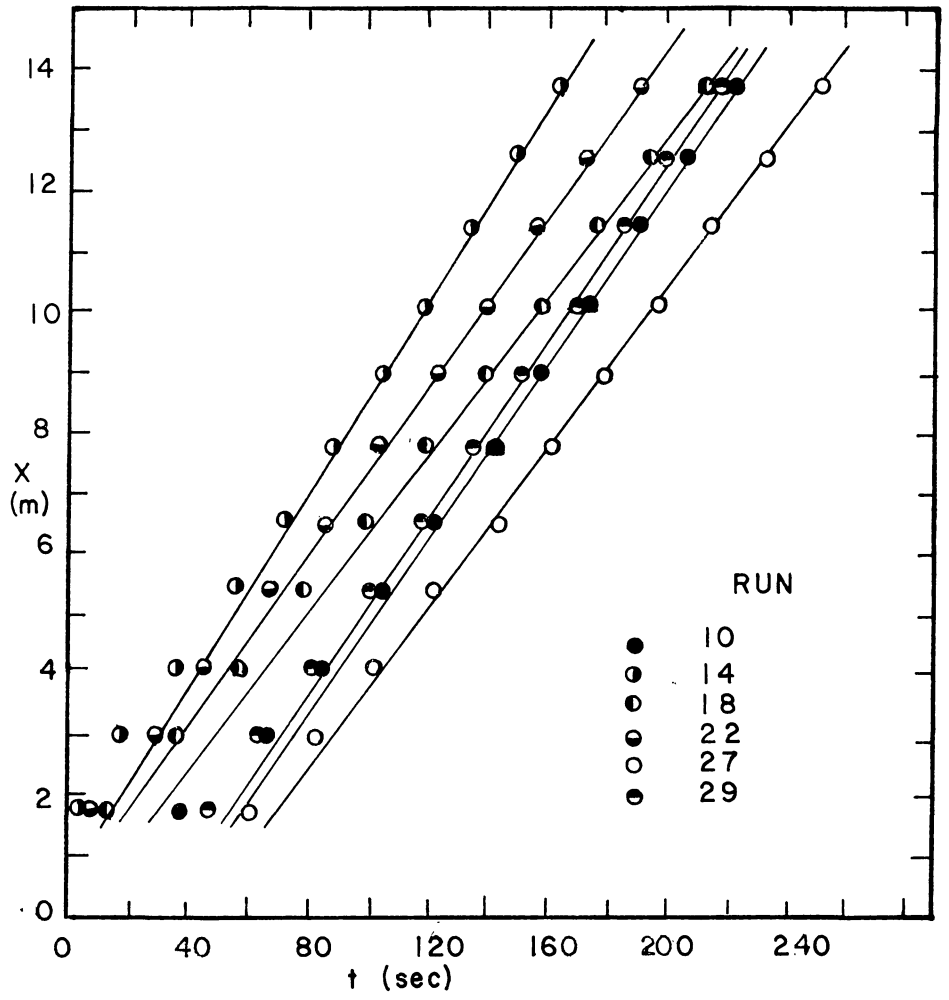

Figure 4-1. Typical Propagation Histories For Density Currents in Series 1.

The density current head left a stratified wake of mixed fluid similar to that described by Britter and Linden (1980). This was only slowly removed from the channel by entrainment and interfacial shear. In spite of the fact that temperature sampling was not initiated until after the density current head had left the inner channel, the influence of this wake was detectable in the temperature records. The temperature racks were installed at 25., 35., 100., and either 400. or 680. cm from the source. The last rack was changed from 400. to 680. cm during the course of the investigation because it was not obvious that the 4 m location was sufficiently far from the source to be free of the near source mixing zone. Approximately 6 minutes of temperature samples at about 12.5 hz were recorded in each experiment. These temperature records show the interface at the downstream becoming more sharp with time

Table 4-1. Experimental Conditions for Series 1 Experiments

RUN #	Total Discharge liters/sec	b_o cm	$\rho_{amb.}$ gm/ml	$\rho_{disch.}$ gm/ml	T_a °C	T_d °C	H cm	g'_o/g'
7	1.993	1.643	1.0001	1.0086	18.1	4.67	24.3	1.90
8	1.615	1.643	1.0001	1.0086	17.95	4.9	23.9	1.86
9	2.459	1.643	1.0001	1.0083	17.5	4.1	24.6	*
10	1.065	1.643	1.0001	1.0083	17.45	4.51	23.3	1.63
11	1.334	1.643	1.0001	1.0083	17.48	5.12	23.6	1.74
12	2.295	1.643	.9999	1.0080	17.2	4.25	24.5	1.96
13	1.623	1.643	.9999	1.0080	19.3	4.33	23.9	1.92
14	2.780	1.643	.9997	1.0083	19.8	4.56	24.9	1.72
15	1.746	1.643	.9997	1.0083	19.8	4.87	24.0	1.88
16	1.759	1.643	.9999	1.0071	19.3	4.2	12.2	1.30
17	1.209	1.643	.9999	1.0071	19.15	4.5	11.6	1.47
18	0.897	1.643	.9999	1.0071	19.05	4.91	11.4	1.57
19	1.619	1.643	1.0000	1.0073	18.5	4.22	12.1	1.33
20	1.546	1.643	1.0000	1.0073	18.15	4.34	12.0	1.38
21	1.041	1.643	1.0000	1.0073	18.2	4.85	11.5	1.52
22	2.186	1.643	1.0000	1.0062	20.5	4.36	12.6	1.21
23	1.388	1.643	1.0000	1.0062	20.2	4.63	11.8	1.39
24	1.006	1.643	1.0000	1.0062	20.2	5.15	11.4	1.53
25	2.118	1.643	1.0000	1.0067	18.6	4.69	17.2	1.50
26	1.431	1.643	1.0000	1.0067	18.6	5.03	16.5	1.62
27	1.098	1.643	1.0000	1.0067	18.6	5.02	16.2	1.68
28	1.912	1.643	1.0001	1.0059	17.2	4.37	17.0	1.52
29	2.819	1.643	1.0001	1.0059	17.2	4.47	17.4	1.30

* Not computed, thermistor racks installed too low.

apparently due to the removal of the mixed fluid left in the wake of the density current head. Figure 4-2 indicates the nature of the influence for Run 17; it was found that the change in temperature profiles is not too important over the entire record but nearly undetectable in the last one-fourth of the temperature record. Nevertheless, it was decided to only use the last 800 (or 1600 for some experiments in which a longer sampling time was used) samples to define the temperature profiles.

The experiments were divided approximately equally between stable and unstable flows as distinguished visually by the occurrence of salt water touching the surface. Figs. 4-3 through 4-5 are photographs of the near field for different relative layer thickness and indicate some of the qualitative features of the flow. Photographs from Run 8 in which no detectable roller region is visible are presented in Fig. 4-3. Although the flows are still stable in Fig. 4-4, the occurrence of recirculation in the mixing zone is clear. Fig. 4-5 shows flows which are unstable (Run 22 was very clearly unstable while Run 23 is a flow which is very close to the transition between stable and unstable flow). The occurrence of unstable flow was very poorly defined, since near the transition to unstable flows (hereafter referred to as incipient instability), a very thin layer of fresh water passed above the salt water with only occasional touching of the surface by the salt water. Visual observations in the unstable flows also indicated that fluid at the water surface could be moving upstream over a portion over the flume width and downstream over the remainder. This did not appear to be directly related to the previously mentioned variations in the source opening since the upstream flow sometimes was at the

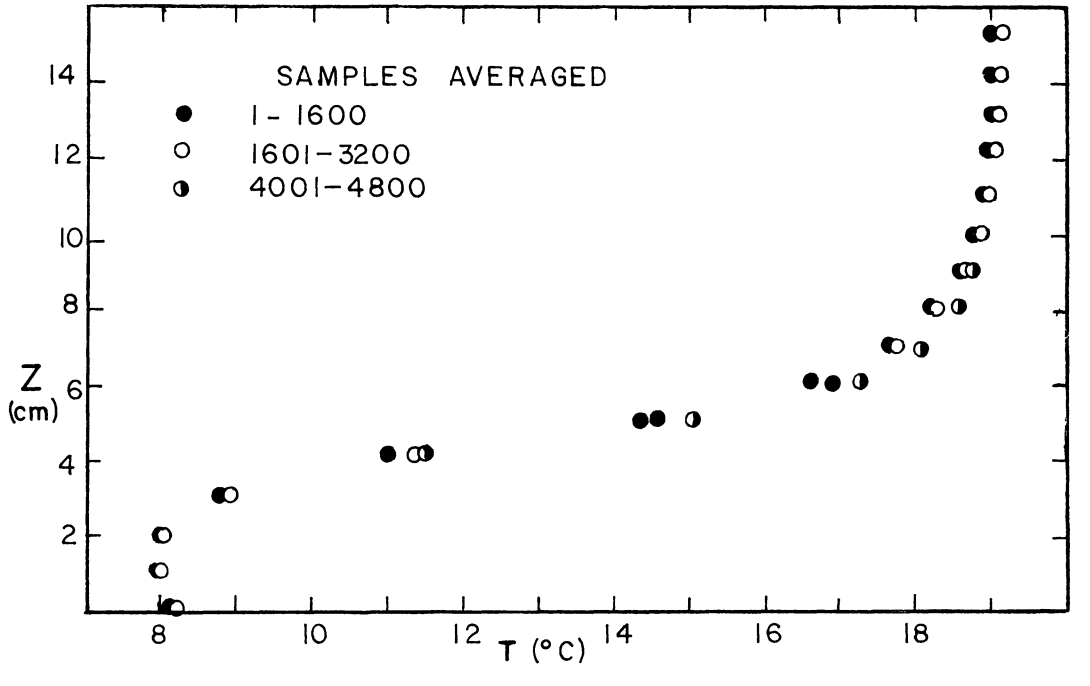

Figure 4-2. Changes of Temperature Profiles With Time.

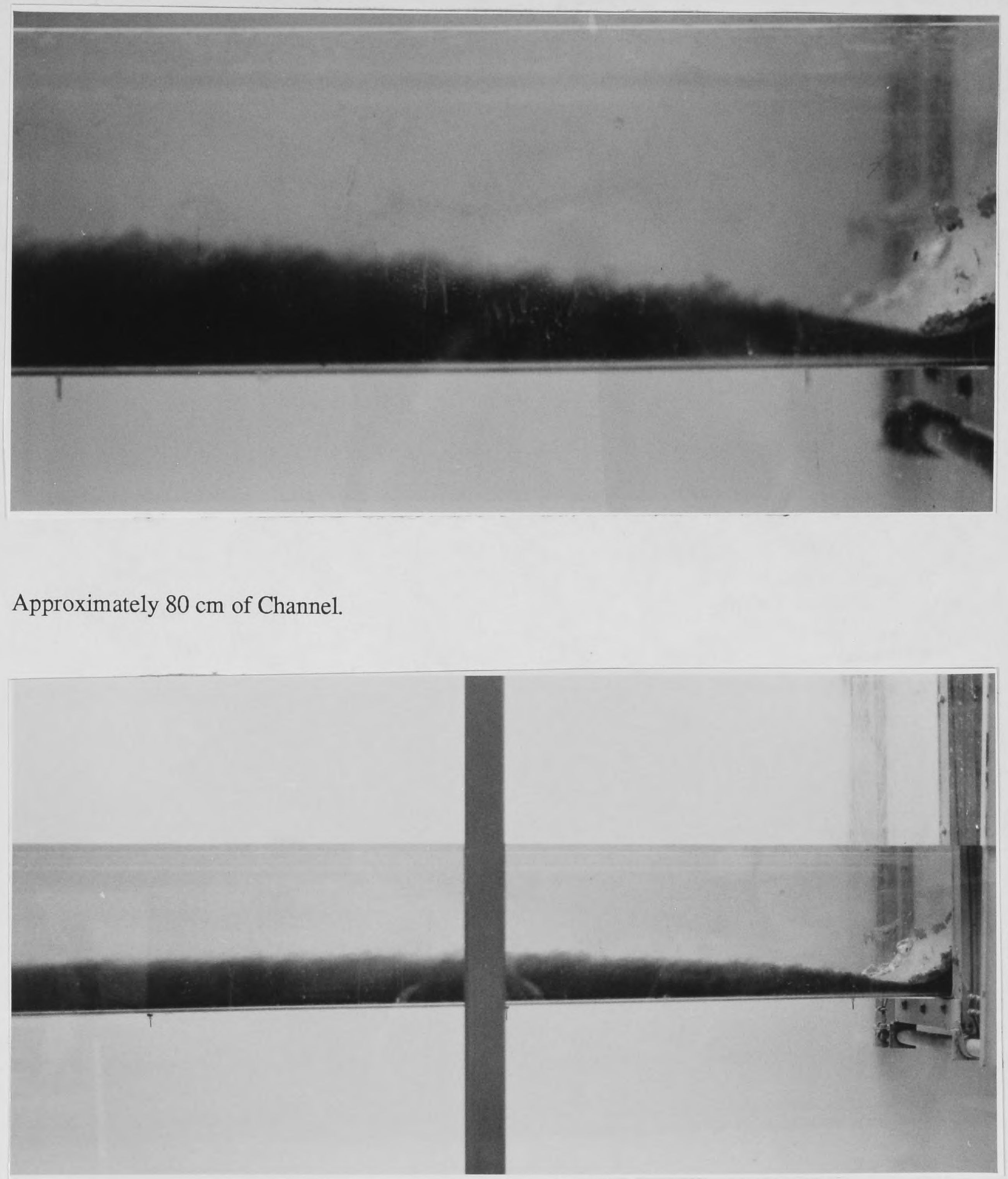

Approximately 80 cm of Channel.

Approximately 2 m of Channel.

Figure 4-3. Flow With No Observable Roller Region (Run 8)

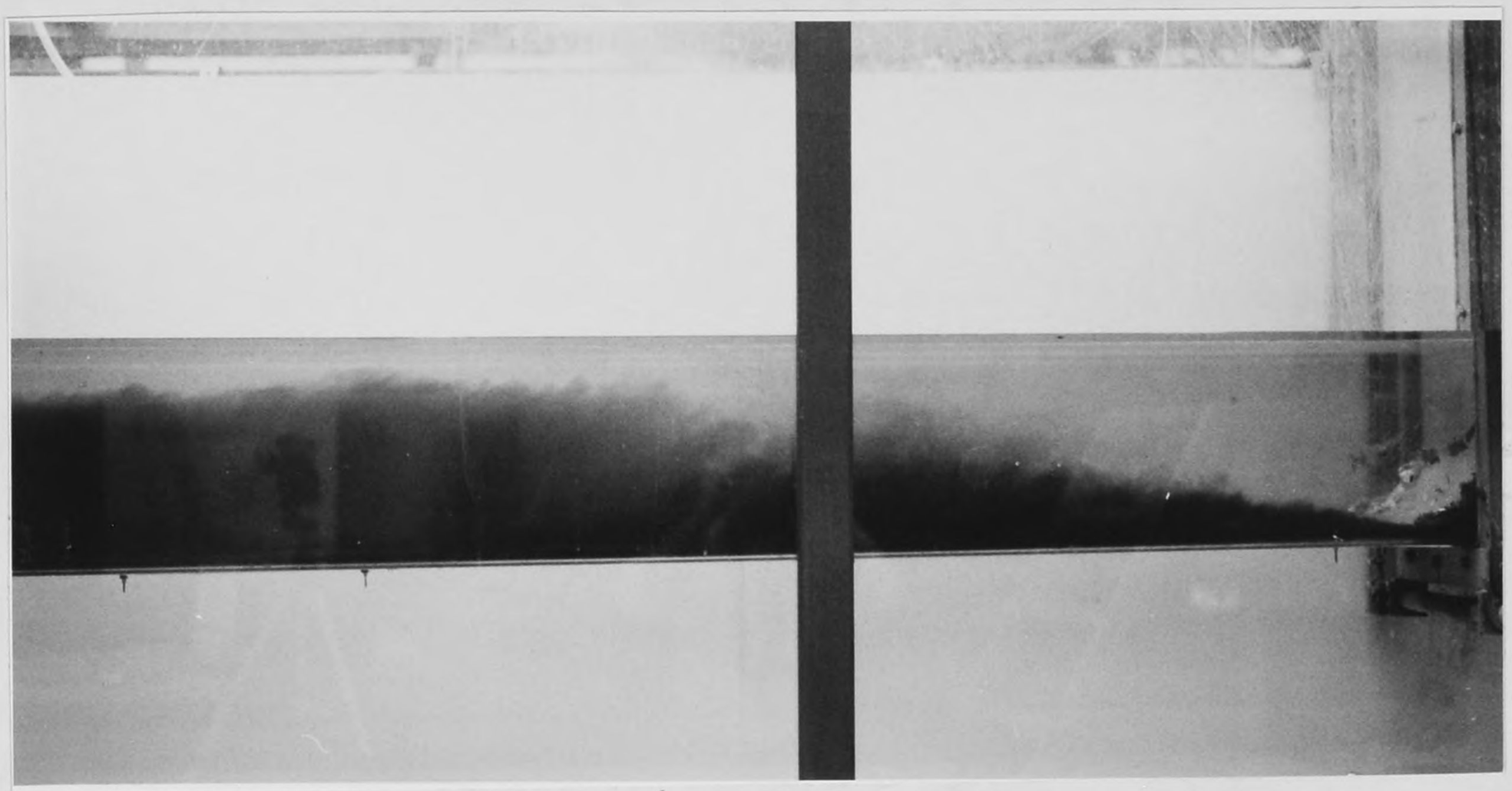

RUN 7

RUN 18

Figure 4-4. Experiments with Stable Flow and Observable Roller.

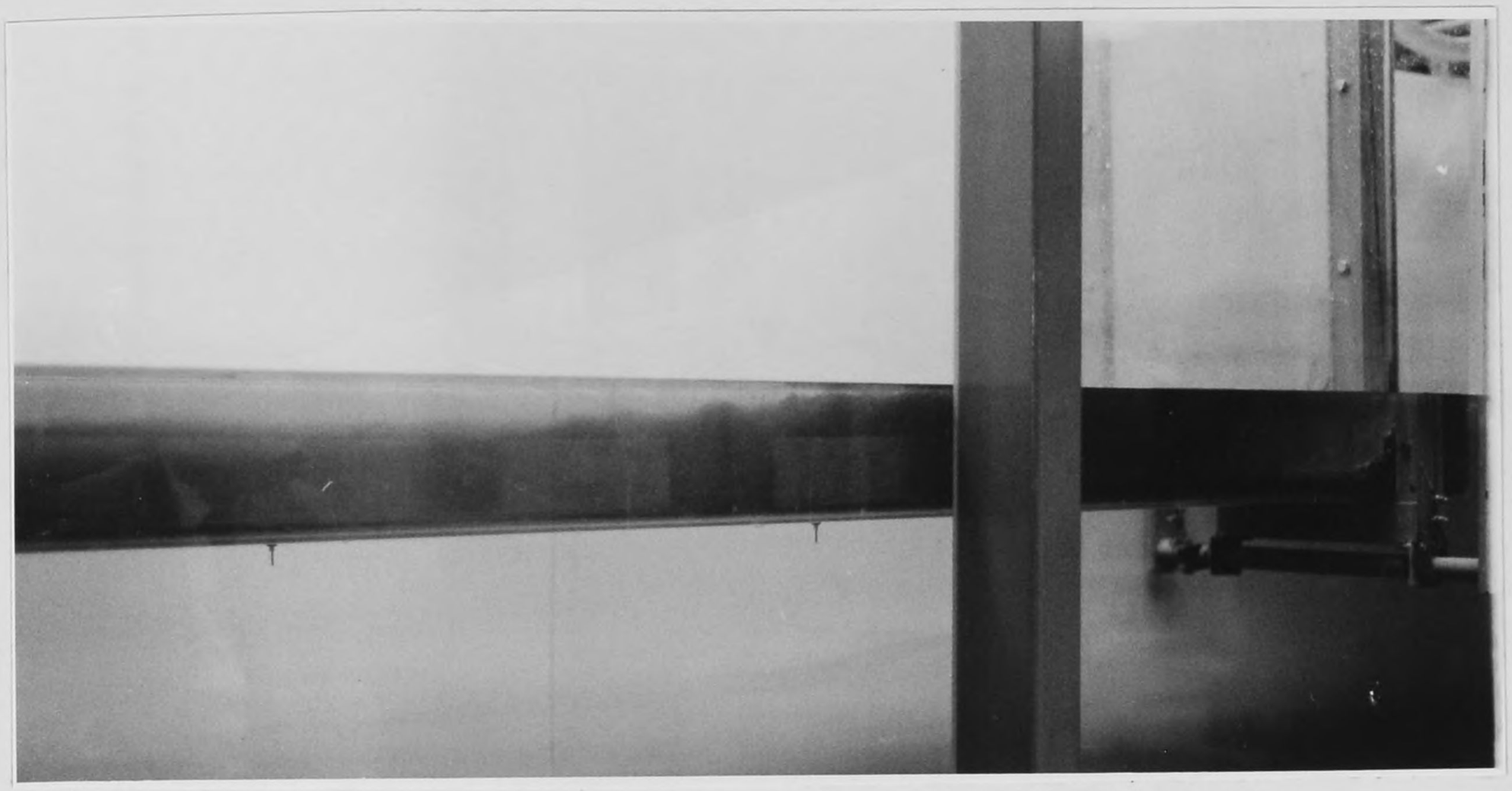

Run 22

Run 23

Figure 4-5. Experiments with Unstable Flow.

center of the flume and other times along one side. These instabilities resulted in a significant counterflow, even for the unstable flows. Salt water at the density interface could be observed to be moving upstream for up to 2-3 m downstream from the source even though the highly turbulent region was perhaps only half that length. This indicates that there is not a circulation (driven by internal stresses) set up in the fresh water layer such as noted by Singh and Shah (1971) for plunging density currents or for the related problem of intruding density wedges. In their experiments, the secondary layer is not at rest as assumed in the simple theory, but is driven by internal friction to provide a recirculation zone with no net flow. In the present experiments with unstable flows, there is a definite net upstream flow near the surface over the entire mixing zone. This implies that a description of the exchange process must involve some other important physical flow principle. Jirka and Harleman (1979) avoid this problem by specifying the flow to be internally critical and to detach at a particular location which was constant for all source conditions. However the detachment point was variable in these experiments and there is no obvious reason to indicate that the flow was internally critical.

Statements by previous researchers that the entrainment vanishes as the source is submerged (e.g. Wilkinson and Wood (1971)) are approximate only and should not be regarded as an accurate description of the flow field; other evidence collected in the second series of experiments supports this argument. In general, the complete flooding of the source (i.e. a roller above the dense layer or salt water moving upstream along the entire interface) corresponded very nearly to the incipient instability condition. Recirculation of the salt water along a portion of the interface was also observed for many of the stable flows although the source was not flooded.

Although it was especially apparent for the unstable flows, the free water surface level was found to drop above the source rather than rise to a stagnation point as described in Eq. 2-7. It is felt that this may be due to the fact that the pressure distribution near the source is not hydrostatic, a fact that has been noted for free jets, e.g. Miller and Comings (1957) and others. Although attempts were made to include a source underpressure in the governing equations, it didn't make enough difference in the computed results to justify inclusion due to its speculative nature. However, the results are compared below with the assumption of a level water surface as a result of these observations. Additional consideration of this effect is warranted in further data interpretation.

The distance to collapse of the source turbulence was observed to be on the order of 0.8-2.5 meters in general agreement with the findings of Stefan and Hayakawa. The dense layer is characterized by an increase in thickness up to a maximum for stable flows with very little change in the bottom temperatures from the rack at 100 cm to the one further downstream. The mixing zone in some experiments with large source discharges lasted beyond the 1 m location and further increases in dilution are observed at the downstream measurement location. Fig. 4-6 shows the velocity profile at 100 cm and the temperature profiles at 100 and 680 cm for one experiment in which both types of information were obtained. The velocity profile downstream did not satisfy continuity by a considerable amount and it is suspected that the source discharge was recorded incorrectly for that

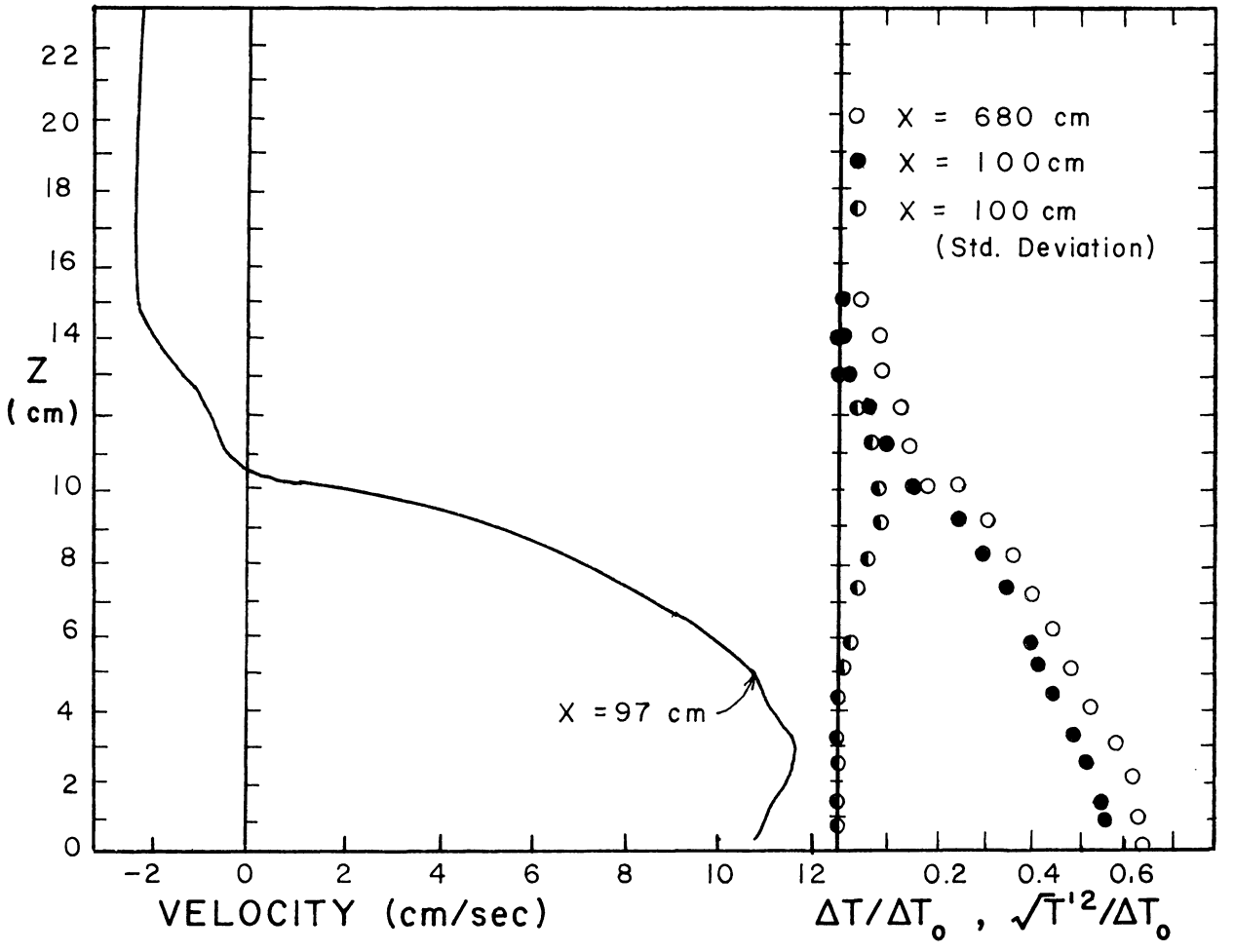

Figure 4-6. Velocity and Concentration Profiles For Stable Flow (Run 8).

particular velocity measurement. Temperatures are presented in the form of $\Delta T/\Delta T_o = (T_a-T)/(T_a-T_d)$ with T_a and T_d the ambient and discharge temperatures, respectively. The small change in the temperature profiles indicates only minor mixing between the two locations. The idea of a layer collapse into a smaller thickness is not so obvious from this figure, but Fig. 4-3 also indicates little apparent collapse as well.

Self-similar temperature and velocity profiles were not found; this is most evident from the results of another experiment with unstable conditions given in Fig. 4-7. Of course, this result should hardly be surprising given the complex nature of the flow. However, the temperature profiles are quite different. Also, the temperature profiles in Fig. 4-6 for the stable flow are different from those observed by Schläpfer for similar flows with large source openings (about equal to the final layer thickness so that

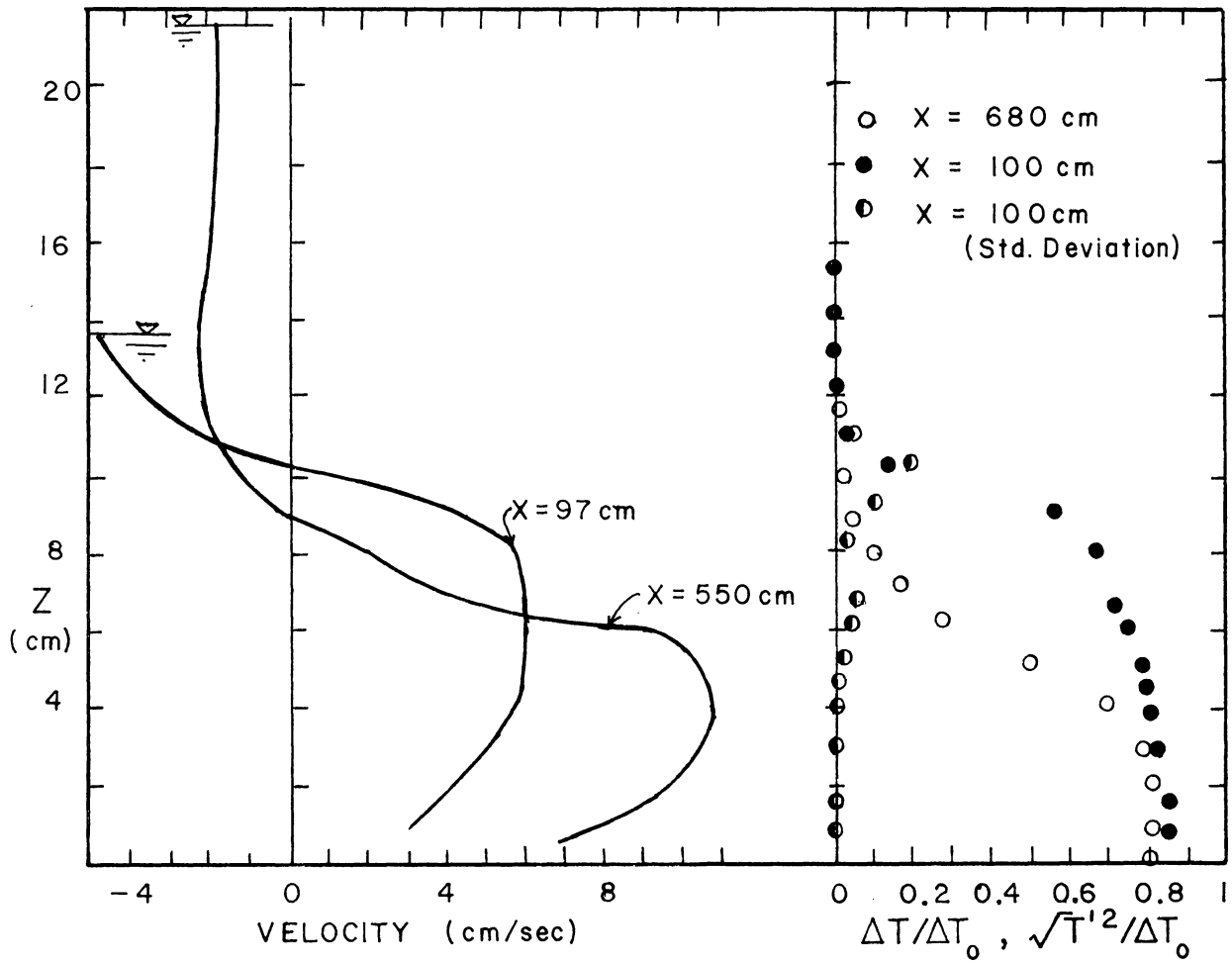

Figure 4-7. Velocity and Concentration Profiles For Unstable Flow (Run 23).

there is essentially no near-source mixing). Both velocity and temperature profiles for all unstable flows clearly indicate the collapse of the mixing layer. Standard deviations of the temperature records at each probe are also presented in Fig. 4-6 and 4-7 and show a quite intermittent flow in the recirculation or roller zone in contrast to the remainder of the flow.

The momentum factor γ_1 in Eq. 2-8 was found to be of the order of 1.15 while γ_2 could reach much larger values due to the fact that the region of upstream flow is generally less than $H-h_1$. At large layer thicknesses, the discrepancy between the two is significant and suggests a more appropriate definition of layer thicknesses may be required.

The temperature profiles at the downstream location were numerically integrated to provide the density scale from which S can be estimated from Eq. 2-11. These are compared in Fig. 4-8 against the theoretical prediction from Eqs. 2-13 and 2-14, both with and without the stagnation pressure included

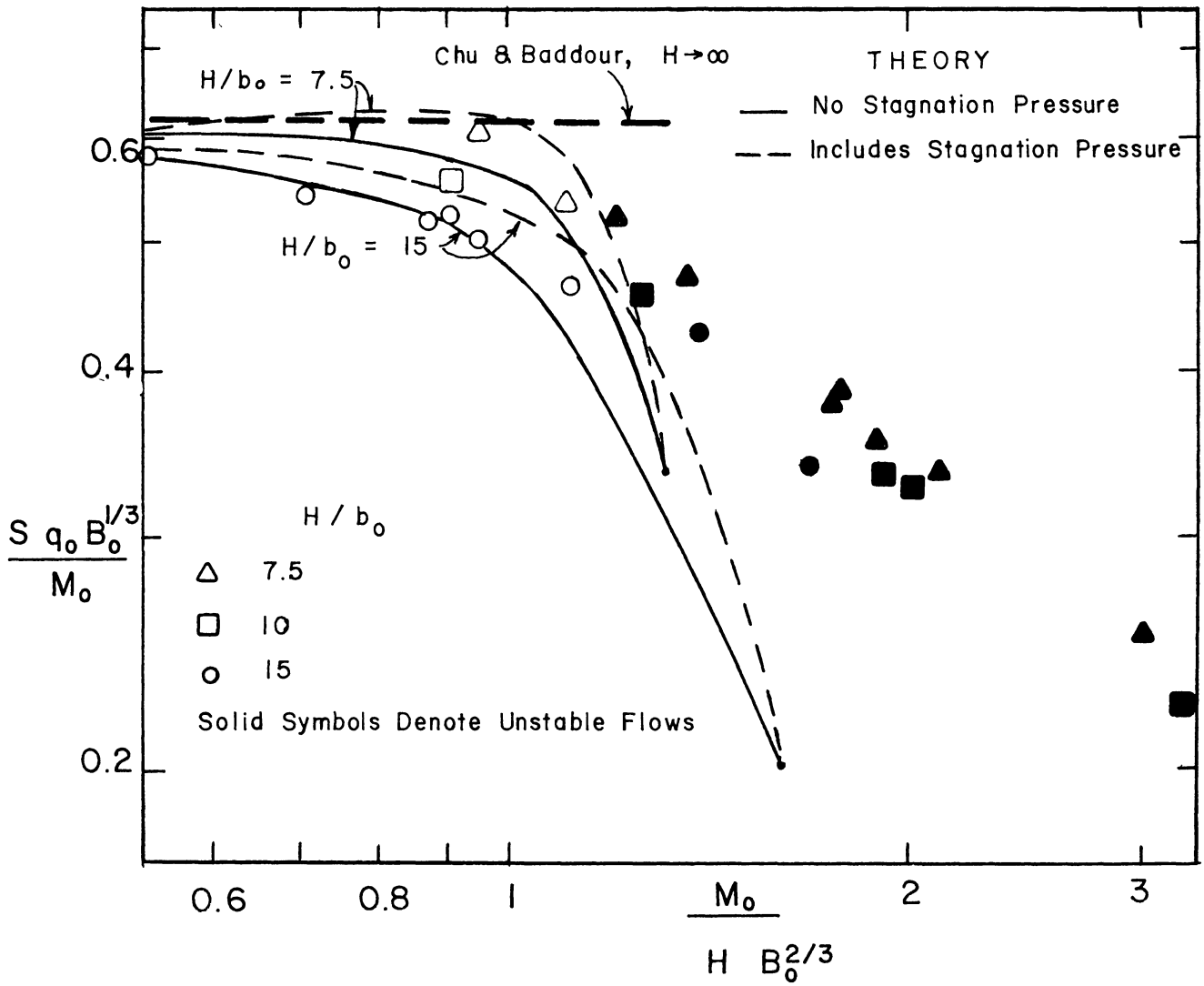

Figure 4-8. Comparison of Observed and Predicted Dilutions.

in the formulation. The theoretical curves correspond to the smallest and largest depths. γ_1 was assigned a value of 1.15 in all analyses while γ_2 was set at 1.25. The other factors were set to unity and the effect of the depth change due to the sloping bottom has been included in the analysis although it only contributes about a 1-2% influence on the results. Other quantities such as the weight component down the slope or bottom friction were estimated to have an insignificant effect over a distance of about 100 cm assumed for the mixing zone length and also partially cancel each other. In terms of the formulation in Eqs. 2-13 and 2-14, only the choice of factors γ_1 and γ_2 have an influence greater than about 2-3%. The solutions are nondimensionalized according to the infinite depth solution,

Eq. 2-15, and the experimental results of Chu and Baddour (1984) which should correspond roughly to this limiting state are also indicated. The data are indicated as visually observed stable oir unstable flows. The predicted transition conditions for onset of unstable flows as defined by Eq. 2-17 are also noted on the curves for the different depths.

The theoretical curves with and without the stagnation pressure included diverge from each other only for certain ranges of source conditions. The lack of agreement for the predictions with the stagnation pressure included is generally within the experimental uncertainty that may be possible due to the estimate of source thickness. It was found that any correction due to this effect would result in further inconsistencies in the predictions; therefore it was concluded that there is not a significant error associated with the source effect. This indicates that the inclusion of the stagnation pressure in the formulation is not justified, and it also conflicts with the visual observations of water surface changes. In general, the agreement with the theory assuming a level water surface is well within experimental uncertainty except as the unstable condition is approached. In these circumstances, the dilution does not drop as rapidly as predicted by the theory; and the dilution did not go to unity at the onset of instability.

If one computes the criterion for onset of the unstable flow condition as given by Eq. 2-17, the agreement with the observations is satisfactory, but not precise. It should be realized however, that the visual layer thickness is different than the scale h_1, so there may not necessarily be a correspondence between predicted and observed values. Also, the upper layer volume flux did not vanish in accordance with the theoretical argument, so the criterion should not necessarily be expected to be valid. The data appear to be in better agreement with the approximate condition

$$H B_o^{2/3}/M_o \approx 1.25 \qquad 4\text{-}1$$

As mentioned previously, the extreme lack of two-dimensionality associated with the unstable flows led to the conclusion that it would be futile to attempt to describe the results with a two dimensional model. Therefore, a description by dimensional analysis guided by the nondimensional forms of Eqs. 2-13 and 2-14 was attempted. The results in Fig. 4-9 show that the most significant variable for the unstable flows appears to be $\mathbf{F}_*^2 = q_o^3/B_o H^3$ and other choices of nondimensional parameters resulted in less satisfactory correlation. Except for the one experiment right at the transition to unstable flow, all data fall within 3% of the indicated empirical curve. Of course, the dilution should approach a limit of 1.0 in the limit as $\mathbf{F}_* \rightarrow 1$ and it is recognized that due to the lack of variation of source width in the experiments, q_o and M_o can be regarded as equivalent parameters. It is not intuitively obvious that the dilution should increase with source buoyancy flux B_o and this result needs to be examined further. However, this sort of relationship is also implied for flows with density current head control, Eq. 2-31, and therefore this finding may imply that the location of the detachment point is controlled by some type of density controlled exchange process which in turn controls the total dilution. It may be worthwhile

to consider if the exchange process can be described on the basis of an energy loss argument, e.g. that the discharge dissipates a maximum amount of energy in this configuration or some similar argument.

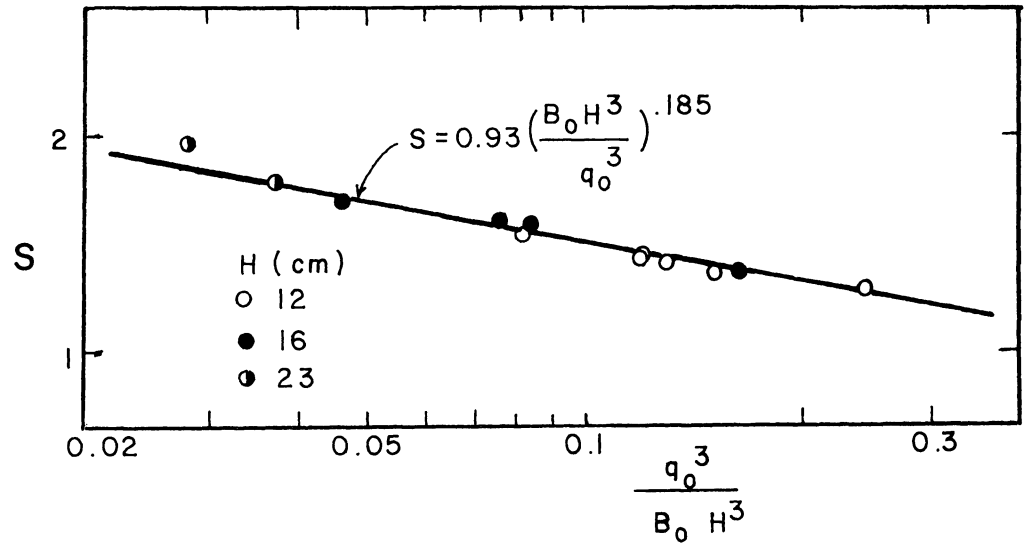

Figure 4-9. Observed Dilutions For Unstable Flows.

Series 2 - Constant Depth Experiments

Objectives

This set of experiments was intended to examine the more general situation of the density jump with a variety of downstream controls somewhat similar to Wilkinson and Wood (1971) except that the effect of the limited depth was also to be examined in these experiments. Also, the entrainment of ambient fluid was to be measured whereas Wilkinson and Wood concentrate only on the measurement of layer depths. Stefan and Hayakawa (1972) also measure entrainment rates for some experiments similar to these except that they only examined flows in which the layer was less than the entire depth. Also, their channel was relatively short with a withdrawal device which establishes the downstream control. The experiments of Chu and Baddour (1984) are similar in this latter regard.

With the rather interesting flow behavior anticipated for the density current, it was desirable to look at this problem as one case of possible downstream control. It was also of interest to examine the case of friction control from the point of view of establishing the behavior when the downstream layer submerges the source since this may be of great practical importance. A desirable objective is to evaluate how significant the friction effect must be to produce significant decreases in mixing. From this, the relative importance of interfacial friction in prototype applications can be more readily assessed.

Results

27 different experiments were performed in this series; the conditions for each are provided in Table 4-2 Hydrogen bubble measurements were also made for several cases as noted in the table; again these were separate experiments and there is not always an exact correspondence of all test parameters. Runs 1A-14A were made with a 14.4 m length of inner channel while the remainder were made with a 4.8 m long channel. Temperature records were lost for runs 5A and 15A, so only a limited amount of information is available from those experiments. Most of the experiments have visual observations of the density current head propagation history recorded on the original data sheets; information for the others can be extracted from the temperature records since the bottom probes were installed during these experiments. In addition, photographs were often taken, both of the density current head and the final steady state flow as noted in the table. There were also a few experiments in the final set of series (described in the next section) performed with no ambient current (four temperature measurements and 6 hydrogen bubble velocity profiles). These are essentially the same experiments as those in the 14.8 m long channel, except for the slightly different source configuration.

Table 4-2. Experimental Conditions for Series 2 Experiments

RUN #	Discharge liters/sec	b_o cm	$\rho_{amb.}$ gm/ml	$\rho_{disch.}$ gm/ml	T_a °C	T_d °C	H cm	Velocity Profile Dens.	Curr.	Steady
1A	0.855	1.0	1.0001	1.0077	16.9	4.8	23.3			
2A	0.681	1.0	1.0000	1.0077	18.6	4.8	23.1			
3A	1.490	1.0	0.9999	1.0073	18.3	4.75	23.9			
4A	1.423	1.0	1.0000	1.0048	17.5	4.85	23.8	x		
5A	1.379	1.0	1.0000	1.0047	17.5	4.80	12.2			
6A	1.423	1.0	1.0000	1.0101	17.6	5.05	12.0			
7A	1.194	1.0	1.0001	1.0073	18.0	4.75	51.6			
8A	0.741	1.0	1.0000	1.0083	17.7	6.45	51.2			
9A	0.563	1.0	1.0000	1.0083	17.8	6.25	51.1			
10A	0.796	1.0	0.9999	1.0099	19.5	4.85	51.3			
11A	0.897	1.0	1.0001	1.0090	20.4	4.45	51.3			
12A	1.473	6.6	1.0000	1.0046	20.4	4.83	51.8			
13A	1.561	9.9	0.9999	1.0023	20.3	4.46	30.7			
14A	1.710	8.8	0.9999	1.0023	19.0	5.09	30.8			
16A	0.937	1.23	0.9999	1.0065	19.2	5.28	50.6	x		x
17A	0.998	1.23	1.0000	1.0041	18.1	4.44	50.7			
18A	2.326	1.23	1.0000	1.0049	18.7	4.35	51.7	x		x
19A	2.419	1.23	1.0001	1.0087	18.1	4.35	51.7			
20A	0.956	1.23	0.9998	1.0071	20.0	4.45	23.4	x		x
21A	2.383	1.23	0.9997	1.0072	19.6	4.25	24.5			
22A	0.584	1.23	0.9998	1.0071	19.5	4.8	23.3			
23A	0.662	1.23	0.9998	1.0066	19.1	4.9	23.3			
24A	1.306	1.23	0.9998	1.0038	19.4	4.5	23.7			
25A	1.473	1.23	1.0000	1.0043	18.0	4.88	11.7	x		
26A	0.563	1.23	1.0000	1.0043	18.0	5.6	11.25	x		x
27A	1.059	1.23	0.9999	1.0051	18.8	4.6	11.5	x		x

The data in the shorter (4.8 m long) channel were normally with the downstream plate installed so that a free overfall condition did not occur at the channel exit. In some cases, the plate was installed after an initial measurement with the free overfall. For these experiments, the temperature records consist of groups of 1600 samples/probe with different plate positions. Typically, the first group consisted of the measurement of the unsteady density current with succeeding groups of measurements at steady state conditions with different degrees of downstream blockage. Runs 16A and 17A have six and seven groups of data, respectively, while the others have two to four. The original data sheets describe the details of these and would need to be referred to in any data reduction effort. In a few cases, special types of measurements were made; for example, measurements of the unsteady internal wave propagation that was observed after the density current reached the end of the channel as discussed below. In this entire series of experiments, there are approximately 75 different test conditions and a considerable amount of data processing is required to extract all of the information. In the case of the density current head data, some sort of moving average of the temperatures will be required to properly interpret the data. This has not been done at present except for a few cases. Appendix A describes the format in which the data is stored.

Information on the observed propagation histories of the density current head provides some quite interesting observations. Typical propagation histories for several experiments are given in Fig. 4-10. It can be seen that propagation velocities are quite constant over the length of the channel except in a few instances, such as Runs 2A and 12A. These runs were with the lowest source discharges and smallest layer thicknesses and are probably influenced by viscous effects. Therefore, the data interpretation for these experiments should not probably be considered within the framework of the analysis of Chapter 2, since the effect of friction was ignored in the theoretical development. It was always possible to distinguish the experiments with small layer thicknesses from those with larger ones by the nature of the flow in the vicinity of the density current head. Photographs of the flow at the heads for typical conditions are given in Fig. 4-11 and show quite clear differences. The small head thicknesses show considerable mixing behind the heads while little or none is apparent at the larger thickness. Easily apparent is the fact that a layer thickness much greater than .347 H can be achieved. Also interesting is the fact that there is apparently little change from the head thickness to the steady layer thickness for the case of large layer thickness. Many of these experiments were visualized by injecting dyed fluid (which was then more dense than the ambient fluid but less than the discharge fluid) along the bottom of the first one to three meters of the channel. From observations of the flow, the dye flowed up over the head (Fig. 4-12) and then was entrained into the head itself and both transported along the channel and left in the wake of the head. The dye was usually carried in the head over the entire length of the channel although it decreased in concentration with distance. This does not correspond to the suggestion by Simpson and Britter (1979) that the entrainment occurs along the channel bottom at the nose. In fact, the dyed fluid in some cases appeared to be pushed ahead of the density current. Other experiments were made with the dye injection in the source fluid and no apparent

difference between the two flows is seen although the visualization is different. In some cases the source dye was turned on after the density current was already started. In these cases, the dye caught up with the front and then exited through the wake for the flow with small layer thickness, but the effect was not so obvious at greater layer thicknesses.

The dye layer thicknesses are much greater than the theoretical limit of .347 H as suggested by Kranenburg (1978). Fig. 4-13 is a photograph of a long section of the density current for Run 25A and the large layer thickness extends far behind the head. In general, the layers for experiments with large thickness are more or less constant behind the head and then increase further away due to friction. Although Kranenburg includes an friction effect in his analysis (with a kU^2 term to decribe the energy loss and k is the friction factor), it is does not appear that this is sufficient to describe the large layer thicknesses observed. In his analysis of other data, he suggests a value for k of 0.5-1.0 which seems quite high compared to expected values for steady state friction factors which may be on the order of 0.02-0.03. Therefore it is possible that the effect he attributes to friction is due to some other effect; e.g. the theory he discusses neglects mixing between the layers . With his recommended values of k,

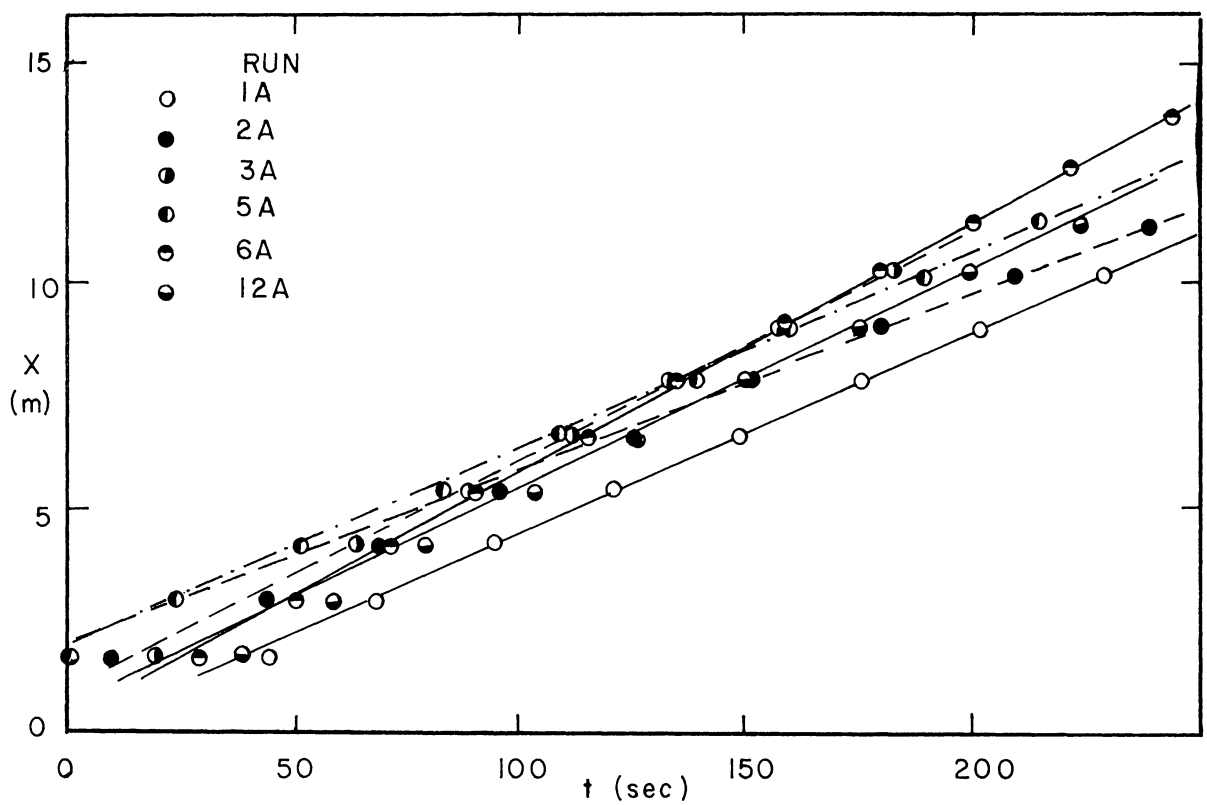

Figure 4-10. Typical Density Current Speeds for Series 2 Experiments.

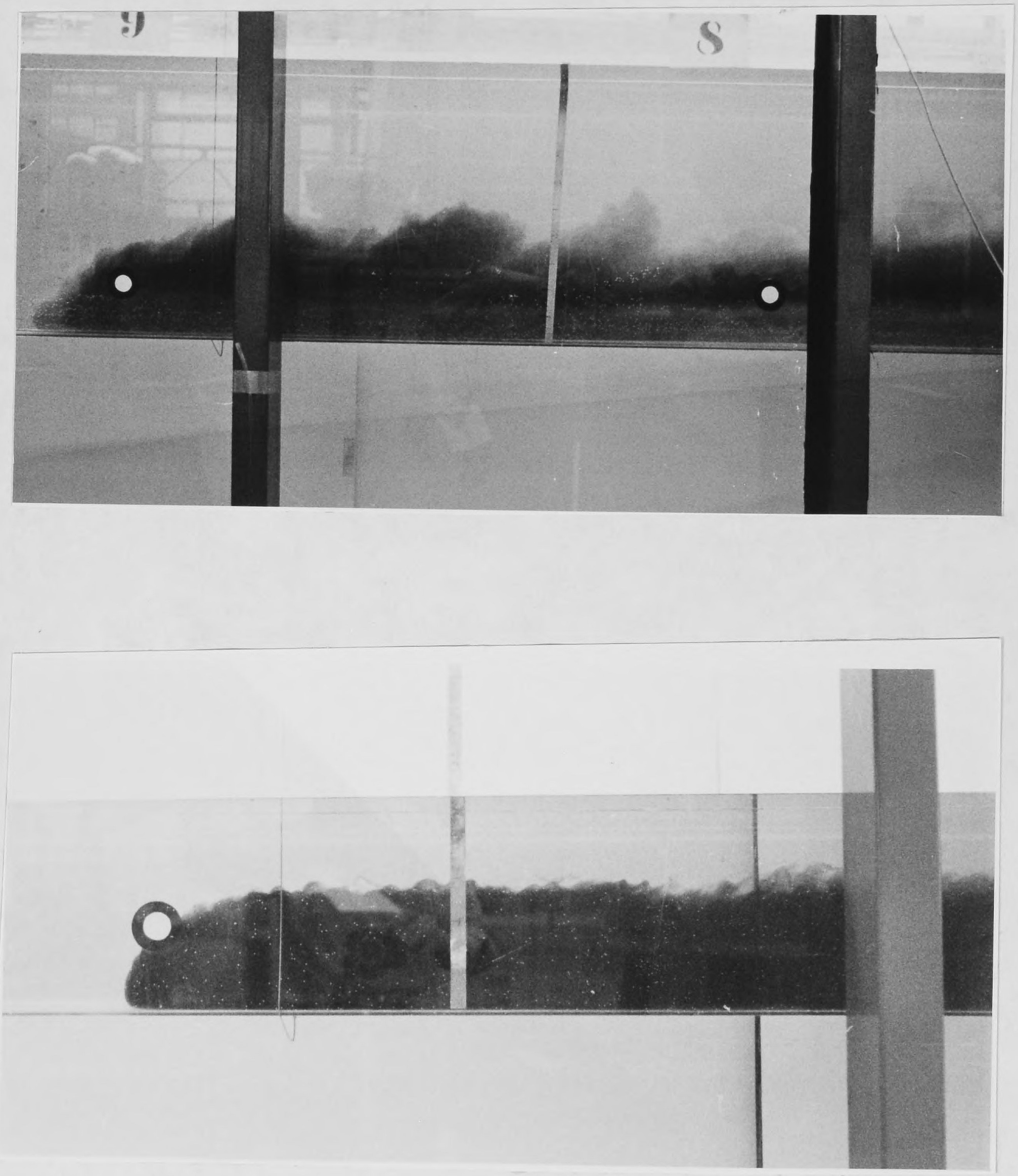

Figure 4-11. Density Current For a.) Thin (Run 7A) ; b.) Thick Layers (Run 3A).

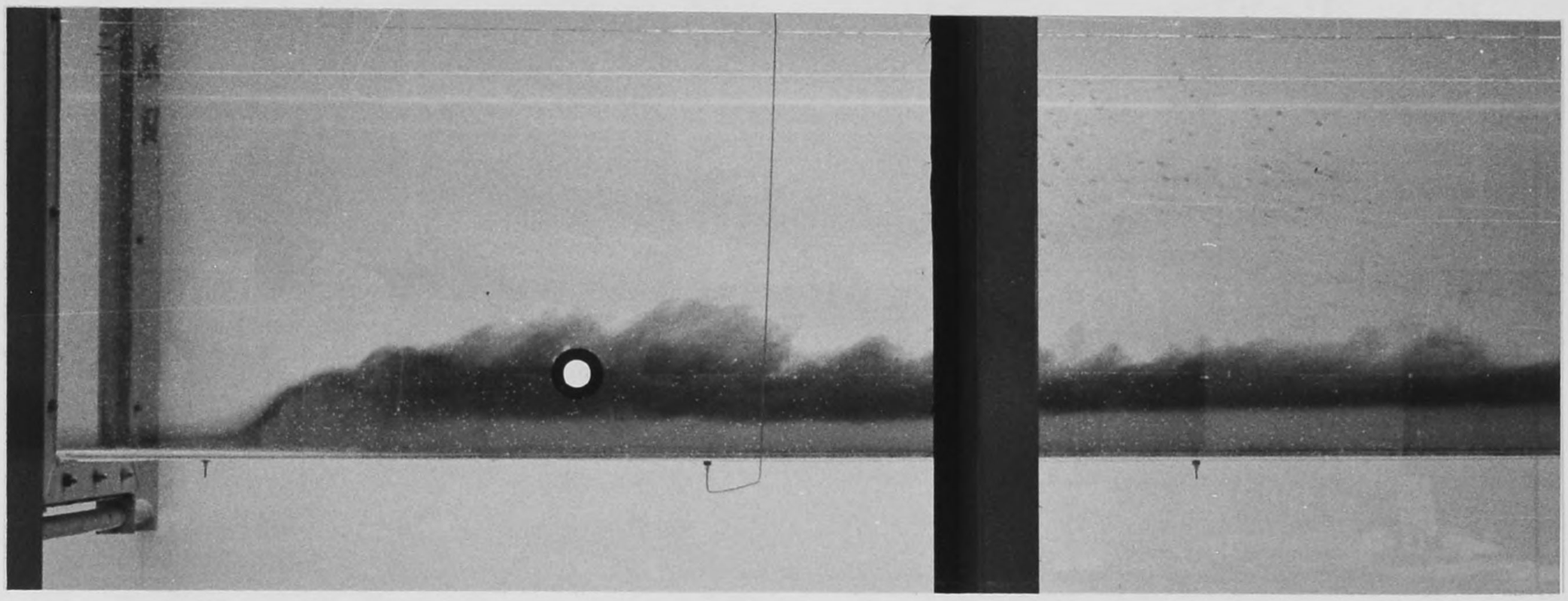

Figure 4-12. View of Density Current with Dye at Channel Bottom (Run 10A).

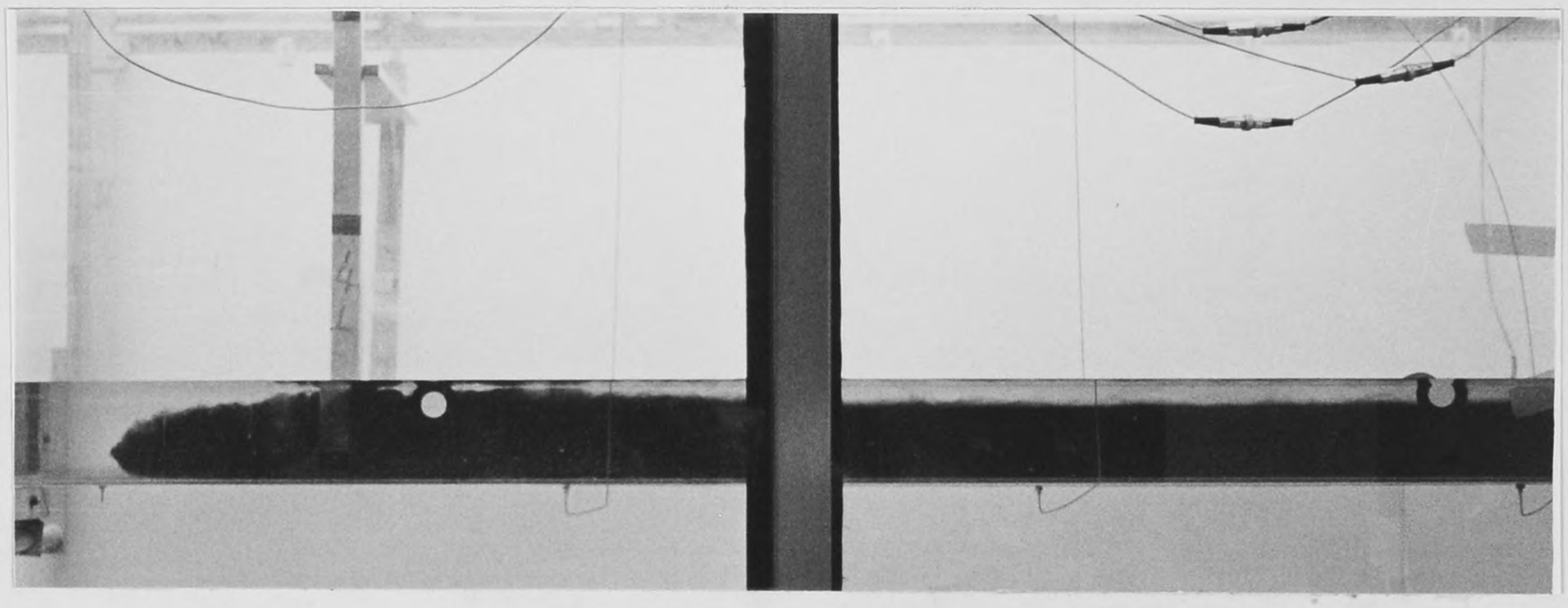

Figure 4-13. Photograph of Density Current From Run 25A.

the maximum η only increases to about 0.43 according to the Fig. 5 in his paper. In order to achieve the visual layer thickness in some of the experiments, values of k in excess of 100 would be required.

It can be argued that the visual layer thickness is not a good measure of the layer thickness, especially in light of the observations by Simpson and Britter (1978) of a significant wake behind the head. However, in Run 25A, both velocity and temperature data can be used to establish the layer thicknesses with alternative definitions. The profiles of each at two different locations behind the head (actually times later than the passage of the head at a single location) for the experiment in Fig. 4-13 are given in Fig. 4-14. The times given are relative to the passage of the density current at the measurement location. It can be seen that the head thickness by whatever measure employed will be far in excess of the critical limit and that there does not appear to be a significant wake with reversed flow near the top of the layer. If one uses Eq. 2-21 along with the occurrence of critical flow in the return layer ($U_2^2/(g'h_2) = 1$), the following relation can be derived:

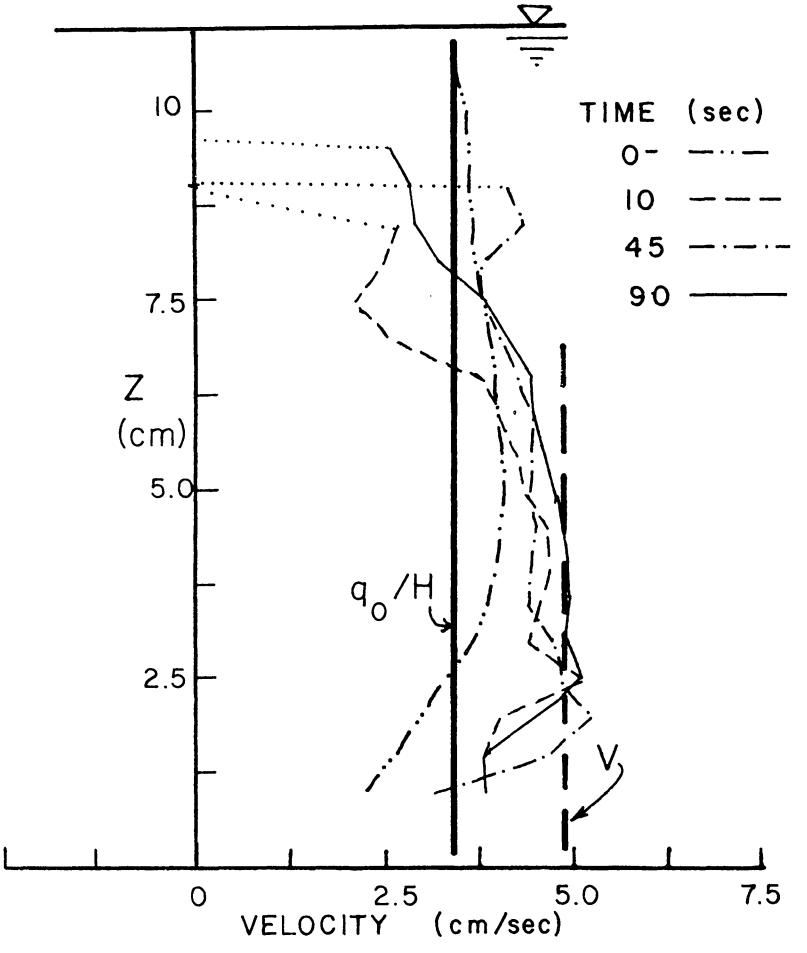

Figure 4-14a. Velocity Profiles at Different Times For Run 25A.

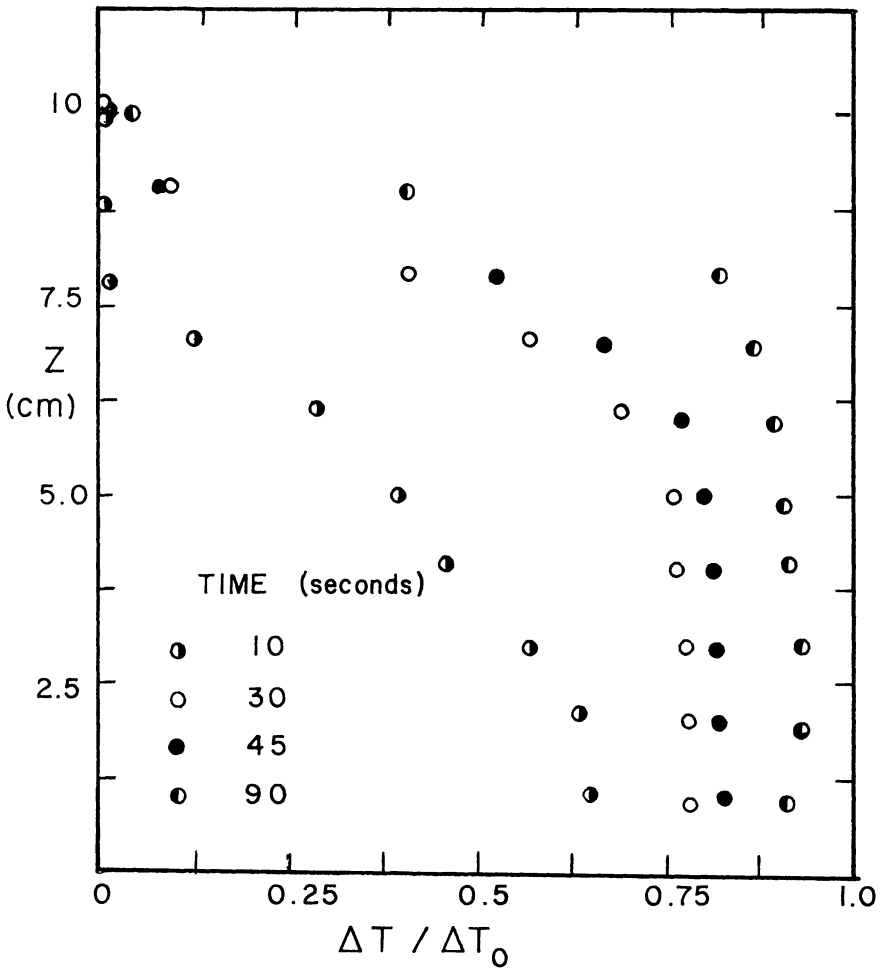

Figure 4-14b. Concentration Profiles at Various Times for Run 25A.

Table 4-3. Density Current Property Data.

RUN #	$(V-q_o/H)^2V/B$	computed η	visual η	
1A	0.325	0.47	0.55	
3A	0.244	0.50	0.57	THICK DENSITY
5A	0.073	0.64	0.63	CURRENTS
25A	0.069	0.70	0.77	
10A	0.578	0.39	0.25	THIN DENSITY
12A	0.516	0.41	0.28	CURRENTS

$$\frac{(V - q_o/H)^2 V}{B} = \frac{h_2^3}{h_1 H^2} = \frac{(1-\eta)^3}{\eta} \qquad 4\text{-}2$$

The left hand side of Eq. 4-2 is independent of the definition of the layer thickness and values for several different experiments are given in Table 4-3. The lack of agreement with the value of 0.8 for a maximum $\eta = 0.347$ is very evident. Therefore, the theory by Kranenburg is invalidated regardless of the choice of layer thicknesses. However, if one uses the value of the constant in Table 4-3 to compute η required to satisfy the equation, the corresponding values are given in a column of the table and are comparable with the visual thicknesses estimated from the photographs which are also given. The correspondence is quite clear only for those experiments with large head thicknesses. Therefore, it appears that the basic idea of a critical flow state is still valid but the theory needs to be revised.

For smaller η values, the results do not indicate a correspondence with the critical flow condition which agrees with the idea that critical flow only occurs for large layer thicknesses. However, there are some obvious discrepancies suggested by the results in Table 4-3 for thin density currents as well. The parameter in the table from Eq. 4-2 represents the densimetric Froude number of the density current head as in Eq.2-29 and should have a value no less than 0.8 which occurs at $\eta = 0.347$. For smaller values of η, the Froude number should be larger. This is not the case for the experimental data presented in Table 4-3 and for the other experiments performed. There are no density currents with a supercritical head speed as implied by Benjamin's theory. It is important to recognize that this method for computation of the Froude number does not rely upon an arbitrary definition of the layer thickness and so avoids the difficulties posed by Britter and Simpson (1978) in which they essentially describe the problem as a three layer flow. This raises major questions regarding the validity of Benjamin's theory for any of the flows studied and whether or not the condition discussed in Chapter 2 where the density current does not provide the downstream control can be attained. Since there are a limited number of experiments to answer these questions, they remain unanswered as this report is written. Further experiments to address these questions are planned for the immediate future. In particular, the question of whether there is a fundamental difference between the density currents from supercritical and subcritical source discharges will be examined.

The temperatures within the layer were found to decrease continuously during the density current head propagation as seen in the results in Fig. 4-14. Since this was also observed in the experiments in Series 1, it is not clear that this represents a truly unsteady nature to the flow or whether it is a secondary effect of minor importance in the interpretation of the results. A careful study of both velocity and temperature profiles is required before definite conclusions can be drawn. However, since

the density current speeds were basically constant, it is expected that the flows may be treated as steady state to a first approximation.

Experiment Run 9A was conducted without draining the tank after the preceding experiment. In this situation, a thin salt water layer remained on the channel bottom when the experiment was begun. The density current propagation is indicated in the photographs in Fig. 4-15. The nonlinear internal waves are similar to those reported by Amen and Maxworthy (1980) and Maxworthy (1980) associated with intrusions in stratified fluids and must be due to the residual stratification at the inner channel bottom. This indicates that in some prototype problems with a small degree of stratification, the propagation of the density current may be significantly different from that in an unstratified environment.

Internal wave propagation also occured in every experiment when the density current head passed from the channel, i.e. when the control was switched to the free overfall at the downstream end. After the density current left the channel, the layer thicknesses always increased and the dilutions decreased. The influence was apparent in the form of internal waves which propagated upstream and flooded the source region which in turn reduce the entrainment region and the volume flux in the layer. This would in turn tend to reduce the layer thickness and thus the control depth at the downstream end of the channel. Fig. 4-16 are photographs of the interfacial waves in an extreme situation where the downstream end was partially blocked, but similar though smaller waves occurred in the other experiments. This complicated feedback system resulted in a very long time for the flow to approach steady state. The thickness and concentration scales (Eqs. 2-5 and 2-6) for a particular probe rack are indicated in Fig. 4-17 as functions of time and clearly indicate the wavelike nature of the flow adjustments. This particular experiment was in the 4.8 m channel and the motions are still apparent in the temperature record after 1000 seconds. In general, about 25 minutes was required in the longer channel before the amplitudes of these temperature oscillations decreased sufficiently to approximate the flow as steady state. Independent verification with the conductivity measurements showed the same thing, i.e. steady state was not achieved for long periods of time. Consequently, nearly all experiments in the longer channel were run 33 minutes to get a sufficiently long temperature record. In the 4.8 m channel, the time to steady state was more like 8 to 10 minutes; in fact, the reason the shorter channel was used was mainly to be able to study more than one downstream condition in the same experiment. Nevertheless, the range of experimental discharges that could be studied were much more limited than in the first series due to these long times required to attain steady state.

The temperature racks were placed at 35, 100, 615, and 1230 cm from the source for the first group of experiments and at 35, 100, 247 and 432 cm for the second. The furthest downstream rack was intended mainly to provide a definition of the downstream condition. The flow appeared to be of the free overfall type as indicated in the photograph in Fig. 4-18. However, vortices with vertical axes were observed to be generated in the upper layer. Since the critical depth doesn't necessarily occur precisely at the end of the channel, it was decided to directly measure the downstream condition.

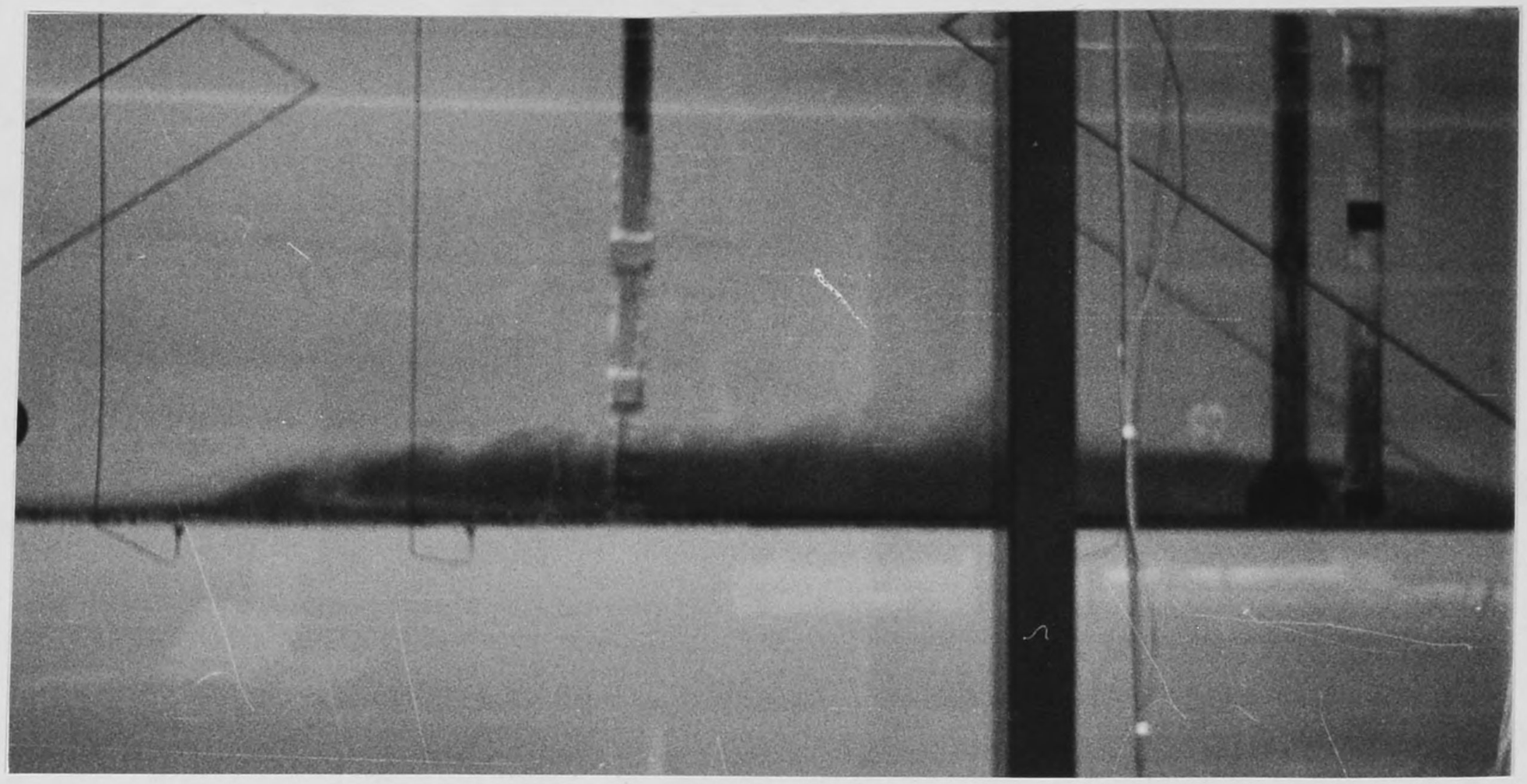

Density Current at About 1.5 m From Source.

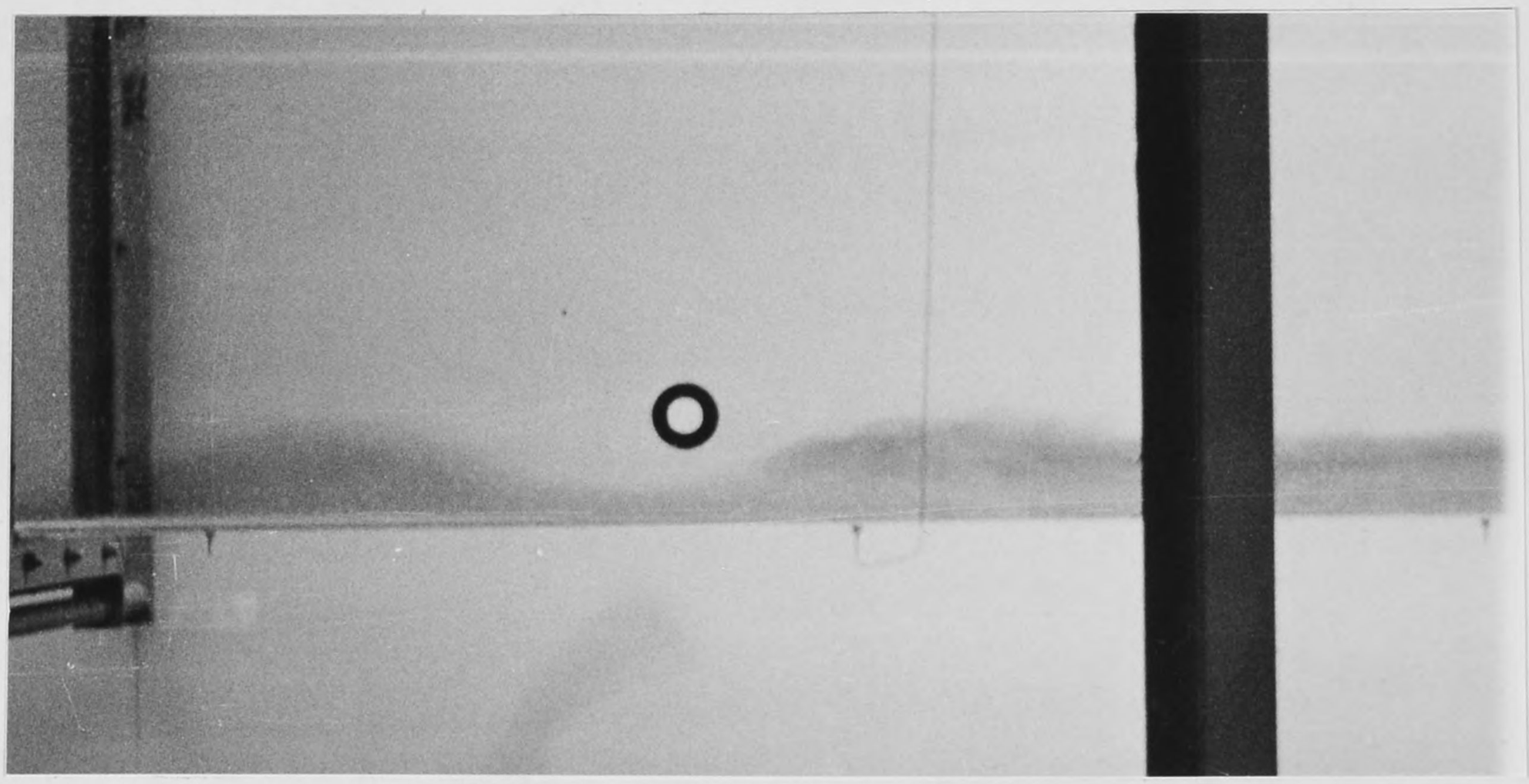

Density Current At About 4 m from Source.

Figure 4-15. Photographs of Density Current In Internally Stratified Fluid.

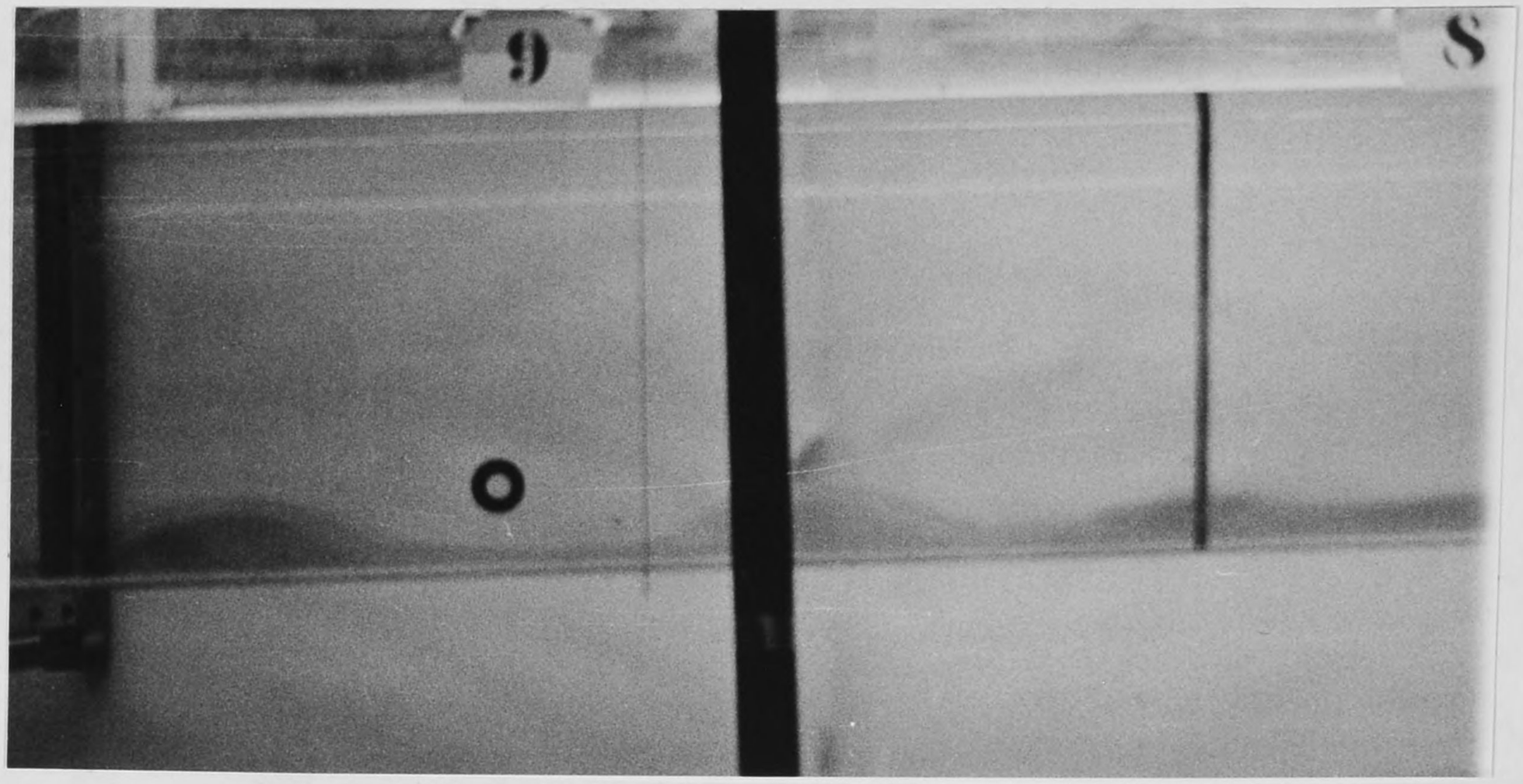

Density Current at About 9 m from Source.

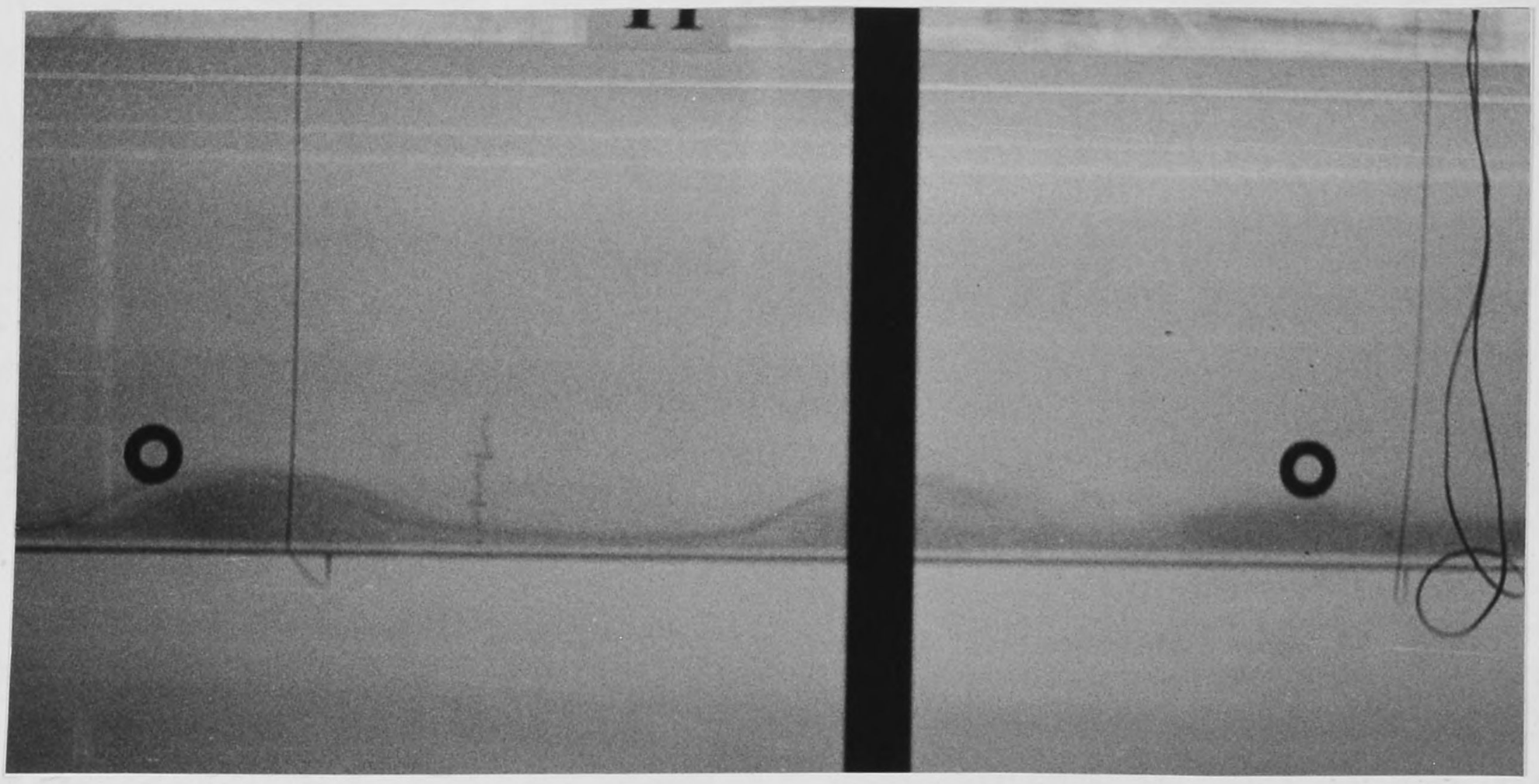

Density Current at About 11 m from Source.

Figure 4-15(continued). Nonlinear Internal Waves.

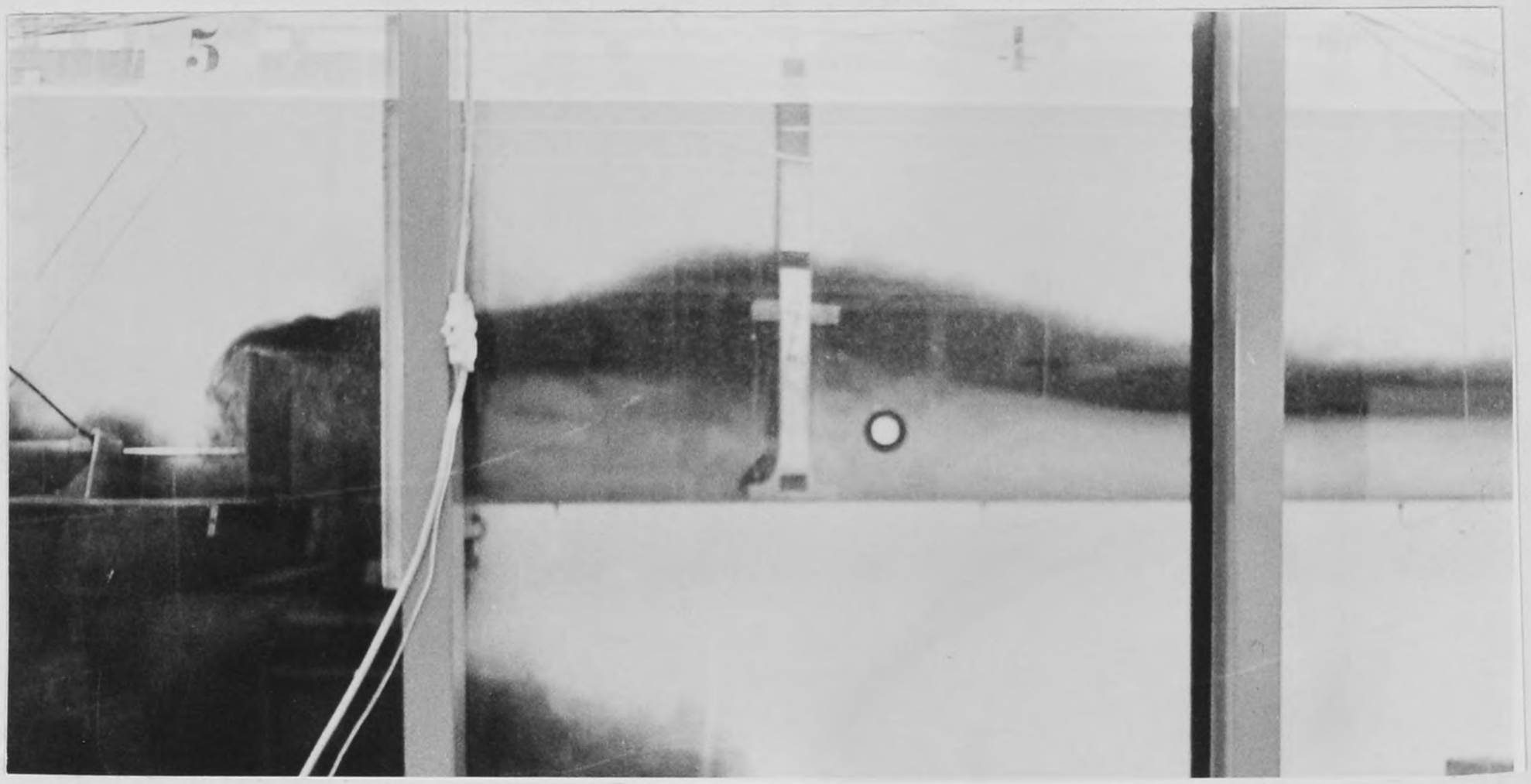

Figure 4-16. Photograph of Interfacial Wave Due to Channel End Effect (Run 17A).

It was found to be possible to completely halt the near-source dilution in contrast to the case in the first series. These were for a few experiments in which the ambient fluid formed a clear intrusion wedge such as described by Singh and Shah (1971) or Denton (1980b). So long as the wedge penetrated up to the source mixing zone, then dilution occurred, i.e. there was a net upstream flow in the secondary layer. The wedge formation never occurred during the propagation of the density current, but always during the approach to steady state after the head had left the channel. This lends support to the concept of the shifting of the downstream control under these circumstances.

The occurrence of near-source dilution was found even for cases of extreme downstream blockage. Although sucessively less dilution occurred with increasing blockage, it was impossible to halt the mixing until the wedge formation occurred; when this occurred, the wedge generally propagated fairly rapidly downstream until it reached an equilibrium position. In experiment 22A, the layer thickness with the unblocked end was on the order of 9 cm. A series of different degrees of blockage that created successively higher layers up to about 21 cm were studied. Fig. 4-19 is a photograph of the source region a short time after the dye supply was turned off in the discharge. There is very little dilution in the clearly defined roller region and all entrainment is observed to occur at the downstream end of the roller, i.e. just near the location of the turbulence collapse. Again, this indicates that the often-quoted suggestion that entrainment stops when the roller blocks the jet is only a qualitative argument that should not be used in place of the overall momentum balance given in Chapter 2.

Otherwise, generally similar observations as to the nature of the flow as noted in the first series were also found in these experiments. Since the data analysis is incomplete, a presentation of results similar to that for the experiments in Series 1 is not provided herein.

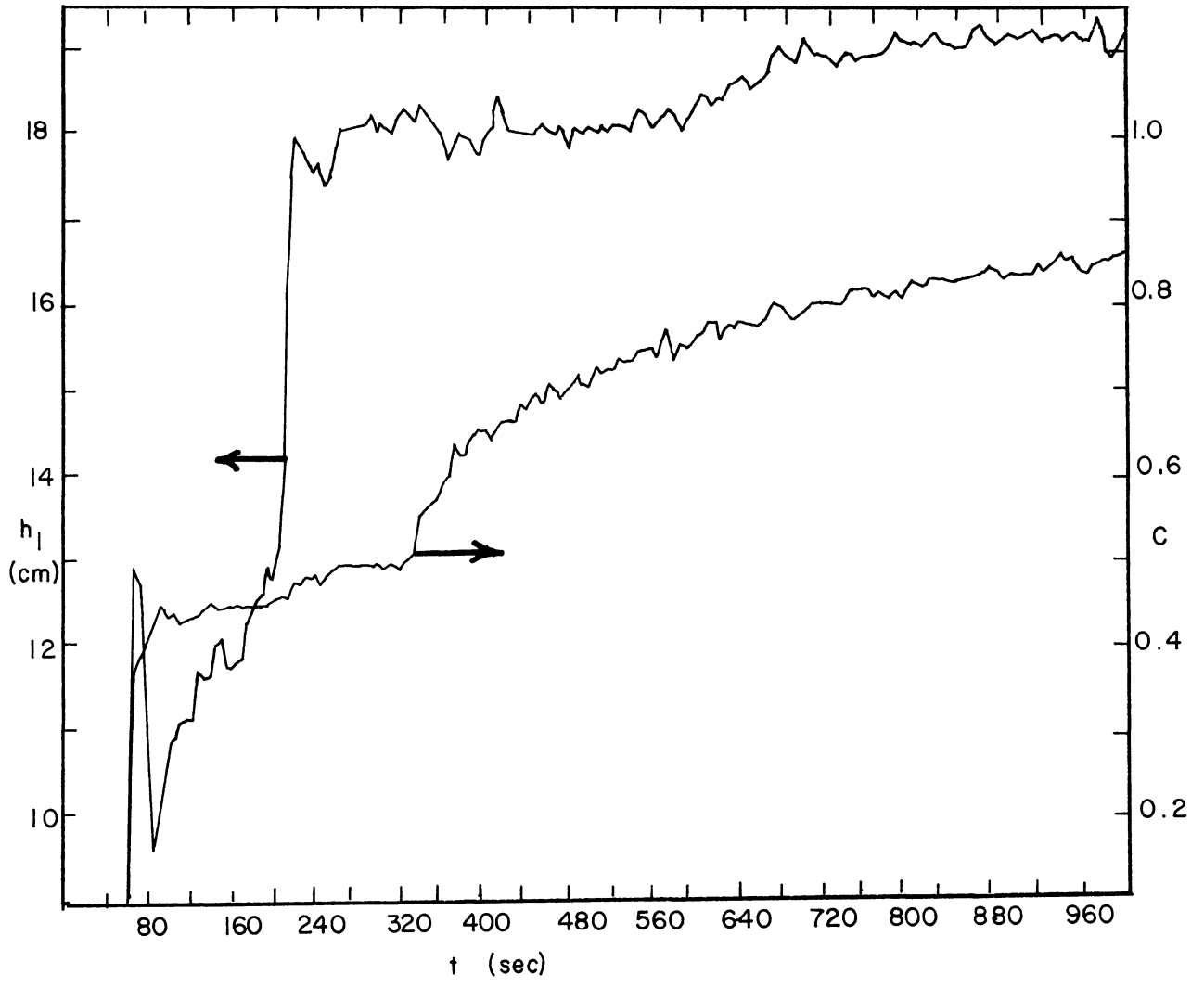

Figure 4-17. Time Histories of Layer Thickness and Concentration for Run 17A.

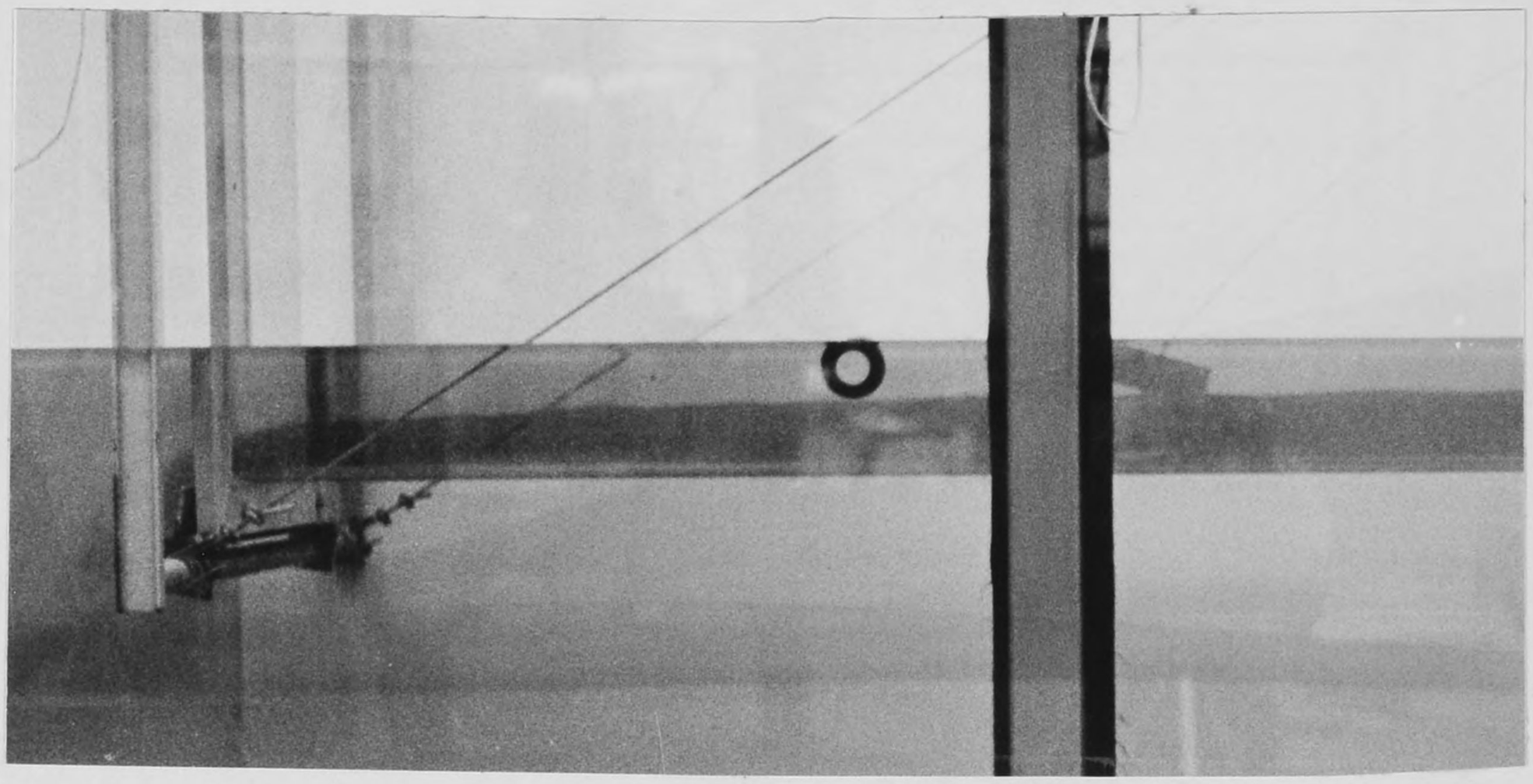

Figure 4-18. Downstream End Condition for Unblocked Channel (Run 6A).

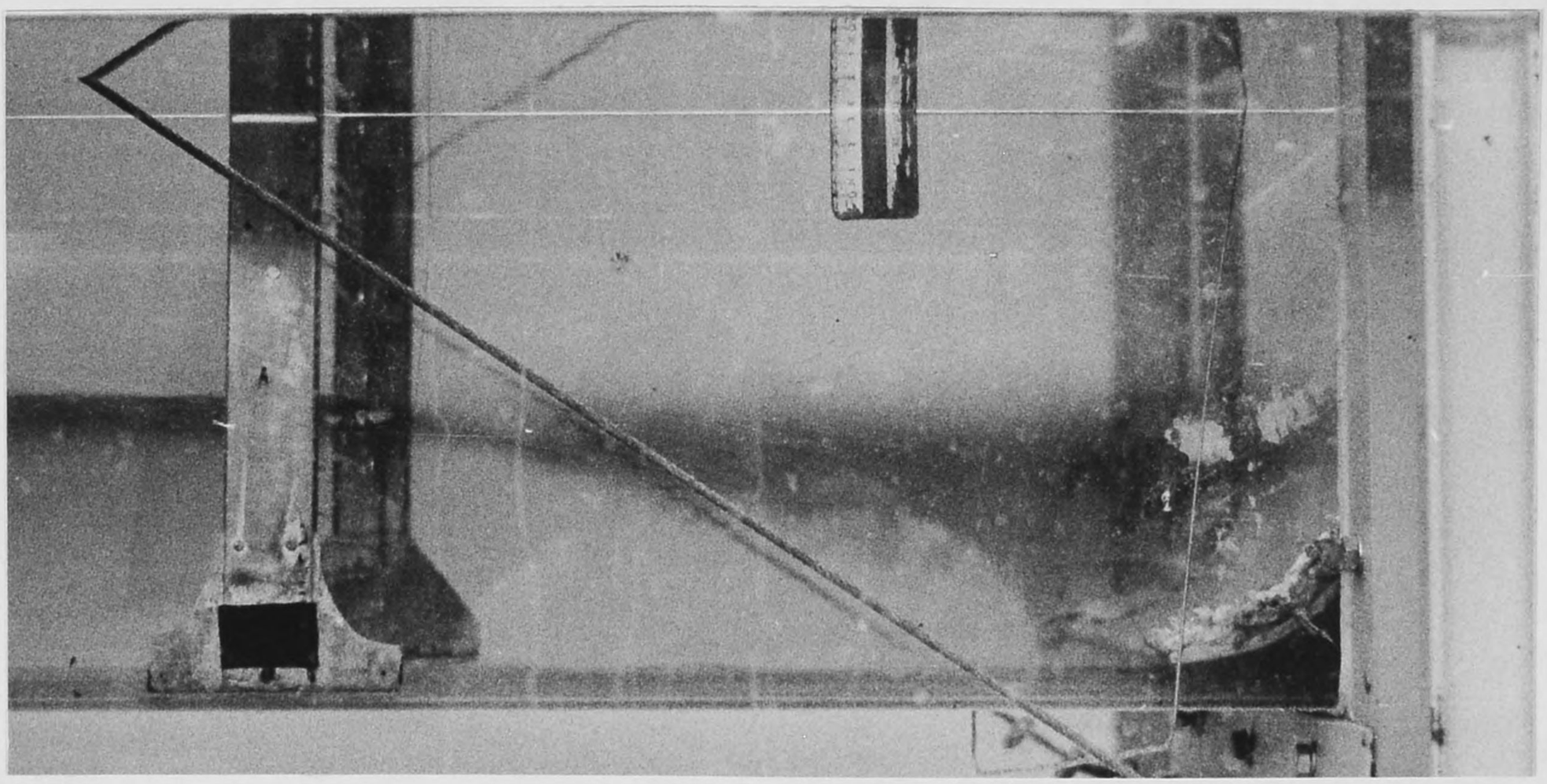

Figure 4-19. Visualization of Roller Region for Downstream Blocked Flow.

Series 3 - Constant Depth Experiments With Ambient Current

Objectives

This final set of experiments in many ways is independent of the first two although there are many parallels. The main objective was to add another aspect to the problem, especially since Wood and Simpson (1984) do not provide measures of entrainment rate and the results of Bewick (1974) are ambigous. Bewick found only marginal agreement with the theory developed in Chapter 2 and attributed this to departures of the velocity and density profiles from their assumed uniform values. However, it has already been discussed how these effects can be included in the analysis and the results from the first series of experiments in this study appear satisfactory in most regards. With respect to the basic momentum balance with significant layer depths, there are some excellent test cases to the theory. For example, one condition is when the flow in the upper layer is reversed downstream from the mixing zone. Also there is another situation where the discharge just entrains all the ambient flow. These criteria can be judged much more easily than, e.g., the occurrence of unstable flows. Since all previous experiments in this study represent cases of counterflow and also since the theory indicates enhanced entrainment for coflowing cases, it was decided to perform these types of experiments.

There is also little information available on the propagation of a density current in a coflowing stream, although, according to the simplified theories, the problem should be the same except for a coordinate transformation. However, from the results in the previous series, there are good reasons to question the validity of the basic approach and the experiments provide a good means of further examining various aspects of this problem.

Results

The number of experimental parameters becomes nearly unmanageable from the point of view of experimental design for this problem. However an attempt was made to try to study all relevant influences. The slot opening was fixed for the reasons discussed in Chapter 3. The source density was maintained at a single value for all experiments except for the last fifteen for which the salt concentrations were approximately tripled. There are thus two groups of experiments with respect to this variable. Primary experimental variables are the depth, discharge, and ambient velocity. Typically, the experiments were performed at a particular depth keeping either the discharge or the ambient velocity fixed while the other parameter was varied over a range of four or five values. In some cases, the zero ambient flow was studied as well although the experiments were designed to complement the experiments in series 2 as much as possible; the data in series 2 correspond to the zero ambient velocity case of several experiments in this section.

A total of 43 different temperature measurements were made. Table 4-4 summarizes the tests and experimental conditions. In general, it is correct to visualize these experiments as analogous to those in the long channel in series 2 except for the addition of an ambient flow. One important difference in the

experimental configuration, however, is that if the source discharge was stopped and the ambient flow continued to circulate in the flume, the salt water could be flushed out of the inner channel. This led to the decision to try to obtain hydrogen bubble data for most experiments. The experimental procedure was altered to make the hydrogen bubble measurement in the density current, then stop the salt water flow, and circulate the ambient flow for several minutes until all salt water was flushed from the inner channel. Then the temperature measurement was performed along with photographing the flow and the visual observations of the density current propagation. After completion of the temperature measurement, hydrogen bubble measurements of the steady state were usually made. Therefore there are almost three times as many velocity profiles as for series 2. In some cases, zero ambient velocity hydrogen bubble measurements were made at the beginning of the experiment. The notes in Table 4-4 indicate the nature of the information collected. Appendix A also describes the format and measurement conditions in more detail.

The time to steady state for the flows varied considerably depending upon the ambient velocity but generally were much reduced compared to the experiments in the second series. In general, it can be stated that unless the flow in the upper layer was reversed, which it was in some cases, then the time to approach steady state usually lay in the range of 5-15 minutes with the shortest times for the largest ambient velocities. The data therefore consist of various sampling frequencies and record lengths. In many experiments , the temperatures were sampled at a higher frequency within the density current and at a lower frequency thereafter.

The thermistor racks were located at 37, 100, 564 and 1240 cm from the source in a similar fashion to those in series 2. In general, it was observed that the mixing region was advected further downstream, e.g. compare the general nature of the flow in Fig. 4-20 with that indicated in Fig. 4-3. Therefore the rack at 564 cm was not always downstream of the point where the turbulence was damped and there are a few experiments where it is not clear from visual observations whether the mixing completely ceased over the length of the channel. Since there was an ambient input of fluid from the upstream side, the flow did not generally recirculate as in the other cases, although this was possible for very low ambient velocities. However, the flow can still mix over the entire depth. There were several interesting phenomena that were observed during the experiments. In one case, the flow velocity downstream was uniform over the entire depth but there was a thin (approximately 1 cm) unmixed layer at the free surface. In other cases, an intrusion wedge was observed to form (the layer extended over the entire depth in the region near the source); in these cases the flow in the upper layer was essentially stagnant far downstream and all of the ambient flow was entrained by the source discharge. It was possible with proper combinations of source and ambient discharges to find the conditions that were associated with reversal of flow in the upper layer or mixing over the entire depth. Both of these were not necessarily possible for a given ambient flow, for example, but these types of transition cases were defined insofar as possible.

Table 4-4. Experimental Conditions for Series 3 Experiments.

RUN #	Source Disch. l/sec	Ambient Disch. l/sec	b_o cm	$\rho_{amb.}$ gm/ml	$\rho_{disch.}$ gm/ml	T_a °C	T_d °C	H cm	Velocity Profile Dens. Curr.	Steady
1B	0.924	4.65	1.098	1.0001	1.0052	17.4	4.8	50.3	x	x
2B	0.897	2.40	1.098	1.0001	1.0052	16.5	4.9	50.3	x	
3B	1.199	9.5	1.098	1.0003	1.0054	15.8	4.6	50.5		x
4B	0.936	9.6	1.098	1.0003	1.0054	16.0	4.55	50.3	x	x
5B	1.623	9.5	1.098	1.0001	1.0052	17.4	4.75	50.7		x
6B	1.615	4.76	1.098	1.0002	1.0052	16.7	4.65	50.7		x
7B	1.615	2.37	1.098	1.0004	1.0052	16.9	4.7	50.7		x
8B	1.615	1.68	1.098	1.0001	1.0055	17.2	4.62	50.7		x
9B	1.615	0.0	1.098	1.0002	1.0054	16.2	4.5	50.7		x
10B	1.696	2.04	1.098	1.0002	1.0052	16.6	4.7	23.4		x
11B	1.561	2.04	1.098	1.0000	1.0058	18.5	5.15	23.3	x	x
12B	1.297	2.04	1.098	1.0001	1.0052	17.6	4.9	23.2		x
13B	0.988	2.08	1.098	1.0000	1.0053	18.6	4.6	23.0	x	x
14B	1.179	2.04	1.098	1.0000	1.0053	18.1	4.66	23.1		x
15B	0.681	1.97	1.098	1.0000	1.0052	17.8	4.8	22.8	x	
16B	1.00	6.0	1.098	1.0001	1.0051	18.2	4.9	23.0	x	x
17B	1.00	4.1	1.098	1.0002	1.0051	17.5	4.85	23.0		x
18B	1.00	3.02	1.098	1.0001	1.0052	17.9	4.65	23.0		x
19B	1.00	1.07	1.098	1.0002	1.0056	17.6	5.23	23.0	x	x
20B	1.00	1.72	1.098	1.0001	1.0053	17.4	4.83	11.3	x	
21B	1.00	0.88	1.098	1.0000	1.0053	17.6	4.78	11.3		x
22B	1.0	0.58	1.098	1.0000	1.0053	18.0	4.94	11.3		x
23B	1.538	1.96	1.098	1.0001	1.0052	17.5	4.95	11.6	x	x
24B	1.37	1.07	1.098	1.0001	1.0055	17.7	4.94	23.2	x	x
25B	1.608	1.07	1.098	1.0000	1.0052	17.3	4.79	23.3		x
26B	1.608	4.1	1.098	1.0000	1.0050	17.1	4.78	23.3	x	
27B	1.414	4.1	1.098	1.0000	1.0050	16.6	4.90	23.2		x
28B	0.988	0.0	1.098	1.0000	1.0122	19.1	5.07	23.0	x	x
29B	0.988	1.0	1.098	1.0000	1.0122	18.3	5.07	23.0	x	x
30B	0.924	4.1	1.098	1.0001	1.0123	17.9	4.80	22.9		x
31B	0.924	1.82	1.098	1.0001	1.0123	18.0	4.97	22.9		
32B	1.440	1.0	1.098	0.9999	1.0121	19.2	4.90	23.2	x	x
33B	1.178	1.03	1.098	1.0000	1.0122	18.2	4.87	23.1		x
34B	1.746	1.05	1.098	1.0000	1.0123	17.8	4.79	23.4	x	x
35B	1.012	0.0	1.098	1.0000	1.0122	17.7	4.79	50.4	x	x
36B	1.012	2.48	1.098	1.0000	1.0121	17.8	4.38	50.4		x
37B	0.975	9.5	1.098	1.0000	1.0124	17.5	4.38	50.4	x	x
38B	0.963	9.5	1.098	1.0001	1.0124	17.3	4.75	50.4		x
39B	1.024	4.7	1.098	1.0000	1.0122	18.0	4.40	50.4		x
40B	2.279	0.0	1.098	1.0001	1.0122	17.1	4.43	51.2		x
41B	2.353	2.21	1.098	1.0000	1.0118	17.6	4.79	51.2		x
42B	2.383	5.1	1.098	1.0001	1.0128	16.5	4.50	51.3	x	x

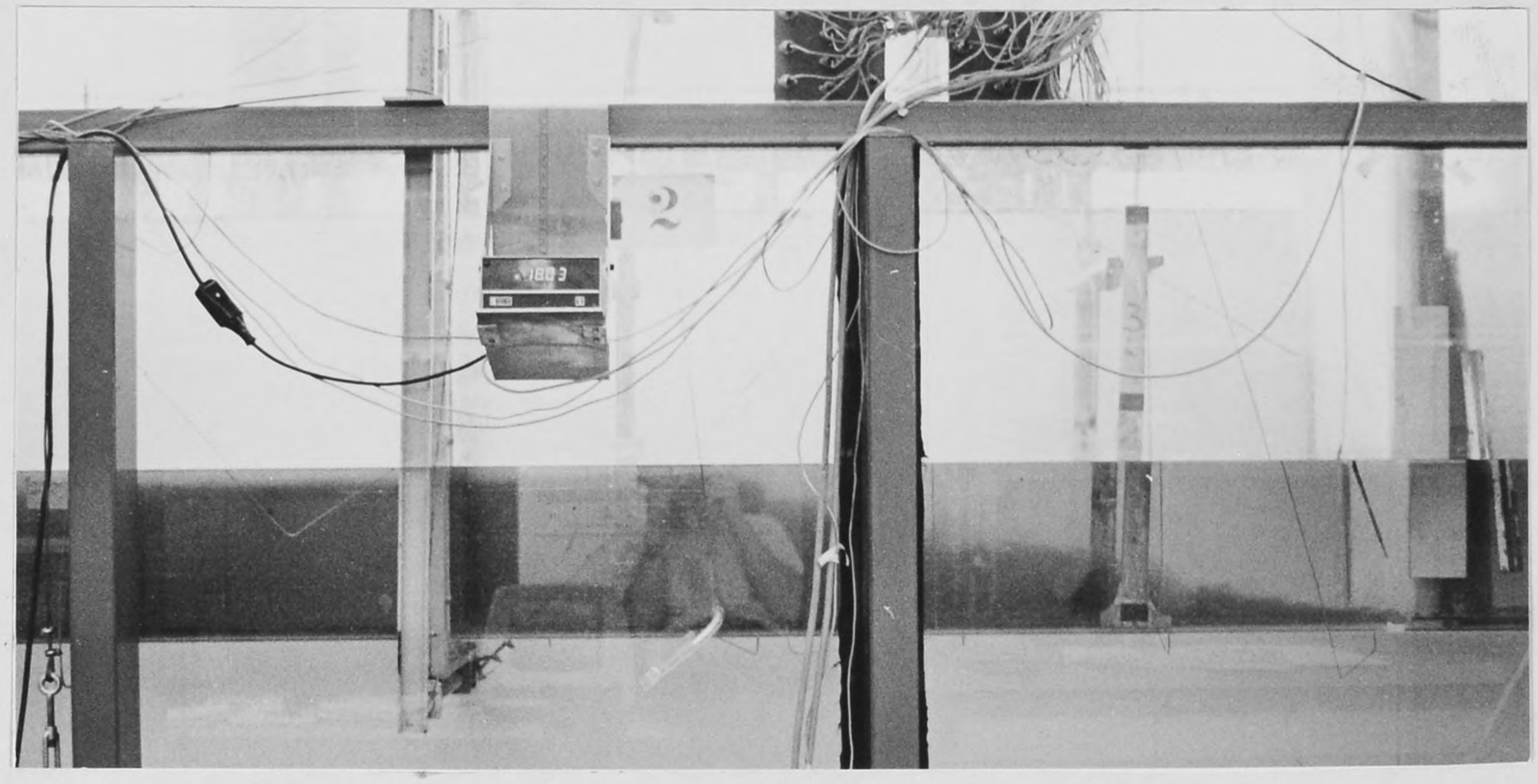

Figure 4-20. Near-source Mixing Region for Run 34B.

The behavior of the density currents was generally similar to those in Series 2. However there was one major difference at the highest ambient velocities. Figure 4-21 provides a plot of the density current propagation histories for several typical experiments and generally indicates constant velocities. Again, as in the Series 2 experiments, but in contrast to the sloping channel experiments, the velocities decrease slightly with distance along the channel. However, it can also be seen that there is a significant initial region (which apparently is the near-source mixing zone) in which the flow is still evolving and the density current speeds are not constant. At the highest ambient velocities, the density current head was very nondistinct and was often smaller than the layer depths behind. An explanation for this effect is not obvious from previous theories and this aspect of the problem requires further study.

Fig. 4-22 is a photograph of an experiment that was performed with a very small (approximately 0.5 cm) layer of salt water on the channel bottom. The density current can be seen to be forcing the salt water ahead of it to the extent that the salt water thickness is significantly increased at downstream locations and the density current is lifted off the bottom. One purpose in this experiment was to examine the effect of bottom friction since it was reasoned that a density current propagating over a salt water layer would experience less friction than over the channel bottom itself. The propagation histories for successive experiments indicate only a minimal increase in the propagation speed when the

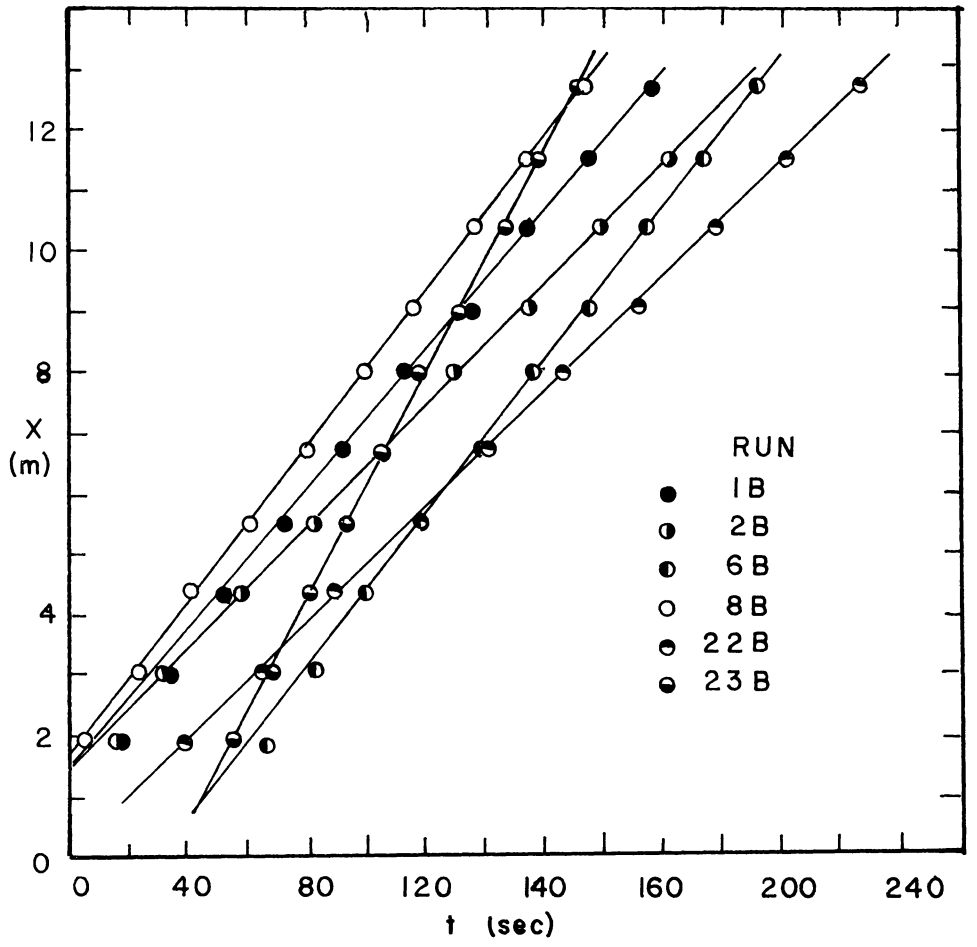

Figure 4-21. Density Current Propagation Histories for Series 3 Experiments.

salt water layer is present. However, the effect is essentially negligible (about 1 percent), thereby adding more support to the argument that Kranenburg's (1978) analysis describing the effect of friction losses is more likely to be describing some other influence such as mixing behind the density current head.

Because of the short time between the completion of these experiments and the writing of this report, very little data analysis has been performed for these experiments. A considerable amount of data analysis will be required to address the basic experimental objectives.

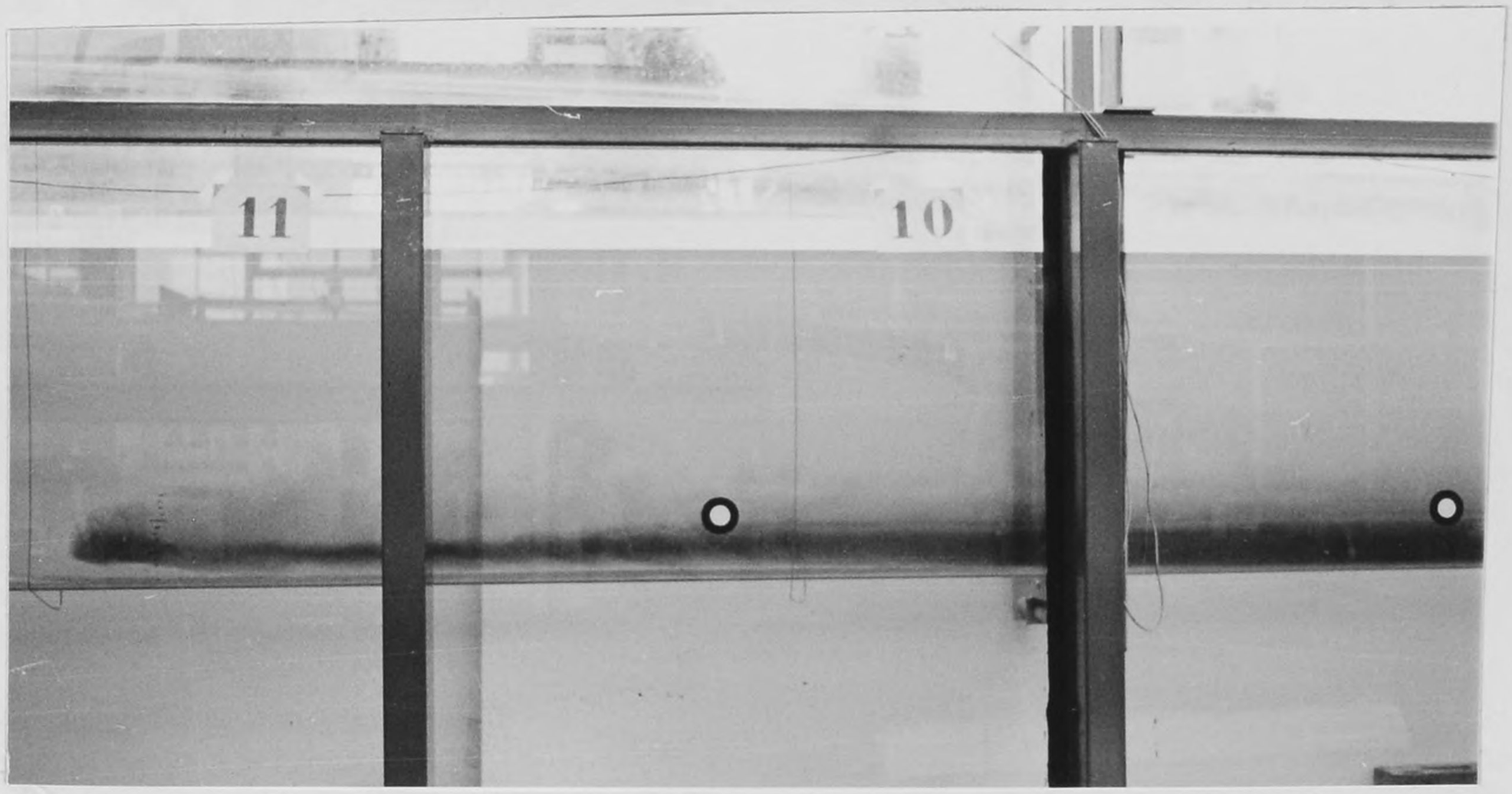

Figure 4-22. Photograph of Density Current Propagating Over Salt Water Layer (Run 7B).

CHAPTER 5
SUMMARY

Although the major purpose of this report is to document the experimental investigation, enough of an initial interpretation of the results obtained has been completed to suggest some tentative conclusions. Also, the value of the data in obtaining certain types of information can be judged.

The first comment is that the basic formulation suggested by Wilkinson and Wood (1971) appears to be a valid and useful tool for predicting the near-field dilution for a variety of potential applications. This makes a strong argument for the comment that turbulent mixing is more a function of the characteristics of the bulk flow rather than the turbulent structure, although it is also clear that there is probably a complex interaction between the two. Nevertheless, the characterization of the bulk flow only in terms of assumed uniform (or otherwise guided by experimental observations) profiles is probably adequate for the types of predictions that are generally required for engineering purposes. The verification contained herein is for the case of no downstream control. The effect of the limitation due to depth is very pronounced. This indicates the role of depth as an important parameter in the determination of dilutions. Surface buoyant jets theories that ignore this effect should perhaps be viewed with suspicion in cases of large relative layer thickness unless rigorously verified. Another important question is whether the jet theories describe the changes in the length of the mixing zone due to coflowing or counterflowing streams.

The observations for unstable near field flows clearly repudiate much of the reasoning behind the simple blocking corrections. Since dilution is observed to occur even when the layer extends over the entire depth, the layer effect cannot simply be treated in the sense of considering the layer to represent a rigid obstacle with respect to exchange between the fluid layers. Instead, the overall dynamics clearly allow, and in fact prescribe mixing even when the source discharge is significantly blocked by the partially mixed fluid.

The analysis and theories for the density current have indicated these to be largely inconsistent with previous theories and in need of new approaches. Very few previous efforts have concentrated on putting this into the framework of a useable theory, i.e. being able to predict the density current characteristics from an arbitrary source discharge. The analysis and experimental results presented herein show this to be a many-faceted problem and one that cannot be resolved on the basis of a single line of reasoning. The analysis for the conditions of density current control on near source mixing implies that there may be conditions where the density current may control source mixing and vice versa. Most importantly, it has been demonstrated that existing theories are inadequate to explain features of the present experimental observations and alternate approaches have been suggested.

Although this is somewhat a matter of judgement, there are several potential application areas for the experimental data described herein. The following areas are identified as possible uses for the

different data (other than those described within this report):

1. Interfacial friction data. In the series 2 experiments and some of the series 3 experiments, the profiles are reasonably well described in at least two locations. The flows are subcritical and stable except for some mixing due to bottom turbulence. Therefore it should be possible to predict the interface by Schijf and Schönfeld equations and thereby estimate the interfacial friction factors. Bottom friction factors for the inner channel has been estimated previously and corrections for wall shear should perhaps be made. As Abraham, et al (1979) point out, there are likely to be some important differences in friction factors between different types of problems. Much of the previous data from other studies is from experiments on intrusion wedges. A critical problem in this case is in the applicability of the theories as discussed by Denton (1980) Therefore, the data herein may provide a useful supplement to the existing data base.

2. The coflowing data can be used to examine buoyant jet theories, since the source regions were generally unsubmerged. A potental problem is the changes in ambient velocity in the external stream. However there are a few relatively deep cases where the layer thickness is not large and the data for those cases would be especially useful in that regard.

3. The density current problem when propagating on a sloping bottom; measurements of propagation speeds and head thicknesses were made for the experiments on a sloping bottom. This data may also be useful in checking the validity of the formulation for constant depth situations. The value would lie in the change in relative layer thickness with distance along the channel and the effect on the density current propagation characteristics.

BIBLIOGRAPHY

Abraham, G., Karelse, M., and van Os, A.G. (1979) "On the Magnitude of Interfacial Shear of Subcritical Stratified Flows in Relation with Interfacial Stability" **Journal of Hydraulic Research**, Vol. 17, No. 4, pp. 273-286.

Amen, R. and Maxworthy, T. (1980) "The Gravitational Collapse of a Mixed Region into a Linearly Stratified Fluid," **Journal of Fluid Mechanics**, Vol. 96, pp. 65-80.

Baddour, R.E. and Abbink, H. (1983) "Turbulent Underflow in a Short Channel of Limited Depth", **Journal of Hydraulic Engineering, ASCE**, Vol. 109, No. 5, pp. 722-740.

Beltaos, S. and Rajaratnam, N. (1973) "Plane Turbulent Impinging Wall Jets", **Journal of Hydraulic Research**, Vol. 11, pp. 29-59.

Benjamin, T.B. (1968) "Gravity Currents and Related Phenomena," **Journal of Fluid Mechanics**, Vol. 31, pp. 209-248.

Bewick, D. (1974) "Entraining Hydraulic Jumps in Two Layer Flows," M.S. Thesis, University of Canterbury, Christchurch, New Zealand.

Britter, R.E. and Linden, P.F. (1980), "The Motion of the Front of a Gravity Current Travelling Down an Incline", **Journal of Fluid Mechanics**, Vol. 99, pp. 531-543.

Britter, R.E. and Simpson, J.E. (1978) "Experiments on the Dynamics of a Gravity Current Head," **Journal of Fluid Mechanics**, Vol. 88, pp. 223-240.

Bühler, J. (1974) "Model Studies of Multiport Diffusers in Unstratified, Stagnant or Flowing Receiving Waters," Ph.D. Dissertation, University of California, Berkeley, California.

Bühler, J. (1977) "On Buoyant Surface Layers Generated by Wastewater Discharged from Submerged Diffusers," **Proceedings, 17th International Congress of the IAHR**, Baden-Baden, Germany, Vol. 1, pp. 325-332.

Bühler, J. (1983) "On Integral Scales for Jetlike Flows", **Proceedings 8th Australasian Fluid Mechanics Conference**, University of New Castle, New South Wales, Australia, pp. 8C9-8C12.

Cederwall, K. (1971) "Buoyant Slot Jets into Stagnant or Flowing Environments," W. M. Keck Laboratory of Hydraulics and Water Resources, Rept. KH-R-25, California Institute of Technology, Pasadena, California.

Champagne, F.H., Pao, Y.H., and Wygnanski (1976), "On the Two-Dimensional Mixing Region", **Journal of Fluid Mechanics**, Vol. 76, pp. 209-250.

Chen, J.C. (1980) "Studies on Gravitational Spreading Currents," W.M. Keck Laboratory of Hydraulics and Water Resources, Rept. KH-R-40, California Institute of Technology, Pasadena, Calif.

Chu, V.E. and Baddour, R.A. (1984) "Turbulent Gravity Stratified Shear Flows," **Journal of Fluid Mechanics**, Vol. 138, pp. 353-378.

Denton, R.A. (1981) "The Role of Bed Slope in Determining the Length and Stability of Density Wedges" in **Aspects of Stratified Flow in Man-Made Reservoirs**, Chapter 2, Report 20, Institut Wasserbau III, University of Karlsrühe, Karlsrühe, Germany.

Denton, R.A. (1981a) "Density Current Inflows into a Run of the River Reservoir", in **Aspects of Stratified Flow in Man-Made Reservoirs,** Chapter 1, Report 20, Institut Wasserbau III, University of Karlsrühe, Karlsrühe Germany.

Denton, R.A. (1981b) "The Role of Bed Slope in Determining the Length and Stability of Density Wedges" in **Aspects of Stratified Flow in Man-Made Reservoirs**, Chapter 2, Report 20, Institut Wasserbau III, University of Karlsrühe, Karlsrühe, Germany.

Ellison, T.H. and Turner, J.S. (1959) "Turbulent Entrainment in Stratified Flows", **Journal of Fluid Mechanics**, Vol. 6, pp. 423-448.

Engelund, F. (1976) "Hydraulics of Surface Buoyant Jets", **Journal of the Hydraulics Division, ASCE**, Vol. 102, HY9, pp. 1315-1325.

Faust, K.M. (1977) "Zweidimensionale Ausbreitung in einem Geschichteten Fluid," Report SFB 80/E/104, Sonderforschungsbereich 80, University of Karlsrühe, Karlsrühe, Germany.

Faust, K.M. (1981) "Intrusion of a Density Front in a Stratified Environment," in **Aspects of Stratified Flow in Man-Made Reservoirs**, Chapter 3, Rept. 20, Institut Wasserbau III, University of Karlsrühe, Karlsrühe, Germany.

Faust, K.M. and Plate, E.J. (1984) "Experimental Aspects of Intrusive Gravity Currents Entering Stably Stratified Fluid," **Journal of Hydraulic Research**, Vol. 22, 5, pp. 315-326.

Gartrell, G. (1979) "Studies on the Mixing in a Density Stratified Shear Flow" W.M. Keck Laboratory of Hydraulics and Water Resources, Report No. KH-R-39, California Institute of Technology, Pasadena, California.

Gartrell, G. (1980) "Vertical Flux Measurements in a Density Stratified Shear Flow", **Proceedings, Second International Symposium on Stratified Flows**, Vol. 1, Trondheim, Norway, pp. 301-314.

Hayakawa, N. (1970) "Internal Jump in Co-current Stratified Fluid", **Journal of the Engineering Mechanics Division ASCE**, Vol. 96, EM5, pp. 797-800.

Henderson, F.M. (1966) "Open Channel Flow", Macmillan, New York, New York.

Isaacson, M., Koh, R.C.Y. and Brooks, N.H. (1983) "Plume Dilution for Diffusers with Multiport Risers," **Journal of Hydraulic Engineering**, Vol. 109, 2, pp. 199-220.

Jirka, G.H. and Harleman, D.R.F. (1973) "The Mechanics of Submerged Multiport Diffusers in Shallow Water," R.M. Parsons Laboratory for Water Resources and Hydrodynamics, Rept. 169, Massachusetts Institute of Technology, Cambridge, Mass.

Jirka, G.H. and Harleman, D.R.F. (1979) "Stability and Mixing of a Vertical Plane Buoyant Jet in Confined Depth," **Journal of Fluid Mechanics**, Vol. 94, No. 2, pp. 275-304.

Jirka, G.H. (1982) "Turbulent Buoyant Jets in Shallow Fluid Layers," **Turbulent Jets and Plumes**, W. Rodi, ed., Pergamon Press.

Koh. R.C.Y. (1971) "Two-Dimensional Surface Warm Jet", **Journal of the Hydraulics Division, ASCE**, Vol. 97, HY6, pp. 819-836.

Koh, R.C.Y. and Brooks, N.H. (1975) "Fluid Mechanics of Waste Disposal in the Ocean," **Annual Review of Fluid Mechanics**, Vol. 7, pp. 187-211.

Koh, R.C.Y. (1976) "Buoyancy-Driven Gravitational Spreading," **Proceedings, 15th Coastal Engineering Conference**, Honolulu, Hawaii, Vol. 4, pp. 2956-2975.

Koh, R.C.Y. (1983) "Wastewater Field Thickness and Initial Dilution," **Journal of Hydraulic Engineering**, Vol. 109, No. 9, pp. 1232-1240.

Kranenburg, C. (1978) "Internal Fronts in Two Layer Flow," **Journal of Hydraulics Division, ASCE**, Vol. 104, HY10, pp. 1449-1453.

Lee, J.H.W. and Jirka, G.H. (1981) "Vertical Round Buoyant Jet in Shallow Water", **Journal of the Hydraulics Division, ASCE**, Vol. 107, HY12, pp. 1651-1675.

Long. R.R. (1970) "Blocking Effects in Flow Over Obstacles", **Tellus**, Vol. 22, pp. 471-480.

Long, R.R. (1977) "The Influence of Shear on Mixing Across Density Interfaces", **Journal of Fluid Mechanics**, Vol. 79, pp. 481-497.

Looney, M.K. and Walsh, J.J. (1984) "Mean-Flow and Turbulent Characteristics of Free and Impinging Jet Flows", **Journal of Fluid Mechanics**, Vol. 147, pp. 397-429.

Manins, P.C. (1976a) "Intrusion into a Stratified Fluid," **Journal of Fluid Mechanics**, Vol. 74, 3, pp. 547-560.

Manins, P.C. (1976b) "Mixed Region Collapse in a Stratified Fluid," **Journal of Fluid Mechanics**, Vol. 77, 1, pp. 177-183.

Maxworthy, T. (1980) "On the Formation of Nonlinear Internal Waves from the Gravitational Collapse of Mixed Regions in Two and Three Dimensions," **Journal of Fluid Mechanics**, Vol. 96, pp. 47-64.

Miller, D.R. and Comings, E.W. (1957), "Static Pressure Distribution in the Free Turbulent Jet", **Journal of Fluid Mechanics**, Vol. 3, pp. 1-16.

Pryputniewicz, R.J. and Bowley, W.W. (1975) "An Experimental Study of Vertical Buoyant Jet Discharges Into Water of Finite Depth," **ASME Journal of Heat Transfer**, Vol. 97, pp. 274-281.

Rajaratnam, N. (1976) "Turbulent Jets", Elsevier Scientific Publishing Co., Amsterdam, The Netherlands.

Rajaratnam, N. and Subramanyan, S. (1985) "Plane Buoyant Surface Jets and Jumps" **Journal of Hydraulic Research**, Vol. 23, pp. 131-146.

Rigter, B.P. (1970) "Density Induced Return Currents in Outlet Channels," **Journal of the Hydraulics Division, ASCE**, Vol. 96, HY2, pp. 529-546.

Roberts, P.J. W. (1977) "Dispersion of Buoyant Wastewater Discharged from Outfall Diffusers of Finite Length," W.M. Keck Laboratory of Hydraulics and Water Resources, Rept. KH-R-35, California Institute of Technology, Pasadena, Calif.

Rodi, W. (1980) "Turbulence Models and Their Applications in Hydraulics-A State of The Art Review," International Association for Hydraulic Resaearch.

Ryskiewich, B.S. and Hafetz, L. (1975) "An Experimental Study of the Free Surface Effect on a Buoyant Jet," General Dynamics Corporation Rept. PB-239.536, Groton Connetticut.

Schijf, J.B. and Schönfeld, J.C. (1953) "Theoretical Considerations on the Motion of Salt and Fresh water" **Proceedings, Minnesota International Hydraulics Convention**, Minneapolis, Minnesota, pp. 321-333.

Singh, B. and Shah, C.R. (1971), "Plunging Phenomenon of Density Currents in Reservoirs", La Houille Blanche, Vol. 9, No.1, pp 59-64.

Simpson, J.E. and Britter, R.E. (1979) "The Dynamics of the Head of a Gravity Current Advancing Over a Horizontal Surface," **Journal of Fluid Mechanics**, Vol. 94, pp. 477-496.

Simpson, J.E. and Britter, R.E. (1980) "Experiments on the Dynamics of the Front of a Gravity Current," **Proceedings, 2nd International Symposium on Stratified Flows**, Trondheim, Norway, pp. 174-183.

Stefan, H. and Hayakawa, N. (1972) "Mixing Induced by an Internal Hydraulic Jump", **Water Resources Bulletin, American Water Resources Association**, Vol. 8, No. 3, pp. 531-545.

Stolzenbach, K.D. and Harleman, D.R.F. (1973) "Three Dimensional Heated Surface Jets," **Water Resources Research**, Vol. 9, pp.138-153.

Tamai, N., Wiegel, R.L. and Tornberg, G.F. (1969) "Horizontal Surface Discharge of Warm Water Jets," **Journal of the Power Division, ASCE**, Vol. 95, PO2, pp. 253-276.

Turner, J.S. (1973) "Buoyancy Effects in Fluids" Cambridge University Press.

Wallace, R.B. (1981) "Two Dimensional Buoyant Jets in a Stratified or Crossflowing Ambient Fluid," Ph.D. Dissertation, University of Michigan, Ann Arbor, Michigan.

Wallace, R. B. and Wright, S.J. (1980) "Buoyant Jet Behavior Near the Maximum Rise," **Proceedings, ASCE Hydraulics Division Specialty Conference**, Chicago, Illinois, pp. 356-365.

Wallace, R. B. and Sheff, B.B. (1984) "Measurements to Quantify Wastewater Fields Produced by Outfall Diffusers," OWRT Project Report, Michigan State University, East Lansing, Michigan.

Wallace, R.B. and Wright, S.J. (1984) "Spreading Layer of a Two-Dimensional Buoyant Jet," **Journal of Hydraulic Engineering**, Vol. 110, No. 6, pp. 813-828.

Wilkinson, D.L. and Wood, I.R. (1971) "A Rapidly Varied Phenomenon in a Two Layer Flow," **Journal of Fluid Mechanics**, Vol. 47, 2, pp. 241-256.

Wilkinson, D.L. and Willoughby, M.A, (1981) "Velocity Measurement with Hydrogen Bubbles-Wake Correction" **Journal of Hydraulic Research**, Vol. 19, No. 2, pp. 141-153.

Wong, D.R. (1984) "Buoyant Jet Entrainment in Stratified Fluids," Ph.D. Dissertation, University of Michigan, Ann Arbor, Michigan.

Wong, D.R. and Wright, S.J. (1985) "Submerged Turbulent Jets in Linearly Stratified Fluids", **Proceedings, International Symposium of Jets and Cavities**, ASME Winter Annual Meeting, Miami Beach, Florida, pp. 141-152.

Wood, I.R. and Simpson, J.E. (1984) "Jumps in Layered Miscible Fluids," **Journal of Fluid Mechanics**, Vol. 140, pp. 329-342.

Wright, S.J. (1977) "Mean Behavior of Buoyant Jets in a Crossflow," **Journal of the Hydraulics Division, ASCE**, Vol. 103, HY5, pp. 499-513.

Wright, S.J., Wallace, R.B., and Wong, D.R. (1980) "Buoyant Discharge from Outfall Diffuser into Stratified Fluid," **Proceedings, 2nd International Symposium on Stratified Flows**, Trondheim, Norway, Vol. 2, pp. 871-880.

Wright, S.J., Wong, D.R., Wallace, R.B., and Zimmerman, K.E. (1982) "Outfall Diffuser Behavior in Stratified Ambient Fluid," **Journal of the Hydraulics Division, ASCE**, Vol. 108, HY4, pp. 483-501.

Wright, S.J., Roberts, P.J.W., Wong, D.R. and Bradley, N.E. (1984) "Surface Dilution of Submerged Buoyant Jets", unpublished manuscript.

Wright, S.J. (1985) Discussion to "Wastewater Field Thickness and Initial Dilution," **Journal of Hydraulic Engineering**, Vol. 111, No. 5, pp. 891-896.

Wright, S.J. (1985) "Global Constraints on Buoyant Jet Mixing in Confined Environments" **Proceedings, International Symposium of Refined Flow Modelling and Turbulence Measurements**, Iowa City, Iowa. Chapter A-13, pp. 1-10.

Wright, S.J. and Bühler, J. (1986) "Control of Buoyant Jet Mixing by Far Field Spreading," to be published in **Proceedings, ASCE Specialty Conference, Advancements in Aerodynamics, Fluid Mechanics, and Hydraulics**, Minneapolis, Minnesota.

Yih, C.S. and Guha, C.R. (1955) "Hydraulic Jump in a Fluid System of Two Layers", **Tellus**, Vol. 7, No. 3, pp. 358-366.

Yuan, M. (1984) "Pressurized Surges," M.S. thesis, University of Minnesota, Minneapolis, Minnesota.

APPENDIX A
DATA FILE DESCRIPTION

This appendix describes the format under which the basic data files have been stored and the means by which they can be retrieved. Also, an explanation of any unusual aspects of particular data file structures is provided to help in any data retrieval effort. All files were written on either a PDP 11/45 or a VAX and the tapes are compatible with the standard DEC format which is ANSI labelled and with ASCII character coding. In all cases, a subroutine to read the data files has been written and tested; on any magnetic tape, there is a copy of this routine as well as the program that originally wrote the data file. With the information in this appendix and the retrieval subroutines, the appropriate information can be accessed.

Hydrogen Bubble Velocity Profiles

All of the raw data files were processed on the PDP 11/45 with a modification of the program UBUBBK written by Daniel Schläpfer. Various versions of this program were used to process all data files. As originally written, the program read a raw data file with the name BUBBLEnn.DAT with nn any integer and wrote a file UBUBBLKnn.DAT. Because there were approximately 250 velocity profiles, this naming procedure was modified to clearly distinguish among them. 85 profiles consisting of all the data from the first two series of experiments followed the above naming system. Table A-1 provides the description of the experiments associated with a particular data file. These are identified according to the temperature measurements that they approximately correspond to. Also, for the measurements behind the density current head, the experiments are labeled according to times after the arrival of the density current at the measurment location. This is also true with respect to the data in Table A-2 below. For the final set of experiments, the first 99 raw data files were named BUBBLKnn.DAT and the processed data files were written as UBUBBLAnn.DAT. The remaining ones had raw and processed data file names of BUBBLCnn.DAT and UBUBBLBnn.DAT respectively. Table A-2 gives the experimental conditions that correspond to each file. Because these data were taken at the same time as the temperature measurement, only those cases where the flow conditions were different from Table 4-4 are noted. For example, sometimes the source discharge was slightly different or the ambient discharge is zero. For the conditions not provided, refer to Table 4-4.

Table A-1. Experimental Parameters Associated with Velocity Profiles for Series 1 and 2 Experiments.

SERIES 1 EXPERIMENTS

Data file	Q_o l/sec	$\rho_{disch.}$ gm/ml	$\rho_{amb.}$ gm/ml	H cm	Matches RUN #	Condition	X cm	Z_o cm
UBUBBLK63	1.630	1.0091	1.0001	23.9	8	Forward Flow	550.	
UBUBBLK64	1.630	1.0091	1.0001	23.9	8	Return Flow	550.	32.
UBUBBLK65	2.219	1.0091	1.0001	24.5	12	Forward Flow	550.	
UBUBBLK66	2.219	1.0091	1.0001	24.5	12	Return Flow	550.	24.
UBUBBLK67	2.219	1.0091	1.0001	24.5	12	Return Flow	550.	24.
UBUBBLK68	1.400	1.0084	1.0000	11.8	23	Forward Flow	97.	
UBUBBLK69	1.400	1.0084	1.0000	11.8	23	Return Flow	97.	22.
UBUBBLK70	1.400	1.0084	1.0000	11.8	23	Return Flow	97.	22.
UBUBBLK71	2.180	1.0084	1.0000	12.6	22	Forward Flow	97.	
UBUBBLK72	2.180	1.0084	1.0000	12.6	22	Return Flow	97.	22.
UBUBBLK73	1.623	1.0091	1.0001	23.9	8	Forward Flow	97.	
UBUBBLK74	1.623	1.0091	1.0001	23.9	8	Return Flow	97.	22.
UBUBBLK75	1.623	1.0091	1.0001	23.9	8	Return Flow	97.	38.
UBUBBLK76	2.219	1.0091	1.0001	12.6	22	Forward Flow	97.	
UBUBBLK77	2.219	1.0091	1.0001	12.6	22	Return Flow	97.	38.
UBUBBLK78	1.400	1.0087	1.0001	11.8	23	Forward Flow	97.	
UBUBBLK79	2.203	1.0087	1.0001	12.5	22	Forward Flow	97.	
UBUBBLK80	2.203	1.0087	1.0001	12.5	22	Return Flow	97.	14.
UBUBBLK81	1.400	1.0087	1.0001	11.8	23	Return Flow	97.	14.
UBUBBLK82	2.219	1.0103	1.0001	24.5	12	Return Flow	36.5	22.
UBUBBLK83	2.180	1.0103	1.0001	12.6	22	Return Flow	36.5	22.
UBUBBLK84	1.400	1.0103	1.0001	11.8	23	Forward Flow	36.5	
UBUBBLK85	1.405	1.0083	1.0000	11.8	23	Forward Flow	97.	

SERIES 2 EXPERIMENTS

Data File	Q_o l/sec	$\rho_{disch.}$ gm/ml	$\rho_{amb.}$ gm/ml	H cm	Matches RUN #	Condi	Z_o cm
UBUBBLK01	1.538	1.0042	0.9999	11.9	25A	Dens. Cur., t = 0 sec	
UBUBBLK02	1.538	1.0042	0.9999	11.9	25A	Dens. Cur., t = 10 sec	
UBUBBLK03	1.538	1.0042	0.9999	11.9	25A	Dens. Cur., t = 30 sec	
UBUBBLK04	1.538	1.0042	0.9999	11.9	25A	Dens. Cur., t = 45 sec	
UBUBBLK05	1.538	1.0042	0.9999	11.9	25A	Dens. Cur., t = 60 sec	
UBUBBLK06	1.179	1.0042	0.9999	11.6	27A	Dens. Cur., t = 0^- sec	
UBUBBLK07	1.179	1.0042	0.9999	11.6	27A	Dens. Cur., t = 10 sec	
UBUBBLK08	1.179	1.0042	0.9999	11.6	27A	Dens. Cur., t = 30 sec	
UBUBBLK09	1.179	1.0042	0.9999	11.6	27A	Dens. Cur., t = 45 sec	
UBUBBLK10	1.179	1.0042	0.9999	11.6	27A	Dens. Cur., t = 90 sec	
UBUBBLK11	1.179	1.0042	0.9999	11.6	27A	Steady State	
UBUBBLK12	0.518	1.0042	0.9999	11.2	26A	Dens. Cur., t = 0 sec	
UBUBBLK13	0.518	1.0042	0.9999	11.2	26A	Dens. Cur., t = 15 sec	
UBUBBLK14	0.518	1.0042	0.9999	11.2	26A	Dens. Cur., t = 30 sec	
UBUBBLK15	0.518	1.0042	0.9999	11.2	26A		
UBUBBLK16	0.518	1.0042	0.9999	11.2	26A	Dens. Cur., t = 45 sec	

Table A-1 (continued)

Data File	Q_o l/sec	$\rho_{amb.}$ gm/ml	$\rho_{disch.}$ gm/ml	H cm	Matches RUN #	Condition	Z_o cm
UBUBBLK17	0.518	1.0042	0.9999	11.2	26A	Dens. Cur., t = 60 sec	
UBUBBLK18	0.518	1.0042	0.9999	11.2	26A	Dens. Cur., t = 90 sec	
UBUBBLK19	0.518	1.0042	0.9999	11.2	26A	Steady State	
UBUBBLK20	1.481	1.0042	0.9999	23.8	4A	Dens. Cur., t = 0 sec	
UBUBBLK21	1.481	1.0042	0.9999	23.8	4A	Dens. Cur., t = 15 sec	
UBUBBLK22	1.481	1.0042	0.9999	23.8	4A	Dens. Cur., t = 30 sec	
UBUBBLK23	1.481	1.0042	0.9999	23.8	4A	Dens. Cur., t = 45 sec	
UBUBBLK24	1.481	1.0042	0.9999	23.8	4A	Dens. Cur., t = 60 sec	
UBUBBLK25	2.219	1.0042	0.9999	52.1	18A	Dens. Cur., t = -5 sec	
UBUBBLK26	2.219	1.0042	0.9999	52.1	18A	Dens. Cur., t = 0 sec	
UBUBBLK27	2.219	1.0042	0.9999	52.1	18A	Dens. Cur., t = 15 sec	
UBUBBLK28	2.219	1.0042	0.9999	52.1	18A	Dens. Cur., t = 30 sec	
UBUBBLK29	2.219	1.0042	0.9999	52.1	18A	Dens. Cur., t = 45 sec	
UBUBBLK30	2.219	1.0042	0.9999	52.1	18A	Dens. Cur., t = 60 sec	
UBUBBLK31	2.219	1.0042	0.9999	52.1	18A	Dens. Cur., t = 90 sec	
UBUBBLK32	2.219	1.0042	0.9999	52.1	18A	Steady State	
UBUBBLK33	0.897	1.0042	0.9999	51.1	16A	Dens. Cur., t = 10 sec	
UBUBBLK34	0.897	1.0042	0.9999	51.1	16A	Dens. Cur., t = 30 sec	
UBUBBLK35	0.897	1.0042	0.9999	51.1	16A	Dens. Cur., t = 45 sec	
UBUBBLK36	0.897	1.0042	0.9999	51.1	16A	Dens. Cur., t = 60 sec	
UBUBBLK37	0.897	1.0042	0.9999	51.1	16A	Steady State	
UBUBBLK38	0.897	1.0042	0.9999	51.1	16A	Steady State	
UBUBBLK39	0.883	1.0071	1.0000	51.1	16A	Dens. Cur., t = 30 sec	
UBUBBLK40	0.883	1.0071	1.0000	51.1	16A	Dens. Cur., t = 45 sec	
UBUBBLK41	0.883	1.0071	1.0000	51.1	16A	Dens. Cur., t = 60 sec	
UBUBBLK42	0.883	1.0071	1.0000	51.1	16A	Steady State	
UBUBBLK43	0.883	1.0071	1.0000	51.1	16A	Steady, Blocked Downstream	
UBUBBLK44	0.988	1.0071	1.0000	23.4	20A	Dens. Cur., t = 0 sec	
UBUBBLK45	0.988	1.0071	1.0000	23.4	20A	Dens. Cur., t = 30 sec	
UBUBBLK46	0.988	1.0071	1.0000	23.4	20A	Dens. Cur., t = 60 sec	
UBUBBLK47	0.988	1.0071	1.0000	23.4	20A	Steady, Blocked Down stream	
UBUBBLK48	0.988	1.0071	1.0000	23.4	20A	Steady State	
UBUBBLK49	0.975	1.0071	1.0000	23.2	20A	Dens. Cur., t = 0- sec	
UBUBBLK50	0.975	1.0071	1.0000	23.2	20A	Dens. Cur., t = 10 sec	
UBUBBLK51	0.975	1.0071	1.0000	23.2	20A	Dens. Cur., t = 30 sec	
UBUBBLK52	0.975	1.0071	1.0000	23.2	20A	Dens. Cur., t = 45 sec	
UBUBBLK53	0.975	1.0071	1.0000	23.2	20A	Dens. Cur., t = 60 sec	
UBUBBLK54	1.146	1.0071	1.0000	23.5	---	Steady State	
UBUBBLK55	1.146	1.0071	1.0000	23.5	---	Steady State	
UBUBBLK56	1.146	1.0071	1.0000	23.5	---	Steady State	
UBUBBLK57	2.219	1.0042	0.9999	52.1	18A	Reverse Flow, Steady	30.
UBUBBLK58	0.975	1.0071	1.0000	23.2	20A	Reverse Flow, t = 30 sec.	30.
UBUBBLK59	0.975	1.0071	1.0000	23.2	20A	Reverse Flow, t = 10 sec.	30.
UBUBBLK60	0.988	1.0071	1.0000	23.2	20A	Reverse Flow, t = 30 sec.	30.
UBUBBLK61	0.883	1.0071	1.0000	51.1	16A	Reverse Flow, t = 30 sec.	30.
UBUBBLK62	1.146	1.0071	1.0000	23.5	---	Steady State	

Note: All Series 2 Velocity Measurements at X = 247 cm

Table A-2. Experimental Parameters Associated with Velocity Profiles for Series 3. Experiments.

Data File	Q_o l/sec	$Q_{ambient}$ l/sec	RUN #	Condition
UBUBBLA01			1B	Steady State
UBUBBLA02			1B	Density Current, t = 0 sec
UBUBBLA03			1B	Density Current, t = 30 sec.
UBUBBLA04			2B	Steady State
UBUBBLA05	0.869		2B	Density Current, t = 15 sec.
UBUBBLA06	0.869		2B	Density Current, t = 30 sec,
UBUBBLA07	0.869		2B	Density Current, t = 45 sec.
UBUBBLA08	0.869		2B	Density Current, t = 60 sec.
UBUBBLA09	0.869		2B	Density Current, t = 75 sec.
UBUBBLA10	0.869		2B	Density Current, t = 90 sec.
UBUBBLA11	0.869		2B	Density Current, t = 120 sec.
UBUBBLA12	0.869		2B	Density Current, t = 150 sec.
UBUBBLA13			3B	Steady State
UBUBBLA14			4B	Steady State
UBUBBLA15			4B	Density Current, t = 30 sec.
UBUBBLA16			4B	Density Current, t = 68 sec.
UBUBBLA17			4B	Density Current, t = 90 sec.
UBUBBLA18			4B	Density Current, t = 120 sec.
UBUBBLA19			5B	Steady State
UBUBBLA20			6B	Steady State
UBUBBLA21			7B	Steady State
UBUBBLA22			7B	Steady State, Return Flow
UBUBBLA23			8B	Steady State
UBUBBLA24			8B	Steady State, Reverse Flow
UBUBBLA25			9B	Steady State
UBUBBLA26			9B	Steady State, Reverse Flow
UBUBBLA27			10B	Steady State
UBUBBLA28			11B	Density Current, t = 0 sec.
UBUBBLA29			11B	Density Current, t = 30 sec.
UBUBBLA30			11B	Density Current, t = 60 sec.
UBUBBLA31			11B	Density Current, t = 90 sec.
UBUBBLA32			11B	Density Current, t = 130 sec.
UBUBBLA33			11B	Steady State
UBUBBLA34		0.0	11B	Density Current, t = 30 sec.
UBUBBLA35		0.0	11B	Density Current, t = 30 sec., Return Flow
UBUBBLA36		0.0	11B	Density Current, t = 60 sec.
UBUBBLA37		0.0	11B	Density Current, t = 90 sec.
UBUBBLA38		0.0	11B	Density Current, t = 90 sec., Return Flow
UBUBBLA39		0.0	11B	Density Current, t = 120 sec.
UBUBBLA40		0.0	11B	Density Current, t = 180 sec.
UBUBBLA41		0.0	11B	Density Current, t = 185 sec.
UBUBBLA42		0.0	11B	Density Current, t = 185 sec, Return Flow
UBUBBLA43			12B	Steady State
UBUBBLA44			13B	Density Current, t = 85 sec.
UBUBBLA45			13B	Density Current, t = 140 sec.
UBUBBLA46			13B	Steady State
UBUBBLA47			14B	Steady State
UBUBBLA48			15B	Density Current, t = 0 sec.
UBUBBLA49			15B	Density Current, t = 30 sec.
UBUBBLA50			15B	Density Current, t = 90 sec.

Table A-2 (Continued)

Data File	Q_o l/sec	$Q_{ambient}$ l/sec	RUN #	Condition
UBUBBLA51			15B	Density Current, t = 150 sec.
UBUBBLA52			15B	Density Current, t = 160 sec.
UBUBBLA53			16B	Density Current, t = 30 sec.
UBUBBLA54			16B	Density Current, t = 60 sec.
UBUBBLA55			16B	Steady State
UBUBBLA56			17B	Steady State
UBUBBLA57			18B	Steady State
UBUBBLA58		0.0	19B	Density Current, t = 30 sec.
UBUBBLA59		0.0	19B	Density Current, t = 30 sec, Return Flow
UBUBBLA60		0.0	19B	Density Current, t = 90 sec.
UBUBBLA61		0.0	19B	Density Current, t = 90 sec., Return Flow
UBUBBLA62		0.0	19B	Density Current, t = 150 sec.
UBUBBLA63		0.0	19B	Density Current, t = 150 sec, Return Flow
UBUBBLA64		0.0	19B	Density Current, t = 210 sec.
UBUBBLA65		0.0	19B	Density Current, t = 210 sec, Return Flow
UBUBBLA66			19B	Density Current, t = 0 sec.
UBUBBLA67			19B	Density Current, t = 30 sec.
UBUBBLA68			19B	Density Current, t = 60 sec.
UBUBBLA69			19B	Steady State
UBUBBLA70		0.875	20B	Density Current, t = 30 sec.
UBUBBLA71		0.875	20B	Density Current, t = 80 sec.
UBUBBLA72		0.875	20B	Density Current, t = 150 sec.
UBUBBLA73		0.58	20B	No Discharge
UBUBBLA74		0.58	20B	Density Current, t = 0 sec.
UBUBBLA75		0.58	20B	Density Current, t = 30 sec.
UBUBBLA76		0.58	20B	Density Current, t = 45 sec.
UBUBBLA77		0.58	20B	Density Current, t = 60 sec.
UBUBBLA78		0.58	20B	Density Current, t = 90 sec.
UBUBBLA79			21B	Steady State
UBUBBLA80			22B	Steady State
UBUBBLA81			23B	Density Current, t = 15 sec.
UBUBBLA82			23B	Density Current, t = 30 sec.
UBUBBLA83			23B	Density Current, t = 60 sec.
UBUBBLA84			23B	Steady State
UBUBBLA85		1.0	24B	Density Current, t = 0 sec.
UBUBBLA86		1.0	24B	Density Current, t = 30 sec.
UBUBBLA87		1.0	24B	Density Current, t = 90 sec.
UBUBBLA88		1.0	24B	Density Current, t = 150 sec.
UBUBBLA89			24B	Steady State
UBUBBLA90			25B	Steady State
UBUBBLA91			26B	Density Current, t = 30 sec.
UBUBBLA92			26B	Density Current, t = 60 sec.
UBUBBLA93			26B	Density Current, t = 90 sec.
UBUBBLA94			27B	Steady State
UBUBBLA95			28B	Density Current, t = 0 sec.
UBUBBLA96			28B	Density Current, t = 30 sec.
UBUBBLA97			28B	Density Current, t = 90 sec.
UBUBBLA98			28B	Density Current, t = 150 sec.
UBUBBLA99			28B	Density Current, t = 150 sec, Return Flow

Table A-2 (Continued)

Data File	Q_o l/sec	$Q_{ambient}$ l/sec	RUN #	Condition
UBUBBLB01			28B	Steady State
UBUBBLB02			29B	Steady State
UBUBBLB03			29B	Density Current, t = 0 sec.
UBUBBLB04			29B	Density Current, t = 30 sec.
UBUBBLB05			29B	Density Current, t = 90 sec.
UBUBBLB06			30B	Steady State
UBUBBLB07	1.334		32B	Density Current, t = 0 sec.
UBUBBLB08	1.334		32B	Density Current, t = 30 sec.
UBUBBLB09	1.334		32B	Density Current, t = 30 sec., Return Flow
UBUBBLB10	1.334		32B	Density Current, t = 120 sec.
UBUBBLB11	1.334		32B	Density Current, t = 120 sec, Return Flow
UBUBBLB12			32B	Steady State
UBUBBLB13			32B	Steady State, Return Flow
UBUBBLB14			32B	Steady State
UBUBBLB15			32B	Steady State, Return Flow
UBUBBLB16			33B	Steady State
UBUBBLB17			34B	No Discharge
UBUBBLB18	1.667		34B	Density Current, t = 0 sec.
UBUBBLB19	1.667		34B	Density Current, t = 30 sec.
UBUBBLB20	1.667		34B	Density Current, t = 30 sec., Return Flow
UBUBBLB21	1.667		34B	Density Current, t = 90 sec.
UBUBBLB22	1.667		34B	Density Current, t = 90 sec., Return Flow
UBUBBLB23			34B	Steady State
UBUBBLB24			34B	Steady State, Return Flow
UBUBBLB25	1.036		35B	Density Current, t = 30 sec.
UBUBBLB26	1.036		35B	Density Current, t = 90 sec.
UBUBBLB27			35B	Steady State
UBUBBLB28			35B	Steady State, Return Flow
UBUBBLB29			36B	Steady State
UBUBBLB30			37B	Density Current, t = 0 sec.
UBUBBLB31			37B	Density Current, t = 35 sec.
UBUBBLB32			37B	Density Current, t = 95 sec.
UBUBBLB33			37B	Steady State
UBUBBLB34			38B	Steady State
UBUBBLB35			39B	Steady State
UBUBBLB36			39B	Density Current, t = 40 sec.
UBUBBLB37			40B	Steady State
UBUBBLB38			40B	Steady State, Return Flow
UBUBBLB39			41B	Steady State
UBUBBLB40			41B	Steady State, Return Flow
UBUBBLB41		0.0	42B	Density Current, t = 30 sec.
UBUBBLB42		0.0	42B	Density Current, t = 30 sec., Return Flow
UBUBBLB43		0.0	42B	Density Current, t = 60 sec.
UBUBBLB44		0.0	42B	Density Current, t = 60 sec., Return Flow
UBUBBLB45		0.0	42B	Density Current, t = 95 sec.
UBUBBLB46		0.0	42B	Density Current, t = 95 sec. Return Flow
UBUBBLB47			42B	No Discharge
UBUBBLB48			42B	Density Current, t = 0 sec.

Table A-2 (Continued)

Data File	Q_o l/sec	$Q_{ambient}$ l/sec	RUN #	Condition
UBUBBLB49			42B	Density Current, t = 30 sec.
UBUBBLB50			42B	Density Current, t = 30 sec., Return Flow
UBUBBLB51			42B	Density Current, t = 75 sec.
UBUBBLB52			42B	Density Current, t = 75 sec., Return Flow
UBUBBLB53			42B	Steady State, Return Flow
UBUBBLB54			42B	Steady State
UBUBBLB61			31B	Density Current, t = 30 sec.
UBUBBLB62			31B	Density Current, t = 90 sec.
UBUBBLB63			13B	Density Current, t = 30 sec.

Note: All Hydrogen Bubble Measurements For Series 3 Taken at X = 550 cm.

The program used the wake correction of Wilkinson and Willoughby (1981) as discussed in Chapter 3. This correction forced the program to take the logarithm of a negative number if it was applied to the reversed flow, i.e. upstream of the wire. Initially, the photo was just turned upside down and analyzed in a fashion that essentially converts the negative velocities to positive ones. The vertical coordinates then need to be adjusted because of this rotation. This is only true for the data in Table A-1. Therefore, for the reverse flow data, the constant Z_o required is noted, i.e. the true vertical coordinate is related to the value by

$$Z_{true} = Z_o - Z(\text{in data file})$$

For the data in Table A-2, all information on reverse flows is correct as presented, because the program was modified to handle this situation.

The files UBUBBLxnn.DAT have have a consistent format. They are written as direct access files with record length of 512 bytes (128, 4 byte words). There are exactly 110 records in each data file. The records contain the following information:

RECORD	INFORMATION
1	There are six REAL*4 values in this record. In order they are the number of records in the file, the number of velocity profiles, the number of profile points, vertical spacing between profile points, time interval between pulses, and the horizontal location of the wire.
2-101	These contain the data for the individual velocity profiles. In no cases are there actually 100 profiles, so only the first records contain data
102	record of average velocity (of all the profiles) at each vertical point
103	standard deviation at each point
104	minimum velocity computed at each point
105	maximum velocity computed at each point
110	the number of velocities computed for each point

In a few files, the same bubble trace was incorrectly traced twice during the digitizing process while an adjacent one was skipped. Except for the nonlinearity due to the wake correction, this won't change the mean velocity computed. However there will be a near zero minimum velocity and a maximum about twice the average. These can be easily detected by inspection of the results, so the photographs were not re-digitized.

There is a program with the name of BUBLREAD.FOR that was written for the VAX that will read any of the UBUBBLxnn.DAT files and creates a print file that displays all the essential information contained within the file. It is interactive, asking for the names of the data and print files. Both the version of the UBUBBx program and the BUBLREAD program have written to the tapes. The tapes contain both the raw (BUBBLxnn.DAT) and processed data FILES and the programs. Tapes were written with density 1600 BPI and the blocksize is noted on the label.

Temperature Measurement Data

There are some differences in the way the temperature data was collected that requires a little care when analyzing. In general, all processing was done with a file by the name of DATIHW, DAT1IHW, or DAT2IHW, the latter two of which are simply revised versions of the first. At the end of each program, there is a subroutine appended that can be used to recover the information from the processed data files. The raw data files were collected on the PDP 11/34 with the program TEMPME.FTN which is a variation of a similar program by the same name written by Daniel Schläpfer. He also wrote DEFDAT.FTN, of which modified versions processed the raw data files written by TEMPME on the PDP 11/45. These DEFDAT files were then in turn processed by the DATIHW programs. The relationship between the various programs used and the file names are given in Table A-3. There are a few special ones such as 16A in which there are two data records for a single experiment. In those cases, the second set of data files are named HO16B.DAT and HO16BA.DAT, respectively. One major difference is that the first set of data collected measurements from 64 temperature probes, **16** per rack while the last two series sampled 75 probes with **15** per rack. The DEFDAT files did not treat these differently in terms of the probes/rack; therefore, the extra information in the DEFDAT file was deleted in the final processing; this is the essential difference between the DATIHW and the DAT1IHW programs. All of the RUNnnA.DAT and RUNnnB.DAT files and about a third of the RUNnn.DAT files have been saved, so if there are any questions, the original raw data files written by DEFDAT are available in most cases.

Table A-3. Convention for Naming Data Files

SERIES	Raw Data File Written By DEFDAT	Files Written By DATIHW	
		Abbreviated File	Complete File
1	RUNnn.DAT	SLnnA.DAT	SLnn.DAT
2	RUNnnA.DAT	HOnnA.DAT	HOnn.DAT
3	RUNnnB.DAT	HFLnnA.DAT	HFLnn.DAT

Programs DATIHW wrote two data files. They were written on the VAX and are direct access files of record length 512 bytes. The total number of records varies between files. The information in the records is in the following format:

RECORD	INFORMATION
1	All the basic information on the experiment, e.g. source discharge densities, temperatures, etc. plus some variables necessary for interpreting the data. The subroutine READ1 describes all variables except for the third series of experiments; for Series 3 the ambient discharge is recorded in the SLOPE variable, to maintain the file structure. Also NSTART and NSTOP are two variables that were added later describe the statistics as noted below.
2	horizontal coordinates of all probes, ordered by probe number. The probes are numbered 1-15(or 16) for first rack, 16-30 (or 17-32) for the second, etc. Rack numbers refer to the multiplexor connections and **do not** indicate relative position along the channel.
3	vertical coordinates for all probes.
4-7	Times of samples; the computer clock was read between each 16th sample of all probes, i.e. the time is read, then all probes are scanned once, twice, ..., up to 16 times, then the clock is read again.
8	Data related to the density current head. This is only for the sloping bottom experiments, it is blank in the last two. Subroutine RESULTS in DATIHW explains the data stored here.
9	Average temperatures for each probe, but only between NSTART and NSTOP which are sample numbers which were designated in the original data processing.
10	Standard deviations for the same range of samples.
11	the first 256 instantaneous temperatures for probe 1. These are stored as INTEGER*2 values that must be mutiplied by a scale factor (A1 = 0.01) the value of which is stored in Record 1 and used in READ1 to convert to actual temperatures.
12	the first 256 for probe 2.
etc.	until the total number of probes have been processed. Then the next 256 for probe 1, etc. until all data is stored.

The abbreviated files have only the first ten records, i.e. they contain everything except the instantaneous temperatures.

One variation of TEMPME collected data in groups of 200 records (1600 samples) with a sampling pause after each 200 records. The sampling was then manually restarted as desired. This was

primarily used for the second group of the series 2 experiments with the different downstream controls. In a few experiments in the series 3 group, this program was used inadvertently. It's use can be detected by an unusual time gap between adjacent times in the time record. In some time records, it will be noted that the time intervals between 16 samples change. This is due to a change in sampling frequency midway through the experiment. This was only done in the B series of experiments. There is one temperature record that contains data for two separate experiments. This is the 20B experiment; the two are alike except for the ambient velocity. The first 200 records are for an ambient discharge of 1.72 liters/sec while the second 200 are for an ambient discharge of 0.875 liters/sec. Furthermore, information on the density current is not present for the second condition so this experiment was repeated as 21B.

The routine READ1 which is appended to the routines DATIHW, DAT1IHW, and DAT2IHW has been verified. It is slightly different between the first and the last two programs, so may not be interchangeable. It recovers all the information in the first ten records. Then, as an example, it selects a particular rack and probe number within that rack. It then determines the probe coordinates, the mean temperature and standard deviation, and reads the entire temperature record for that probe. It then computes the time (relative to the intiation of the sampling) that the sample was collected by interpolation from the recorded times.

There are a series of tapes. Because of the data file size, tape density is 6250 BPI on some and there are more than one data tape for two of the series. Labels on each give the information; the blocksize is 6144 for each. The processed data files (both complete and abbreviated for each experiment) and the program that was used to process the data was also written. From this program, the READ1 routine can found and modified to meet the specific purposes.

AIIM SCANNER TEST CHART # 2

Spectra

4 PT ABCDEFGHIJKLMNOPQRSTUVWXYZabcdefghijklmnopqrstuvwxyz:'',./?$0123456789

6 PT ABCDEFGHIJKLMNOPQRSTUVWXYZabcdefghijklmnopqrstuvwxyz;:'',./?$0123456789

8 PT ABCDEFGHIJKLMNOPQRSTUVWXYZabcdefghijklmnopqrstuvwxyz;:'',./?$0123456789

10 PT ABCDEFGHIJKLMNOPQRSTUVWXYZabcdefghijklmnopqrstuvwxyz;:'',./?$0123456789

Times Roman

4 PT ABCDEFGHIJKLMNOPQRSTUVWXYZabcdefghijklmnopqrstuvwxyz;:'',./?$0123456789

6 PT ABCDEFGHIJKLMNOPQRSTUVWXYZabcdefghijklmnopqrstuvwxyz;:'',./?$0123456789

8 PT ABCDEFGHIJKLMNOPQRSTUVWXYZabcdefghijklmnopqrstuvwxyz;:'',./?$0123456789

10 PT ABCDEFGHIJKLMNOPQRSTUVWXYZabcdefghijklmnopqrstuvwxyz;:'',./?$0123456789

Century Schoolbook Bold

4 PT **ABCDEFGHIJKLMNOPQRSTUVWXYZabcdefghijklmnopqrstuvwxyz;:'',./?$0123456789**

6 PT **ABCDEFGHIJKLMNOPQRSTUVWXYZabcdefghijklmnopqrstuvwxyz;:'',./?$0123456789**

8 PT **ABCDEFGHIJKLMNOPQRSTUVWXYZabcdefghijklmnopqrstuvwxyz;:'',./?$0123456789**

10 PT **ABCDEFGHIJKLMNOPQRSTUVWXYZabcdefghijklmnopqrstuvwxyz;:'',./?$0123456789**

News Gothic Bold Reversed

4 PT ABCDEFGHIJKLMNOPQRSTUVWXYZabcdefghijklmnopqrstuvwxyz;:'',./?$0123456789

6 PT ABCDEFGHIJKLMNOPQRSTUVWXYZabcdefghijklmnopqrstuvwxyz;:'',./?$0123456789

8 PT ABCDEFGHIJKLMNOPQRSTUVWXYZabcdefghijklmnopqrstuvwxyz;:'',./?$0123456789

10 PT ABCDEFGHIJKLMNOPQRSTUVWXYZabcdefghijklmnopqrstuvwxyz;:'',./?$0123456789

Bodoni Italic

4 PT ABCDEFGHIJKLMNOPQRSTUVWXYZabcdefghijklmnopqrstuvwxyz;:'',./?$0123456789

6 PT ABCDEFGHIJKLMNOPQRSTUVWXYZabcdefghijklmnopqrstuvwxyz;:'',./?$0123456789

8 PT ABCDEFGHIJKLMNOPQRSTUVWXYZabcdefghijklmnopqrstuvwxyz;:'',./?$0123456789

10 PT ABCDEFGHIJKLMNOPQRSTUVWXYZabcdefghijklmnopqrstuvwxyz;:'',./?$0123456789

Greek and Math Symbols

4 PT ΑΒΓΔΕΞΘΗΙΚΛΜΝΟΠΦΡΣΤΥΩΧΨΖαβγδεξθηικλμνοπφρστυωχψζ≧∓'',. / ≦±=≠°><⊁⊀⩾⩽≡

6 PT ΑΒΓΔΕΞΘΗΙΚΛΜΝΟΠΦΡΣΤΥΩΧΨΖαβγδεξθηικλμνοπφρστυωχψζ≧∓'',. / ≦±=≠°><⊁⊀⩾⩽≡

8 PT ΑΒΓΔΕΞΘΗΙΚΛΜΝΟΠΦΡΣΤΥΩΧΨΖαβγδεξθηικλμνοπφρστυωχψζ≧∓'',. / ≦±=≠°><⊁⊀⩾⩽≡

10 PT ΑΒΓΔΕΞΘΗΙΚΛΜΝΟΠΦΡΣΤΥΩΧΨΖαβγδεξθηικλμνοπφρστυωχψζ≧∓'',. / ≦±=≠°><⊁⊀⩾⩽≡

White

Black

Isolated Characters

e	m	1	2	3	a
4	5	6	7	o	°
8	9	0	h	I	B

A4 Page 6543210

MESH HALFTONE WEDGES

65

85

100

110

133

150

A4 Page 6543210

RIT ALPHANUMERIC RESOLUTION TEST OBJECT, RT-1-71

PRODUCED BY GRAPHIC ARTS RESEARCH CENTER

ROCHESTER INSTITUTE OF TECHNOLOGY, ONE LOMB

MEMORIAL DRIVE, ROCHESTER, NEW YORK 14623